NOTICE

The quality of this microform is heavily dependent upon the quality of the original thesis submitted for microfilming. Every effort has been made to ensure the highest quality of reproduction possible.

If pages are missing, contact the university which granted the degree.

Some pages may have indistinct print especially if the original pages were typed with a poor typewriter ribbon or if the university sent us an inferior photocopy.

AVIS

La qualité de cette microforme dépend grandement de la qualité de la thèse soumise au microfilmage. Nous avons tout fait pour assurer une qualité supérieure de reproduction.

S'il manque des pages, veuillez communiquer avec l'université qui a conféré le grade.

La qualité d'impression de certaines pages peut laisser à désirer, surtout si les pages originales ont été dactylographiées à l'aide d'un ruban usé ou si l'université nous a fait parvenir une photocopie de qualité inférieure.

ISBN 0-315-56352-4

DEVELOPMENT AND APPLICATION OF A THREE-DIMENSIONAL TWO-FLUID NUMERICAL ALGORITHM FOR SIMULATION OF PHASE REDISTRIBUTION BY BENDS AND OBSTRUCTIONS

by

M.B. Carver

Thesis submitted in partial requirements for the degree PhD.

Department of Mechanical Engineering, University of Ottawa.

Thermalhydraulics Development Branch

Chalk River Nuclear Laboratories

Chalk River, Ontario K0J 1J0

1987 April

DEVELOPMENT AND APPLICATION OF A THREE-DIMENSIONAL TWO-FLUID NUMERICAL ALGORITHM FOR SIMULATION OF PHASE REDISTRIBUTION BY BENDS AND OBSTRUCTIONS

by

M.B. Carver

Thesis submitted in partial requirements for the degree PhD.

Department of Mechanical Engineering, University of Ottawa.

Abstract

This thesis describes research work to complete the development, testing, modelling and validation of a numerical technique for simulating three dimensional two-fluid flow. Numerical methods for simulating two-fluid flow were developed. The constitutive relationships required to model interphase friction and effective viscosity and their interaction are developed. The model is used to simulate phase redistribution caused by obstructions and bends, and computed results are compared to available experimental measurements.

TABLE OF CONTENTS

LIST OF TABLES IN THE TEXT

LIST OF TABLES IN APPENDICES

LIST OF FIGURES IN THE TEXT

LIST OF FIGURES IN THE APPENDICES

NOMENCLATURE

Variable	Description
A	cross sectional area of control volume face
B	imbalance matrix
a,b,c,e	coefficients of linear equations
C	Convective flux
d	differential operator
D	continuity imbalance or Diffusive flux
Fr	Froude number
g	gravitational constant
k	turbulent energy
l	lengthscale
m	mass flux
M	momentum exchange
P	pressure
Pt	Peclet Number
Q	volumetric flux
R	elbow centreline radius
Re	Reynolds number
r,θ,ϕ	toroidal coordinates
s	slip ratio

S	source term
t	time
U	velocity field vector
u,v,w	velocity components
W_∞	bubble rise velocity
x	generalized coordinate
x,y,z	cartesian coordinates
V	volume.
Z	a term
α	volume fraction
β	relaxation parameter
ε	turbulent dissipation
ξ	general viscosity function
γ	normalized density
ϕ	general variable
Ψ	drag function
Γ	viscous function
μ	viscosity
ρ	fluid density
σ	Prandlt-Schmidt number
τ	stress tensor

SUBSCRIPTS

b	bubble
bs	bubble-slug
c,d	continuous, dispersed phase
c	constant
d	drag
E	effective
FL	full of liquid
FG	full of gass
g	gaseous
h	homogeneous
i	neighbouring point in i direction
i+,i-	after,before in the i direction
I,O	in,out
j	neighboring points in j direction or cartesian vector index
l	liquid
l,g	interphase
ι	pertaining to fluid ι
L	laminar
LO	with respect to ~~liquid~~ only
n	neighbouring point n=N,E,S,W,U,D
o	reference

P,M	plus, minus
p	point in question
r	relative
s	slug
sa	slug-annular
T	turbulent
TP	two-phase
1 , 2	phase 1 , 2

SUPERSCRIPTS

c	computed
o	current
r	relaxed
–	matrix, or average
~	mixture
'	based on volume,or instantaneous
+	dimensionless boundary parameter

SUMMARY

In many kinds of industrial equipment such as boilers, reactors and chemical plants, two fluid mixtures flow through piping systems which include bends or obstructions. Under some conditions these can promote separation of the two fluids, while under others a bend may promote homogenization. Knowledge of their effect on phase distribution is therefore often required for detailed analysis of flow and heat transfer characteristics which govern equipment performance. Correlations are not available for predicting phase distribution in such configurations, nor are standard computational techniques, as a two-fluid model in at least two dimensions is required. The objectives of this research were to develop numerical algorithms to solve such a two fluid model, install these in a three dimensional computer program, to investigate and develop the required constitutive models, and to test and validate the resulting computer program, by applying it to simulate phase redistribution in various configurations, and by comparing computed results to reported experimental data.

Multidimensional computer programs for single-phase flow have been available for some time; however, two-phase flow has usually been treated as a homogeneous mixture, which forces the phases to have identical velocities. A full two-fluid formulation permits the phases to have unequal velocities and thus, separation tendencies induced by gravitational or centrifugal forces can be modelled.

Two-fluid modelling in one dimension is now becoming quite common, but very few computer programs have been developed for multidimensional two-fluid modelling. In this research, those that have been reported were reviewed and their numerical methods were found wanting, so an entirely new numerical approach for two fluids was devised. This was implemented by converting an existing single-fluid two-dimensional computer program to model two fluids and testing it for proof of concept on a number of different applications. These include comparison with experiments on two-phase flow in elbows, in which centrifugal force separates the phases, and on two-phase flows with obstructions which tend to mix the phases. This work lead to several refinements of the algorithm including the development of a method for computing volume fraction implicitly, and an additional algorithm to ensure that computed volume fractions remained within acceptable limits.

The successful application of the algorithms in two dimensions led to the extension of the two-fluid method to three dimensions. Again, the skeleton of an existing single-fluid program was used as a base, and the two-fluid algorithms were superimposed. The resulting program may therefore be used in either single-fluid or two-fluid mode. The three dimensional calculations showed that the two-fluid numerical algorithm developed for 2D situations performed consistently adequately when applied to 3D, so no major changes to the philosophy of the algorithm were necessary.

Because of the considerable expense of three-dimensional computation, the speed of convergence becomes of paramount importance, so methods of enhancing convergence in single phase flow computations were reviewed and extended to the two-fluid case.

Attention was then turned to the physical modelling of the two-fluid motion. Not surprisingly, the interaction of the two-fluids and the resulting phase distribution was found to be a strong function of the model used for interphase momentum exchange, and also was affected significantly by the presence of turbulent stress and its interaction with interphase drag. Definitive models of these interactions have yet to be established. Appropriate methods of modelling these phenomena were developed, in this study and shown to be satisfactory under flow conditions in the bubbly and distributed flow (slug/bubble) regimes.

A number of configurations have been simulated with both single-fluid and two-fluid options. For two-fluid flow, computations of phase distribution in bubbly flow in vertical pipes led to an extension of the turbulence model to two-fluid flow. This was then used to model horizontal two-fluid flow being redistributed by blockages, and also of phase distribution changes during flow around various types of elbows. Computed variations of phase distributions and velocity profiles were compared to reported experimental measurements. In cases where cross-sectional distributions were not reported, the measured variation of cross-sectional averaged values for void and slip were used for comparison, as these quantify the overall relative motion of the phases.

The study has produced a robust numerical algorithm for three-dimensional simulation of two-fluid flow which converges well over a wide range of parameters, and has , together with the physical modelling introduced, been shown to well reproduce empirical measurements of phase redistribution.

ORGANISATION OF THE THESIS

Chapter one is an introduction, with a review of the literature in two-phase flow simulation , models of two-phase flow, and flow regimes.

Chapter two reviews previous numerical techniques , identifies the need for improvement, and describes the development of the new technique devised.

Chapter three describes a number of detailed two-dimensional computations to establish proof of concept for the new method before proceeding to 3-D. Computed results are shown to exhibit experimentally observed trends.

Chapter four describes the extension of the new algorithm to 3-D, and some associated concerns, particularly convergence enhancement.

Chapter five addresses the detailed modelling that is now possible, having established a 3-D computational tool. The basic equations are reviewed in detail, with particular emphasis on the interphase relationships required to simulate vertical bubbly flows, and on the suitable modelling of effective viscosity due to turbulence in such two-fluid flows. Computed velocity and void profiles are compared to measured values.

Chapter six uses the techniques developed in all the previous chapters to simulate three-dimensional two-fluid flow around obstructions, and computed results are compared to experimental measurements.

Chapter seven uses the techniques to simulate three-dimensional two-fluid flow around various elbows, and results are included showing comparisons of void redistibution in the bend for nine different experiments. Some results of sensitivity studies are also included.

Chapter eight has the concluding remarks.

Following the references, Appendix A contains details of the computer implementation, and Appendix B outlines some related computational considerations.

CHAPTER 1. INTRODUCTION

This chapter reviews numerical solution of two-fluid flow, and the pivotal role of the treatment of pressure. The various models of two-fluid flow are introduced and flow regimes are discussed.

1.1 Overview of Two-Phase Flow Simulation

The homogeneous model traditionally used for two-phase flow calculations is based on an assumption of thermal and mechanical equilibrium between phases, and is not capable of predicting flow distribution under conditions which cause departure from these equilibria. The study of models which permit certain departures from equilibrium has progressed considerably in recent years, and rigorous models of one dimensional two fluid flow have been developed. Particular attention has been paid to the well-posedness of these models and a number of benchmark problems have been established, Hancox and Banerjee (1977), Lyczkowski and Sha(1981). Computations, although intricate, are not prohibitive in scale and permit simultaneous solution of all the relevant equations. In contrast, multidimensional thermalhydraulic analyses generate numerical systems which are usually too large for simultaneous solution. The state of multidimensional two fluid modelling is therefore less well advanced. Definitive studies of well-posedness have yet to appear and benchmark problems are rarely used.

Computer codes have been developed for the solution of multidimensional two-phase flow problems but there is little agreement concerning either the form of the equations to be solved, or the selection of a suitable numerical scheme. Among the most important numerical concerns are the manner in which the pressure field is computed, and the effect this has upon the maintenance of continuity.

Even for single-phase, pressure appears in the conservation equations as a secondary variable. The density, energy and velocity components appear as primary variables in the differential equations expressing conservation of mass, energy and momenta respectively, but although pressure is linked to velocity in the momentum equations, it is linked only indirectly to density through the equation of state and has a minor role in the energy equation. An explicit differential equation defining pressure cannot therefore be derived, although, by introducing appropriate derivatives from the equation of state, implicit sets of equations containing pressure as a primary variable can be developed, Ransom and Hicks(1984), Carver(1980). Roache (1976) discusses the role of the pressure in numerical schemes in some detail, and also discusses the hyperbolic nature of the conservation equations. Whether the various forms of the one dimensional two-fluid models successfully maintain hyperbolicity remains a controversy, Ransom and Hicks(1984), and will not be discussed in this report, as the primary intent is to develop multidimensional two-fluid computation schemes.

It is computationally efficient to reformulate the conservation equations to extract pressure from the primary variable solution, by forming an equation which couples pressure throughout the flow field. As this is a Poisson equation, and elliptic in form, the solution now has a primary hyperbolic phase which uses an assumed pressure field followed by a secondary elliptic phase which adjusts the pressure field. Although the pressure equation normally materializes as a linearized matrix equation, the exact forms of pressure equations used are diverse, as a number of simplifying assumptions can be made in different solution schemes. In single-fluid analysis, these simplifying assumptions do not appear to greatly degrade solution accuracy, although they may considerably affect convergence speed. Multidimensional analyses of single-fluid flow and homogeneous two-phase flow appear to originate from one of two major generic sources, the ICE procedures developed at LASL, Harlow and Amsden(1971), and the SIMPLE procedures from Imperial College, Patankar and Spalding(1972). These basic procedures are also in fact quite similar in concept. Both formulate the equations using the staggered grid concept; the velocities being assigned at control volume boundaries thus act between pressures. Both also use the pressure equation concept. They differ principally in the exact form of the pressure equation, the manner in which the equations are formulated over the control volume, the degree of implicitness used in time advancement, and the solution sequence. Variations on these schemes, aimed primarily at improving convergence through quantifying the linkage between pressure and velocities, have been proposed by Patankar,(1980), Raithby and Schneider(1979) and others, and similar concepts have been applied to boundary fitted coordinate systems, Chen et al(1980), and finite element techniques, Baliga et al(1983).

The most appropriate formulation of a problem is often dictated by the geometry to be considered, as a model of the geometry is required as a framework for the analysis. Alternative computational frameworks are reviewed by Sha(1980) and Carver(1984a). A framework which is intermediate to the simple one dimensional and truly multidimensional formulation is the subchannel method frequently used to analyse flow in rod arrays. In this formulation subchannels are defined as parallel flow channels bounded by rod surfaces and fictitious lines between rod centers. The channels are linked laterally through the fictitious parts of the boundary; however, the lateral momentum equations are reduced by replacing all the viscous stress terms by a simple model approximating turbulent interchange between neighbouring pairs of channels. Particular subchannel codes are discussed by Rowe(1973) and Carver et al(1984).

While the subchannel approach is accurate and cost effective for analysing flow in rod bundles it is restricted to such geometries and cannot be applied to other geometries. The approach will not be discussed further here except to mention particular subchannel codes in the context of the models of two phase flow which they utilize.

Multidimensional two-fluid analyses have also evolved from the same ancestors as single-phase analyses, as it is a straightforward matter in principle, although arduous in practice, to extend the techniques to two fluids. In single-fluid analysis, although the pressure equation may take a number of different forms, the rational basis for its derivation is similar. In two-fluid analyses, however, even more care must be taken with the pressure equation, as legitimate alternatives can be founded on fundamentally different bases. The current study has examined the pressure continuity relationships of a number of reported two-fluid schemes listed below. Flaws exist in this area. These may be diminished under conditions in which heat input causes significant phase change, but become serious for adiabatic situations. An alternate formulation has been developed in the current study and has been shown to be superior. Once a consistently satisfactory scheme was developed, it became apparent that reported schemes for modelling interphase friction and its interaction with turbulent stresses were not adequate either. As results were very sensitive to these features, effort was concentrated on developing and testing appropriate constitutive models, rather than improving the accuracy of the numerical technique along the lines explored for single fluids by, for example, Raithby and Schneider(1979), as such refinement is not productive until it can be shown that the models are sufficiently developed to permit the numerical scheme to compute observed phenomena with reasonable felicity.

In order to establish context, two-fluid models are discussed first, followed by concepts of multidimensional analysis for single-phase flow, and finally the new two-fluid scheme developed is presented.

1.2 MODELS OF TWO PHASE FLOW

The formulation of various models of two-phase flow has been discussed by a number of authors over the last two decades. Perhaps the most comprehensive studies have been by Ishii (1975) and Kocamustafaogulari (1971). Recently, models have been labelled EVET, EVUT, etc. to represent equal velocity equal temperature, equal velocity unequal temperature, etc., Hancox and Banerjee (1977). The following is a brief summary of the models.

The assumption of equilibrium produces the simplest model, in which the phases are taken to be homogeneously mixed, and to have equal velocity and equal temperature, hence the terminology EVET model. The two-phase mixture is treated as a single fictitious fluid having properties determined solely by the relative proportion by weight (quality) of vapor in the mixture. Thus, the partial differential equations to be solved are the same as the single-phase flow: conservation of mass, momentum and energy of the mixture; algebraic relationships cater for the two-phase properties and the equation of state for the mixture. The homogeneous model is suitable for conditions in which departures from mechanical and thermal equilibrium are known to be minimal. One dimensional, subchannel, and three dimensional EVET computer codes are described by Moore and Rettig(1975), Rowe(1973) and Carver(1981), respectively.

The classical mixture model was not adequate for modelling details of phase distribution, as any redistribution of phases in a conduit requires a priori that the phases have different velocities. Non-equilibrium models permit the simulation of the motion of each fluid, using the concept of interpenetrating continua. Thus, for cases in which gravitational or centrifugal forces are known to produce a tendency for phases to travel at different speeds, a two-velocity model is required, and an additional relationship is required for relative velocity. Early separated flow models used void correlation instead of the equation of state, and a simple numeric slip factor to impose the higher velocity of the vapor phase in vertical flow. This was later quantified by relating relative velocity to the rise velocity of vapour bubbles in liquid, and radial distribution of vapor under various conditions. This simple drift flux equal temperature model (DFET), uses algebraic relationships for relative velocity, and hence requires the solution of the same three partial differential equations of conservation, but an additional equation, usually based on gaseous phase continuity, is required for void distribution. One dimensional and three dimensional subchannel DFET computer codes are described by Chang and Skears(1977) and Carver et al(1984) , respectively.

None of the above models permits the temperature of either phase to depart from saturation. In order to simulate non-equilibrium phenomena such as subcooled boiling, superheated liquid and flashing, etc., a mechanism which permits these effects must be added. Again, early studies used algebraic relationships, but more rigorous models now use a separate energy equation, and equation of state for each phase and model heat transfer to and between phases. The EVUT model is, therefore, also a four equation model using a mixture momentum equation, and individual energy equations for each fluid. A one dimensional EVUT model is discussed in Ferch(1979).

The advanced drift flux DFUT model is a combination of both of the above, and therefore, requires the solution of five conservation equations, a mixture momentum equation, two energy equations, and two continuity equations. A multidimensional subchannel DFUT model is discussed by Judd et al(1984).

Finally, the full two-fluid models abandon the algebraic definition of relative velocity and instead compute phase velocities using two momentum equations containing models of wall to fluid and fluid to fluid stresses. One dimensional two-fluid models have also been developed in five-equation UVET, Ransom et al(1982) and six-equation UVUT form, Ransom et al(1985) and Mahaffy et al(1981).

It is apparent that with each level of complexity of the two-phase model, additional partial differential equations are added, and hence more involved numerical schemes are required.

One-dimensional simulation permits the modelling of phenomena in which the relationship of the axial velocities of the fluids is of paramount importance, however, phase distribution is considered to be uniform in the cross-sectional or lateral plane. Attempts have been made to incorporate non-uniformity of phase distribution into one dimensional analyses by using appropriate techniques to arrive at a set of conservation equations in which the variables represent cross-sectional averaged quantities. Such methods have been discussed at length by Ishii (1975), Delhaye (1973) and others, and lead to quite complicated expressions. A subset of these models which has found quite common use, because of its simplicity, is the distribution parameter concept introduced by Zuber and Findlay (1965) in their formulation of the one-dimensional drift-flux model.

However, although the distribution parameter approach did permit inclusion of an approximation of distribution effects into one dimensional drift-flux calculations, no generally applicable method of quantifying these parameters has been developed. The most comprehensive protocol developed to date, Chexal (1985) is restricted to vertical flow.

The above methods merely approximate the effects of lateral phase distribution on the axial flow, and in no way model or even convey information about the nature of phase distribution in the lateral plane. In order to model this distribution, at least two dimensions, and frequently three, must be incorporated in the analysis.

1.3 Flow Regimes

As already mentioned, the phases in two-fluid flow are very rarely uniformly mixed, and usually tend to establish some kind of preferred distribution. The fact that, for vertical flow in pipes, this can be compensated for in the one-dimensional equations has been mentioned, and the type of distributions encountered will be discussed in a later chapter. It is relevant to note here that the distribution of the phases and the manner in which the phases interpenetrate is a function of the geometry and orientation of the flow, the density, and viscosity of the phases,surface tension, and the mass flow of each phase. The structure of two phase flow has been studied extensively, and particularly characteristic flow patterns have been identified and termed flow regimes. Boiling flow usually generates a sequence of flow regimes as boiling increases the void fraction progressively, see for example Delhaye(1981). However, in adiabatic conditions, the overall ratio of

volumetric flows remains fairly constant throughout the flow passage, and preferred flow regimes are usually established. The accumulated experimental information has been condensed and presented in the form of flow regime maps. Clearly this cannot be done precisely and requires a certain amount of subjective interpretation and judgement. Clearly also these maps will be somewhat different depending on the orientation of the flow. In popular use are the maps presented by Hewitt and Roberts (1969) and Mundhane(1974) for vertical and horizontal two phase flows respectively. These are given in Figure 1.1. The plots are given in terms of superficial velocity. This is used frequently in two phase flow studies and denotes the velocity which the phase would have if it fully occupied the pipe at the same total volumetric flow; the superficial velocity of phase k is lower than the actual velocity.

Pictorial representation of the flow regimes also involves some subjective interpretation. Pictorial interpretations are given in Figure 1.2. As mentioned, the flow regimes depicted by the maps are the preferred distribution eventually established given the conditions shown, however any change in the geometry will redistribute the flow, and it will take some time, typically 10-20 equivalent diameters for the preferred pattern to restablish.

The techniques developed in this research are applicable only to the distributed flow regimes, as to model the separated flow regimes it would be necessary to track the interface between the fluids and that requires quite different techniques.

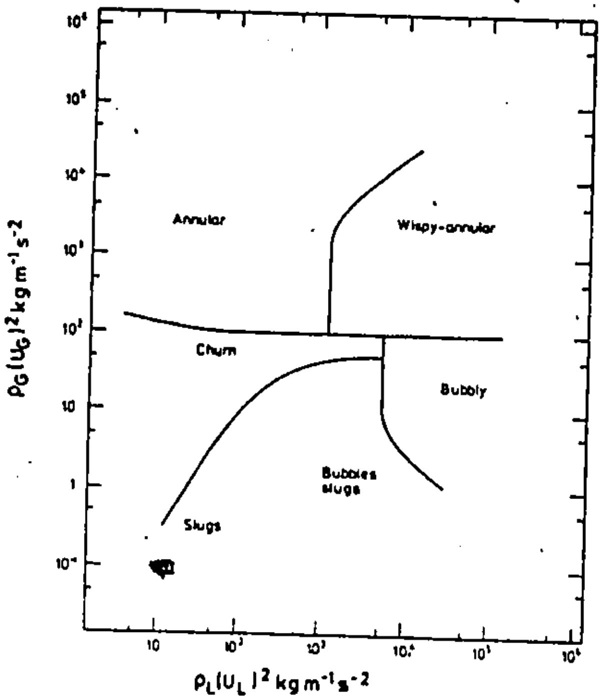

Flow-pattern map obtained by Hewitt & Roberts (1969) for vertical two-phase upward flow.

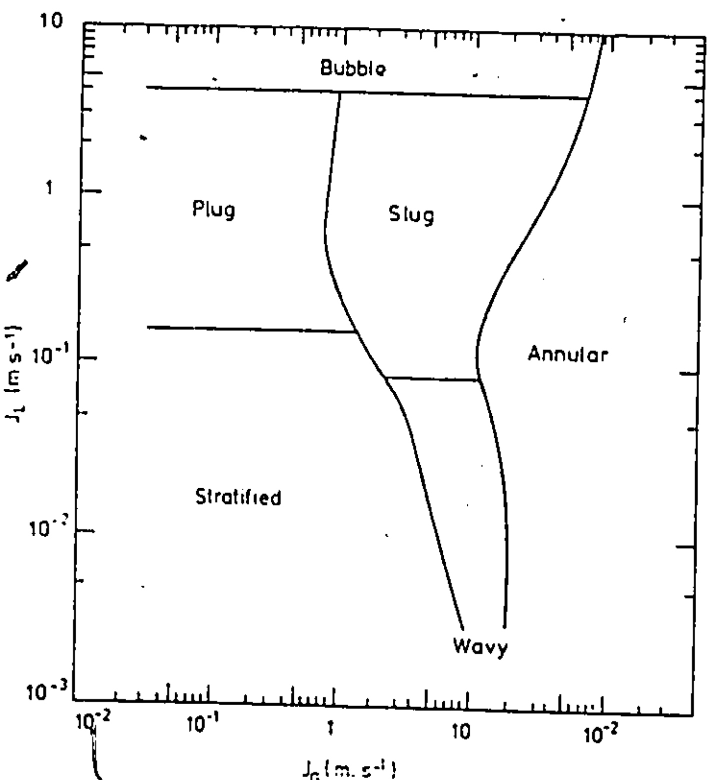

Flow Map Proposed by Mandhane et al. (1974)

Fig. 1.1. Flow Regimes for Adiabatic Two-Phase Flow

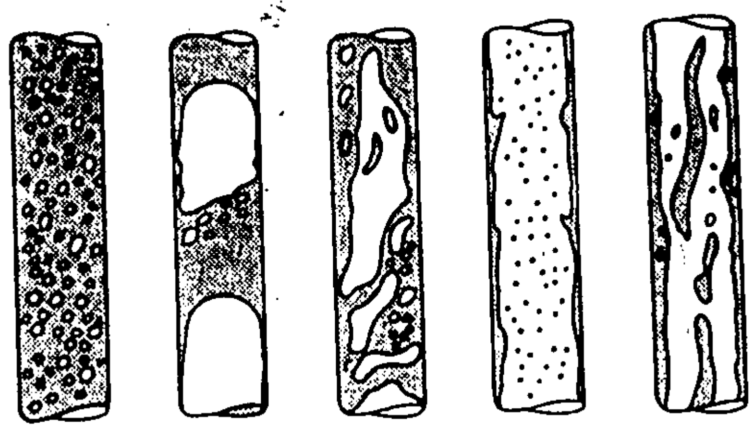

Flow patterns in vertical flow.

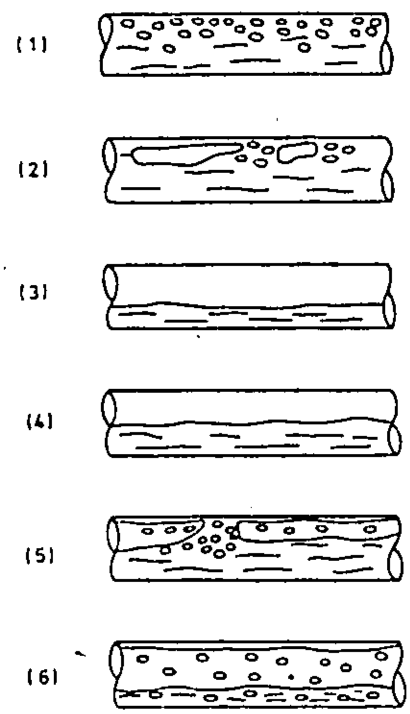

(1) Bubbly flow, (2) Plug flow,
(3) Stratified flow, (4) Wavy flow,
(5) Slug flow, (6) Annular flow

Flow Patterns in a Horizontal Pipe

Fig. 1.2. Flow Patterns for Adiabatic Two-Phase Flow

1.4 Conditions Causing Phase Redistribution

Two common causes of flow redistribution in adiabatic two phase flow are bends and obstructions. The effect on pressure drop of bends and various types of obstructions has been documented in great detail for single phase flows, but although considerable information is also available for two phase flow, it is less precisely established, see for example Chisholm (1969).

The common feature causing flow redistribution in bends and obstructions is the creation of differential forces which tend to separate the phases. In a horizontal bend, for example, a centrifugal force tends to drive the fluids towards the outside of the bend ,thus the heavier fluid displaces the lighter fluid towards the inside. In an obstruction, the heavier fluid is driven around the obstruction while the lighter fluid is displaced into the recirculation area behind the obstruction. Gardner and Neller (1970) discuss both bends and obstructions, and also were the first to give detailed measurements of phase redistribution due to bends. The current research focussed on the computer simulation of flow and phase distribution. This requires multi-dimensional two-fluid analysis. The two necessary ingredients for successful completion of such a simulation are the development of

a) a robust numerical technique for solution of the equations and

b) the development of appropriate constitutive models for use therein.

These will be discussed in the ensuing chapters.

CHAPTER 2. DEVELOPMENT OF THE NUMERICAL SOLUTION TECHNIQUE

In this chapter, the equations governing three-dimensional two-fluid flow are stated, standard techniques for solving the single fluid equations are reviewed ,some techniques proposed in the literature for solving the two-fluid flow equations are examined and found unsatisfactory, and a new technique is developed and shown to be robust and general. Following description of the testing, and extension of the technique, in Chapters 3 and 4 , the equations are revisited and discussed in detail in Chapter 5.

2.1 THE GOVERNING EQUATIONS

Ishii (1975) presents a full formulation of the various models, however, in this study, only the two fluid model of two-phase flow is used, and the studies were restricted to steady adiabatic flow of two incompressible components.

To assemble the equations for adiabatic two component flow, one requires for each fluid an equation of conservation of mass, three equations of conservation of momentum, one for each coordinate direction, plus constitutive relationships for momentum transfer between fluids and between each fluid and the wall. These latter are discussed in chapter 5. Finally, of course, the sum of the volume fractions must be unity.

Following Ishii(1975), the equations are stated here for each fluid ι, discussion of the constitutive relations in Chapter 5.

$$\nabla.(\alpha\rho U)_\iota = 0 \tag{2.1}$$

$$\nabla.(\alpha\rho UU)_\iota = -\alpha_\iota \Delta p + (\alpha\rho)_\iota g + M_{\iota\iota'} + \Gamma_\iota \tag{2.2}$$

In order to address a range of geometries, including radial bends in pipes, the conservation equations have been written in toroidal cylindrical coordinates. Toroidal coordinates have been used for single phase computation by Austin(1971), Soh and Berger(1984) and Pratap(1976), and can be derived from the Cartesian form by straightforward coordinate transformation following procedures outlined in texts on vector algebra such as Chorlton(1967), and using a toroidal coordinate system with parameters assigned as described in Figure 2.1.

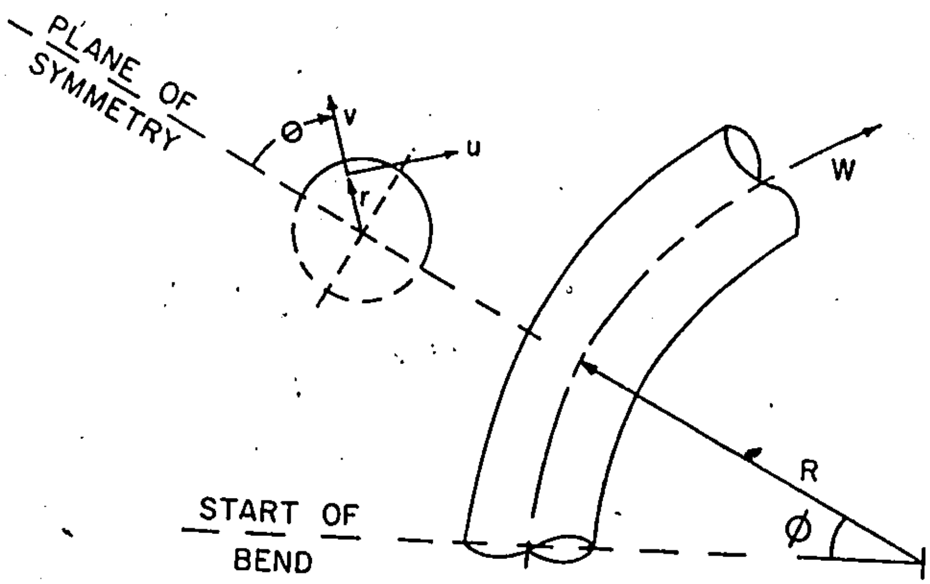

Fig. 2.1 Toroidal Coordinate System

This results in the set of governing equations given in Tables 2.1 and 2.2. The equations are written in terms of α_ι the volume fraction of fluid ι, thus the mass flow in the x direction is $(\alpha\rho u)_\iota A_x$. Note that the reduction to cylindrical polar and thence to cartesian is much more easily accomplished than the transformation, so for general application, it is useful to assemble the equations in toroidal form and introduce simplifications to generate the other coordinate systems where necessary. For example, analysis of a bend between straight lengths of pipe requires three coordinate sets: cylindrical polar, toroidal and cylindrical polar in sequence. The same equations reduced to Cartesian in the cross-section can be used to model flow of a rectangular duct around a bend as noted in Table 2.1. Two dimensional subsets may be readily derived from this latter set.

The equations reduce to the single-fluid case by writing $\alpha_\iota = 1$ and bypassing the interphase drag terms. Note also that, as they should, the equations reduce to the single-fluid equations by addition if the two fluids are identical, as $\alpha_l + \alpha_g = 1$. Finally, the equations as written can also be used to solve for single-phase flow in a porous medium, where α is assigned as the local porosity, i.e., that volume fraction which is available for fluid as opposed to hardware.

Table 2.1

CONSERVATION EQUATIONS FOR ADIABATIC TWO FLUID FLOW TOROIDAL (θ-r-ϕ) SYSTEM

Conservation of Mass

$$\frac{1}{R'r}\left\{ \frac{\partial}{\partial r}(R' r\alpha\rho v)_\iota + \frac{\partial}{\partial\theta}(R'\alpha\rho u)_\iota + \frac{\partial}{\partial\phi}(r\alpha\rho w)_\iota \right\} = 0 \qquad (2.3)$$

Conservation of Momentum

$$\frac{1}{R'r}\left\{ \frac{\partial}{\partial r}(R' r\alpha\rho uv)_\iota + \frac{\partial}{\partial\theta}(R'\alpha\rho u^2)_\iota + \frac{\partial}{\partial\phi}(r\alpha\rho uw)_\iota \right\}$$

$$+ (\alpha\rho uv)_\iota/r + (\alpha\rho w^2)_\iota \sin\theta/R'$$

$$= -\frac{\alpha_\iota}{r}\frac{\partial P}{\partial\theta} + \Psi(u_{\iota'} - u_\iota) + (\alpha\rho_\iota)g\sin\phi\sin\theta + \Gamma_{\theta\iota} \qquad (2.4)$$

$$\frac{1}{R'r}\left\{ \frac{\partial}{\partial r}(R' r\alpha\rho v^2)_\iota + \frac{\partial}{\partial\theta}(R'\alpha\rho uv)_\iota + \frac{\partial}{\partial\phi}(r\alpha\rho vw)_\iota \right\}$$

$$- (\alpha\rho u^2)_\iota/r - (\alpha\rho w^2)_\iota \cos\theta/R'$$

$$= -\alpha_\iota\frac{\partial P}{\partial r} + \Psi(v_{\iota'} - v_\iota) - (\alpha\rho_\iota)\,g\sin\phi\cos\theta + \Gamma_{r\iota} \qquad (2.5)$$

$$\frac{1}{R'r}\left\{ \frac{\partial}{\partial r}(R' r\alpha\rho vw)_\iota + \frac{\partial}{\partial\theta}(R'\alpha\rho uw)_\iota + \frac{\partial}{\partial\phi}(r\alpha\rho ww^2)_\iota \right\}$$

$$- (\alpha\rho w)_\iota(u\cos\theta - v\sin\theta)_\iota/R'$$

$$= -\frac{\alpha_\iota}{R'}\frac{\partial P}{\partial\phi} + \Psi(w_{\iota'} - w_\iota) - (\alpha\rho)_\iota\,g\cos\phi + \Gamma_{\phi\iota} \qquad (2.6)$$

Notes

(i) The equations are written for fluid ι, ι' is the second fluid
(ii) $R' = R + r\cos\theta$
(iii) $\Gamma_{\theta\iota}$, $\Gamma_{r\iota}$, $\Gamma_{\phi\iota}$ are the viscous stress terms (see Table 2.2).
(iv) $\Psi(u_{\iota'} - u_\iota)$ is the interphase friction function
(v) Transform to cylindrical polar along z-axis writing ϕ=z, R'=1, omit algebraic terms involving R, and denote orientation by sinϕ, cosϕ.
(vi) Transform to cartesian polar (bend in rect. duct) by writing θ=x, r=1, omit algebraic terms involving r, and denote orientation by sinθ, cosθ.
(vii) Reduce to single phase form by writing α=1, or for flow through a porous medium by α=volume fraction available to the fluid (porosity).

Table 2.2

VISCOUS STRESS TERMS

$$\Gamma_{\theta} = \frac{1}{R'r} \{\frac{\partial}{\partial r} [R' r\alpha\mu(r \frac{\partial}{\partial r} \frac{u}{r} + \frac{1}{r} \frac{\partial v}{\partial \theta})]$$

$$+ \frac{\partial}{\partial \theta} [2R' \alpha\mu(\frac{1}{r} \frac{\partial u}{\partial \theta} + \frac{v}{r})] + \frac{\partial}{\partial \phi} [r\alpha\mu(\frac{R'}{r} \frac{\partial}{\partial \theta} \frac{W}{R'} + \frac{1}{R'} \frac{\partial u}{\partial \phi})]\}$$

$$+ \frac{\alpha\mu}{R'}(r \frac{\partial}{\partial r} \frac{u}{r} + \frac{1}{r} \frac{\partial v}{\partial \theta}) + \frac{2\alpha\mu}{R'} (\frac{\partial W}{\partial \phi} + v\cos\theta - u\sin\theta)\frac{\sin\theta}{R'} \tag{2.7}$$

$$\Gamma_{r} = \frac{1}{R'r} \{(\frac{\partial}{\partial r} [2R' r\alpha\mu\frac{\partial v}{\partial r}] + \frac{\partial}{\partial \theta} [R' \alpha\mu(r \frac{\partial}{\partial r} \frac{u}{r} + \frac{1}{r} \frac{\partial v}{\partial \theta})]$$

$$+ \frac{\partial}{\partial \phi} [r\alpha\mu(\frac{1}{R'} \frac{\partial v}{\partial \phi} + R' \frac{\partial}{\partial r} \frac{w}{R'})]]$$

$$- \frac{2\alpha\mu}{r} [(\frac{1}{r} \frac{\partial u}{\partial \Theta} - \frac{v}{r}) - \frac{r}{R'} (\frac{\partial w}{\partial \phi} + v\cos\theta - u\sin\theta) \frac{\cos\theta}{R'} \tag{2.8}$$

$$\Gamma_{\phi} = \frac{1}{R'r} \{\frac{\partial}{\partial r} [R' r\alpha\mu(\frac{1}{R'} \frac{\partial v}{\partial \phi} + R' \frac{\partial}{\partial r} \frac{w}{R'}) + \frac{\partial}{\partial \theta} [R' \alpha\mu(\frac{R'}{r} \frac{\partial}{\partial \theta} \frac{w}{R'} + \frac{1}{R'} \frac{\partial u}{\partial \phi})]$$

$$+ \frac{\partial}{\partial \phi} [2\alpha\mu r(\frac{1}{R'} \frac{\partial w}{\partial \phi} + (v\cos\theta - u\sin\theta)/R')]\}$$

$$+ \frac{\alpha\mu}{R'} [(\frac{1}{R'} \frac{\partial v}{\partial \phi} + R' \frac{\partial}{\partial r} \frac{W}{R'}) \cos\theta - (\frac{R'}{r} \frac{\partial}{\partial \Theta} \frac{w}{R'} + \frac{1}{R'} \frac{\partial u}{\partial \phi}) \sin\theta \tag{2.9}$$

2.2 SOLUTION OF THE SINGLE-PHASE FLOW EQUATIONS

In one-dimensional analyses, solutions are frequently obtained simultaneously for all flow variables throughout the field. However, equation systems resulting from multidimensional analyses are too large to permit simultaneous solution and some form of segmentation of the problem is required, with iteration to merge the segments.

2.2.1 Reduction to Discretized Form

In order to solve the equations, it is necessary to write them in discrete form with reference to finite control volumes. To maintain continuous definition of all variables, it is important that all variables are evaluated correctly where averages across grid points are required. The concept of staggered grid facilitates this, and avoids the problematic decoupling of neighbouring pressures which can occur in calculations with collocated grids, Patankar(1980). Scalar variables such as pressure, density and enthalpy are stored at primary node points, whereas velocities are considered to act between pressures as shown in figure 2.2. The momentum equations are thus written for control volumes centered on velocities, whereas, the continuity and energy equations are centered on the primary nodes. A control volume for a general variable ϕ is shown in figure 2.2, and a full description of the assignment of control volumes is given in Appendix A. The detailed integration of the momentum equations is also given in full in Appendix A.

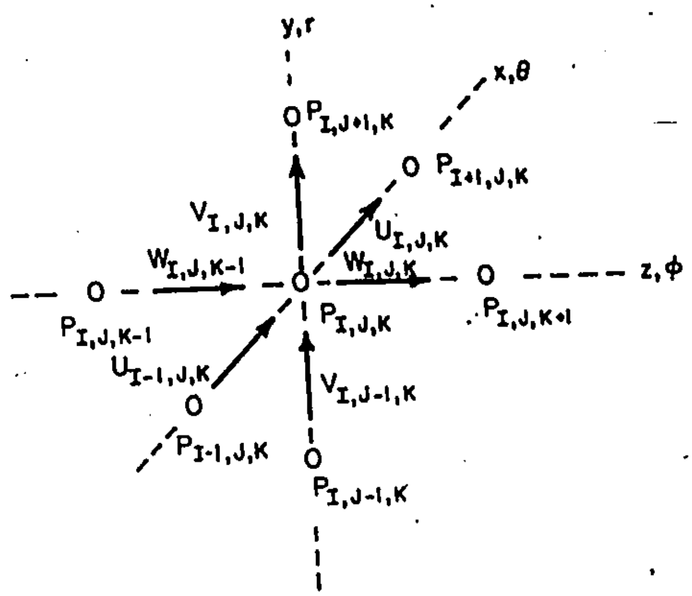

a. Assignment of scalars and vectors

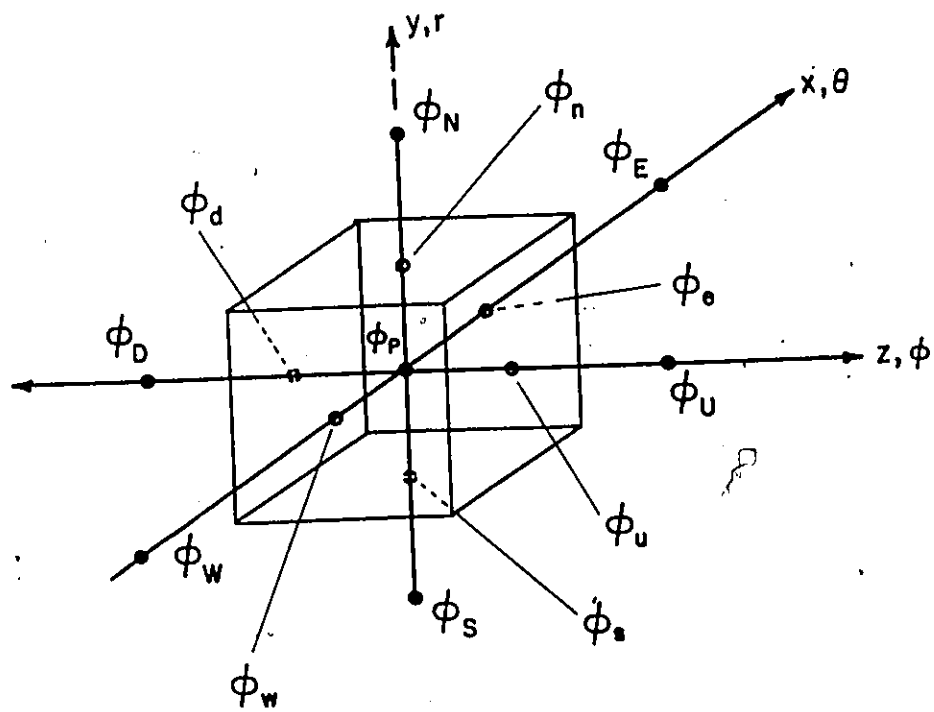

b. Control volume for general variable ϕ

Fig. 2.2 Assignment of Variables and Control Volumes

It would be counterproductive to attempt here to describe the integration and solution of equations 2.2 to 2.9 in complete detail because of the amount of algebra involved. Instead, to illustrate the methodology, the equations will be stated and discussed in cartesian vector notation for brevity. Once the solution sequence is understood, it is a methodical although arduous procedure to apply the same techniques to solve the full toroidal set.

In cartesian vector form for fluid ι the equations become

$$\frac{\partial}{\partial x_j}\{(\alpha\rho u_j)\}_\iota = 0 \tag{2.10}$$

$$\frac{\partial}{\partial x_j}\{(\alpha\rho u_j u_i)\}_\iota + \alpha_\iota \frac{\partial P}{\partial x_i} = S_{i\iota} + \frac{\partial}{\partial x_j}\{\alpha\mu\left(\frac{\partial u_i}{\partial x_j} + \frac{\partial u_j}{\partial x_i}\right)\}_\iota \tag{2.11}$$

The velocity component along coordinate x_i is denoted by u_i and

$$\frac{\partial u_j}{\partial x_j} = \frac{\partial u}{\partial x} + \frac{\partial v}{\partial y} + \frac{\partial w}{\partial z}\,.$$

S_ι contains the remaining source terms from the appropriate equation. For single-phase, the index ι is redundant, but is retained for future reference in the subsequent discussion and application to two-fluids.

2.2.2 Standard Form of Solution

Equations (2.10) and (2.11) can be written in a standard form which combines the pressure, non-cartesian terms and part of the viscous terms in the source term and identifies convection and diffusion fluxes of a parameter ϕ which is unity for equation (2.10), and u,v,w for equation (2.11).

$$\frac{\partial}{\partial x_j}(\alpha\rho u_j\phi) - \frac{\partial}{\partial x_j}\left(\xi\frac{\partial\phi}{\partial x_j}\right) = s' \tag{2.12}$$

This equation can be converted to a form amenable to solution by integrating over the control volume. This is facilitated by converting the left-hand side from a volume integral to an area integral involving the normal flux using the theorem attributed alternately to Green and to Gauss.

$$\iiint(\nabla \cdot \bar{F})dv = \iint(\bar{F} \cdot \bar{n})dA \tag{2.13}$$

Applying this to equation 2.12, and using the directional terminology e,w,n,s,u,d shown in Figure 2.1b gives

$$\begin{aligned}&[(\alpha\rho\phi)_e u_e - \xi_e(\phi_E-\phi_P)/\delta x]A_E - [(\alpha\rho\phi)_w u_w - \xi_w(\phi_P-\phi_W)/\delta x]A_W \\ &+ [(\alpha\rho\phi)_n v_n - \xi_n(\phi_N-\phi_P)/\delta y]A_N - [(\alpha\rho\phi)_s v_s - \xi_s(\phi_P-\phi_S)/\delta y]A_S \\ &+ [(\alpha\rho\phi)_d w_d - \xi_d(\phi_D-\phi_P)/\delta z]A_D - [(\alpha\rho\phi)_u w_u - \xi_u(\phi_P-\phi_U)/\delta z]A_U \\ &\qquad = \iiint s' dv\end{aligned} \tag{2.14}$$

This is further simplified by denoting the convection and diffusion fluxes as C and D respectively.

$$C = \alpha\rho u \ , \ D = \xi/\delta x$$

Hence, equation 2.14 becomes

$$\begin{aligned}&(C_e\phi_e - D_e(\phi_E-\phi_P))A_E - (C_w\phi_w - D_w(\phi_P-\phi_W))A_W \\ &+ (C_n\phi_n - D_n(\phi_N-\phi_P))A_N - (C_s\phi_s - D_s(\phi_P-\phi_S))A_S \\ &+ (C_u\phi_u - D_u(\phi_U-\phi_P))A_U - (C_d\phi_d - D_d(\phi_P-\phi_D))A_D \\ &= \iiint s' dv = s''\end{aligned} \tag{2.15}$$

Providing appropriate expressions for interpolating convection and diffusion coefficients at the control volume faces can be found, equation 2.15 can now be rearranged in the form

$$A_P\phi_P + \sum_n A_n\phi_n = s'' \tag{2.16}$$

$$n = E,W,N,S,U,D$$

For a particular point, this is a simple algebraic equation linking the points to its neighbors. However, the set of equations 2.16 for all points becomes a matrix equation defining the ϕ field.

$$\bar{A}_P \bar{\phi}_P + \sum_n \bar{A}_n \bar{\phi}_n = \bar{S}'' \qquad (2.17)$$

Equation (2.17) is a matrix equation. The value of ϕ obtained from linear equation solution of (2.17) alone is exact when ϕ is a scalar, but when ϕ is a velocity, the nonlinear components are included in the A coefficients, so iteration is required . Furthermore as each of the conservation equations is solved in turn, the coefficients also contain other variables, and further iteration around the full sequence is required.

As noted, the standard solution can be implemented for each equation, provided the correct control volume is used for each ϕ and provided suitable expressions can be obtained for interpolated values at control volume faces. These matters are of considerable importance and have been discussed in detail particularly by Patankar(1980). As detailed discussion would interrupt the flow of the main argument here, these topics are discussed in Appendix A.

2.2.3 Overview of the SIMPLE Scheme for Single-Phase

It is clear that equations (2.10) and (2.11) are coupled matrix equations and that an appropriate solution scheme is required to solve them in concert. For the purpose of illustrating this only, the viscous terms will temporarily be incorporated in the source term.

The solution scheme used in FAITH is a novel extension of the SIMPLE scheme of the single-fluid equations Patankar and Spalding(1972) . The equations (2.10) and (2.11) are first discretized by triple integration over the control volumes for each fluid ι, using the usual staggered grid concept.

$$\sum_i [(\alpha\rho uA)_{i+} - (\alpha\rho uA)_{i-}]_\iota = 0 \qquad (2.18)$$

$$\sum_j [(\alpha\rho u_i u_j A)_{j+} - (\alpha\rho u_i u_j A)_{j-}]_\iota + A\alpha_\iota \, (P_{i+} - P_{i-}) = S_{i\iota} \, V, \qquad (2.19)$$

A and V denote cross-sectional area and volume of the appropriate control volume, and i- or i+ denote upstream and downstream values.

If an initial pressure field is assumed, (2.19) can now be reduced to a form which gives a first estimate of mass flux at point p in terms of the mass fluxes from neighbors n, and the relevant pressure gradient:

$$[a(\alpha\rho u)_p + \sum_n (b\alpha\rho u)_n + e(P_{i+} - P_{i-})]_\iota = S_{i\iota} \, V \qquad (2.20)$$

The coefficients a, b and e contain the appropriate expressions reduced from (2.19), but (2.20) is now linearized, and can be solved in point or matrix form for a new matrix of mass fluxes. However, as the pressure field was not necessarily guessed correctly, the new mass fluxes will not satisfy the continuity equation (2.18) but yield a mass imbalance D:

$$\sum_i [(\alpha\rho uA)_{i+} - (\alpha\rho uA)_{i-}]_l = D_l \tag{2.21}$$

A pressure equation can then be derived in the classical 'SIMPLE' manner. It is necessary to find a new pressure field that will drive D_l to zero. This can be done by using the fact that the mass fluxes in (2.21) will vary with pressure through (2.20), and is accomplished efficiently by the Newton-Raphson technique, which yields

$$dP = -D_l/(dD_l/dP). \tag{2.22}$$

Thus, the required equation for the change in the pressure field, dP, is obtained from rearranging (2.22):

$$\left\{ \frac{dD_l}{dP} \right\} \; dP = -D_l \tag{2.23}$$

An expression for dD_l is readily obtained by differentiating (2.21):

$$dD_l = \sum_i [Ad(\alpha\rho u)_{i+} - Ad(\alpha\rho u)_{i-}]_l = -D_l. \tag{2.24}$$

and from (2.20)

$$d(\alpha\rho u)_{il} = \frac{-1}{a_l} \left\{ \sum_n b_n d(\alpha\rho u)_n + e(dP_{i+} - dP_{i-}) \right\}_l \tag{2.25}$$

Equation (2.25) is handled more readily by neglecting the variations in neighboring mass fluxes, thus, relating changes in each mass flux component at each point to the changes in pressure upstream and downstream, as in SIMPLE. This simplification does not affect the final solution, but as it simplifies the coupling between pressure and velocity, it does affect the convergence rate. A modification which improves on this simplification is discussed in Appendix B, and was in fact used in the later studies. Substituting the simplified equation (2.25)into (2.23) yields a matrix equation defining the changes in the pressure field required to drive D_1 towards zero, in the form

$$\bar{B}\, d\bar{P} = -\bar{D}_1 \tag{2.26}$$

This is a Poisson equation and relates the pressure correction required at each node to reduce the mass flux imbalances existing between nodes. Once this is solved for the pressure matrix, equation 2.25 is used to correct all velocities.

In summary, the procedure is to obtain first estimates of each velocity component from equations 2.19, assemble the divergence vector D from 2.24, and obtain a pressure field from equation 2.26, then correct all velocities from equation 2.25.

2.2.4 The Viscous Stress Terms

To this point only the solution of the conservation equations have been discussed. The viscous stress terms have been presented in Table 2.2 in variable viscosity format to allow for the possibility of incorporating the modelling of turbulent flows using the Boussinesq(1877) or effective viscosity concept. Note that the laminar form of the stress terms is usually quoted in fluid dynamics texts in a shortened form which takes advantage of the constant viscosity and density.

$$\frac{\partial}{\partial x_j}\left[\mu\left(\frac{\partial u_i}{\partial x_j}+\frac{\partial u_j}{\partial x_i}\right)\right]=\mu\frac{\partial^2 u_i}{\partial x_j\cdot\partial x_j} \qquad (2.27)$$

as

$$\frac{\partial}{\partial x_j}\left(\frac{\partial u_j}{\partial x_i}\right)=\frac{\partial}{\partial x_i}\left(\frac{\partial u_j}{\partial x_j}\right)=0 \qquad (2.28)$$

The use of the simplified stress terms in (2.27) is slightly more economical than using the unsimplified form for laminar flow, so during the extension of FAITH to cylindrical and toroidal coordinates, the strictly laminar and additional turbulent terms were identified separately as

$\frac{\partial}{\partial x_j}\left(\mu\frac{\partial u_i}{\partial x_j}\right)$ and $\frac{\partial}{\partial x_j}\left(\mu\frac{\partial u_j}{\partial x_i}\right)$ respectively.

However, (2.28) is true only for constant density flow, so to maintain generality these terms are always evaluated.

Finally it is convenient to introduce the stress vector:

$$\tau_{ij} = \mu\left(\frac{\partial u_i}{\partial x_j} + \frac{\partial u_j}{\partial x_i}\right), \tag{2.29}$$

thus, equation 2.11 becomes for $\alpha = 1$:

$$\rho u_i \frac{\partial u_j}{\partial x_j} + \frac{\partial P}{\partial x_i} = \frac{\partial}{\partial x_j}(\tau_{ij}) + S_i \tag{2.30}$$

2.2.5 Effective Turbulent Viscosity

Turbulent mixing is responsible for the large resistance encountered by flow at Reynolds numbers above a critical value. In one dimension, the effect of turbulent flow is incorporated by using a larger friction factor determined classically from the Moody(1944) diagram. In multidimensional analysis, it is clear that an overall friction factor is unsatisfactory and that an approach which both models turbulent mixing and local resistance close to the walls is required.

This is commonly done by recognizing that flow variables in turbulent flow are not constant but can be regarded as having a fluctuating component and a time averaged component .

$$\phi = \bar{\phi} + \phi' \qquad (2.31)$$

Full development may be found in classic texts such as Schlichting (1979). Equation 2.31 can be used to generate the fluctuating components of both scalars and tensors which are then substituted in the conservation equations. For the continuity equation

$$\frac{\partial}{\partial x_j}(\rho\bar{u}_j) + \frac{\partial}{\partial x_j}(\rho u_j') = 0 \qquad (2.32)$$

and as the first term is zero, the second must be.

Noting $\bar{\phi}' = 0$ by definition, inserting (2.30) and (2.31) into equation 2.11, time averaging all resulting terms, and simplifying yields

$$\rho u_i \frac{\partial \bar{u}_j}{\partial x_j} + \frac{\partial \bar{P}}{\partial x_i} - \frac{\partial}{\partial x_j} \left(\overline{\tau_{ij}} + \overline{\tau_{ij}'} \right) + S_i = 0 \tag{2.33}$$

The only additional term which now appears represents the time averaged fluctuating stress. The derivation shows that the components of this term are

$$\bar{\tau}_{ij}' = \rho \overline{u_i' u_j'} \tag{2.34}$$

and are usually called the Reynolds stress terms.

A number of different ways of modelling the Reynolds stresses have been proposed, see for example Lumley (1983), however, the most common is the use of the Boussinesq concept , in which these stresses are modelled by analogy to laminar stresses such that

$$\bar{\tau}_{ij}' = -\rho \overline{u' v'} = \mu_T \frac{\partial \bar{u}_i}{\partial x_j} \tag{2.35}$$

in analogy to

$$\overline{\tau_{ij}} = \mu_L \frac{\partial \bar{u}_i}{\partial x_j} \tag{2.36}$$

hence equation 2.33 becomes

$$\rho \bar{u}_i \frac{\partial \bar{U}_j}{\partial x_j} + \frac{\partial \bar{P}}{\partial x_i} = \frac{\partial}{\partial x_i} \mu_E \frac{\partial \bar{U}_i}{\partial x_j} + S_i \tag{2.37}$$

where $\mu_E = \mu_T + \mu_L$. As the average notation applies to all the variables, it's use is now discontinued for simplicity, but it is to be understood to be in effect.

2.2.6 Mixing Length Models

One of the simplest concepts of accounting for turbulence is the mixing length concept introduced by Prandtl (1925). This is discussed at some length in Schlichting(1979), and reduces to an expression for the turbulent stresses which relates turbulent viscosity in (2.35) to the geometry by means of a length scale ι.

$$\mu_T = \rho \iota^2 \left| \frac{du}{dx} \right| \tag{2.38}$$

Various enhancements to the theory are discussed by Schlichting(1979), as are methods of deriving expressions for the length scale which agree with accepted velocity profiles for limiting cases. However, no universal formulae have been agreed upon, and differential methods have a more general applicability. Among these the k-ε model of turbulence is now believed fairly generally applicable.

2.2.7 The k-ε Turbulence Model

The k-ε turbulence model was suggested by Harlow and Nakayama (1967), and is in widespread use following a detailed account of the model published by Launder and Spalding (1974).

In the model, the turbulent viscosity is assumed isotropic, and is related to the turbulent kinetic energy k and its rate of dissipation ε, through the equation

$$\mu_T = \rho C_\mu \, k^2/\varepsilon \tag{2.39}$$

The partial differential equations governing the transport of k and ε can be derived from the general transport equation in the form of equation (2.12) by using (2.30) and the same approach used to derive (2.32) and (2.33), except that rather more approximations are involved ,in that simplified models of several terms are introduced, Launder and Spalding(1974). For a derivation in tensor notation see for example Bradshaw, et al (1981).

The resulting equations are

$$\frac{\partial}{\partial x_j}\{ k\rho U_j\} = \frac{\partial}{\partial x_j} (\Gamma_k \frac{\partial k}{\partial x_j}) + G - \rho\varepsilon \tag{2.40}$$

$$\frac{\partial}{\partial x_j}\{ \varepsilon\rho U_j\} = \frac{\partial}{\partial x_j}(\Gamma_\varepsilon \frac{\partial \varepsilon}{\partial x_j}) + C_1 \frac{\varepsilon}{k} G - C_2\rho \frac{\varepsilon^2}{k} \tag{2.41}$$

where

$$\Gamma_k = \mu_T/\sigma_k, \ \Gamma_\varepsilon = \mu_T/\sigma_\varepsilon \tag{2.42}$$

and σ_k, σ_ε are effective Prandtl-Schmidt numbers, taken usually as constant.

Although various values for the constants have been recommended Bradshaw et. al.(1981), the usual values are, Gosman et.al.(1979)

$$[C_\mu, C_1, C_2, \sigma_k, \sigma_\varepsilon] = [0.09, 1.55, 2.00, 1.0, 1.3] \tag{2.43}$$

and the generation term G is

$$G = \tau_{ij} \frac{\partial u_i}{\partial x_j} \tag{2.44}$$

As the turbulence equations 2.40 and 2.41 are in standard form, they may be assembled and solved by the method discussed in 2.2.2.

2.2.9 Boundary Conditions

The imposition of boundary conditions is obviously also critical. For laminar flows, boundary conditions take one of the forms $\phi = c$, $\partial\phi/\partial x = c$.

For variables in the inlet plane, it is possible to specify $\phi = \phi(x,y)$.

Boundary conditions are:

at	$\theta=0,\pi$	$u=0$, $\partial v/\partial\theta=\partial w/\partial\theta=0$
at	$r=d/2$	$u=v=w=0$
at	$r=0$	$v=v_c\cos\theta$, $u=v_c\sin\theta$, $v_c= .5(v_{1,1,k}-v_{1,NJ,k})$
		$\partial w/\partial r=0$

The boundary condition at $r=0$ attempts to minimise errors by recognising that a unique velocity v_c exists at the centre, Austin(1970), Soh and Berger(1984).

For turbulent flows it is necessary to ensure that regions in the neighborhood of walls follow the law of the wall, Launder and Spalding(1974). As the actual implementation of boundary conditions within the program depend on the manner in which the grids and the variable arrays are stored, detailed discussion is left to Appendix A.

2.3. SOLUTION OF THE TWO-FLUID EQUATIONS

2.3.1 Previous Work

Prior to embarking on any development, the computer algorithms proposed for multidimensional two-fluid flow were reviewed in detail in the hope that an existing computer code could be used or an existing algorithm could be implemented. Schemes for multidimensional two-fluid analyses have evolved from the same roots as the one-fluid analyses, and two main families remain evident, those based on ICE, Harlow and Amsden(1971), and those based in SIMPLE, Patankar and Spalding(1972). It became clear on reviewing these that because of the increased degree of freedom available in setting up a two-fluid flow algorithm, the possibilities are more diverse, and the probability of developing a completely consistent scheme is more remote. In particular, it was discovered that the treatment of the pressure and the formulation of the pressure equation was even more critical than for single-fluid flow, Carver(1981). The review included the computer codes KFIX, Rivard and Torrey(1978), KACHINA, Amsden and Harlow(1978), KTIF, Amsden and Harlow(1977) all of which are extensions of ICE; the IPSA algorithms, Spalding et al(1979), Spalding(1980) and an algorithm discussed in detail by Shah, et al (1979). The KFIX code was obtained from the Argonne code centre and tested, but in all tests except the example problems it failed to converge.

This study revealed two common failings. The first was that the treatment of the pressure equation was inconsistent and therefore, was not conducive to maintaining continuity in each fluid. The second was that none of the codes had been shown to reproduce experimental results. The decision was therefore made to develop an algorithm which treated each fluid consistently, thus maintaining conservation of each, to implement this algorithm in a computer program, verify this using parameter studies, and to validate predictions of the code using available experimental data on phase distribution under the influence of gravitational and centrifugal forces which would tend to cause separation.

2.3.2 The Algorithm of Shah, et al.

The algorithm of Shah, et al.(1979) was first reviewed, as this was reported in detail. In this algorithm, the momentum equations are solved individually as for the single-fluid case, and the continuity equations are used to generate a mass imbalance for each fluid, thus, there is an equation (2.21) for each fluid ι, and summing these gives

$$\sum_{\iota=1}^{2} \sum_{i} [(\alpha\rho\mu A)_{i+} - (\alpha\rho\mu A)_{i-}]_{\iota} = D_1 + D_2 \tag{2.45}$$

Using similar arguments to the single-fluid case, equations (2.20), (2.24) and (2.25) can be combined to produce a pressure equation similar to (2.26) but based on (2.45) instead of (2.21).

$$(\bar{B}_1 + \bar{B}_2)\, d\bar{P} = \overline{D_1} + \overline{D_2} \tag{2.46}$$

The authors then state that the pressure correction from (2.46) will not precisely satisfy continuity because of non-linearities, so the volume fraction profile can be computed by solving one of the continuity equations (2.21) with $D_\iota = 0$. The entire sequence must then be iterated.
Because 3D calculations are expensive, exploratory calculations were first attempted in 2D.

In order to test the Shah algorithm in detail, an existing single-fluid two dimensional computer program, a version of TEACH Gosman, and Pun(1974), obtained from the University of Ottawa, Salcudean and Abdelrehim(1980), was extended to provide a two-fluid solution for air-water flow using this algorithm. This program was referred to as TOFFEA for Two-Fluid Flow Equation analysis. Initially, however, convergence was extremely poor. Further study revealed that the lighter fluid was poorly conserved. This is because equation (2.45) imposes a pressure correction based on $D_1 + D_2 = 0$. In the case of $\rho_1 >> \rho_2$, as in air and water, the mass flux imbalance of the light fluid will hardly influence the pressure computation at all and it will not be conserved.

2.3.3 Extensions of the ICE Technique

The algorithms in the codes KFIX, Rivard and Torrey(1978), KACHINA, Amsden and Harlow(1978), KTIF, Amsden and Harlow(1977) and IPSA, Spalding(1979,1980) were then reviewed, and similar inconsistencies were detected. The three codes use the IMF (Implicit Multi-Field) Technique, an extension of ICE, and address the cases respectively of one fluid, both and neither fluid being compressible. Although the equations in ICE appear at first glance to be formulated in a quite different manner to SIMPLE, in fact the method shares several features with SIMPLE, including the staggered grid, and an iteration of the the momentum equations which minimises continuity imbalance by means of a pressure correction.

In KFIX, both fluids are regarded as compressible, and the iteration is based on reducing D_1 for $\alpha_1 \geq 0.5$, otherwise the iteration is based on D_2. In KACHINA the iteration is based on the continuity imbalance of the compressible fluid. KTIF bases the pressure iteration on the imbalance of the sum of the volume fractions, $\alpha_1+\alpha_2-1$.

In all three codes the pressure change is based on an analytical expression for dD/dP. This is most comprehensive in KFIX, where both compressibility and interphase drag are incorporated in this derivative. In spite of this implicit coupling, convergence was found to be very slow. This may be due to the use of Jacobi point iteration instead of the TDMA line iteration used in SIMPLE, and also due to the possibility of an inconsistency arising when void fraction changes through the logic transition at $\alpha=0.5$.

2.3.4 The IPSA Algorithm

The original IPSA algorithm Spalding(1979) was based on the imbalance of volume fractions, and α_1, α_2 were computed separately from each continuity equation (2.21) with $D_i=0$

$$D_\alpha = 1 - (\alpha_1 + \alpha_2) \tag{2.47}$$

Clearly a change in each α is required to drive D_α to zero. The required changes were obtained by formulating (2.21) in the upwind sense using $m=\rho UA$ and I and O for flow into and out of control volume i.

$$\alpha_i \sum_O m_O - \sum_I (\alpha m)_I = 0 \tag{2.48}$$

Hence, neglecting changes in neighbouring α:

$$d\alpha_i = \frac{\sum_I \alpha dm_I - \alpha_i \sum_O dm_O}{\sum_O dm_O} \tag{2.49}$$

dm is obtained from equation (2.25) as before.

Hence, the equation for the pressure correction matrix can be assembled.

$$d\overline{\alpha_1} + d\overline{\alpha_2} = (\bar{B}_{1\alpha}+\bar{B}_{2\alpha})d\bar{P} = -\bar{D}_\alpha \qquad (2.50)$$

This algorithm attempts to simulate more directly the affect of pressure on volume fraction distribution and is thus slightly more implicit than the Shah formulation. However, each equation (2.49) has no information on the variation of the other fluid, and as noted by Carver(1981), the lighter fluid will be changed disproportionately through equation (2.25), and both volume fractions will change in the same direction, an effect which will not always be logical.

2.3.5 The TOFFEA Pressure Correction and Implicit Void Fraction Algorithm

In order to cure the convergence problems inherent in all the above algorithms, a procedure which would treat both fluids consistently was sought. This procedure was developed and reported in Carver(1981). The neglect of the light fluid conservation in equations (2.45) and (2.46) was due to the disparity in densities. This problem was circumvented by normalizing each continuity equation (2.45) by the reference density ρ_0 to give a volumetric conservation equation.

$$\sum_{\iota=1}^{2} \sum_{i} [(\alpha u A \gamma)_{i+} - (\alpha u A \gamma)_{i-}]_\iota = D_1' + D_2' \qquad (2.51)$$

where $\gamma_\iota = \rho_\iota/\rho_{0\iota}$, $D_\iota' = D_\iota/\rho_{0\iota}$.

In this case as $\gamma_\iota \simeq 1$, the phases and their contributions D' to the pressure equation are equally weighted, and a pressure field that imposes continuity in each is computed.

This equation was implemented and tested in the 2D two-fluid TOFFEA code. Further tests showed that while the volumetric pressure equation improved conservation, the rate of convergence was still slow when the continuity equation (2.21) for one fluid was used to solve for the volume fraction α_ι, $\iota=2$. The reason for this was identified as the absence of information about fluid 1 in (2.21).

As two linearized continuity equations are to be solved, any linear combination will yield solutions. The sum of volumetric continuity equations was used to derive a pressure equation implicit in both fluids. The equations used to compute volume fraction must also be implicit in both fluids for efficient convergence. The continuity equations (2.21) may be normalized as before, and then subtracted. Noting $\alpha_1 = 1 - \alpha_2$, requiring $D_1 - D_2 = 0$, and using Q for volumetric flux uA. This yields

$$\sum_i [\alpha_1(Q_1 + Q_2)_{i+} - \alpha_1(Q_1 + Q_2)_{i-}] = (Q_{i+} - Q_{i-})_2 \qquad (2.52)$$

This is a further linear matrix equation implicit in both fluids, and defining the pressure field necessary to drive $D_1' - D_2'$ to zero. Hence, the combination of (2.51) and (2.52) drives both $D_1' + D_2'$ and $D_1' - D_2'$, so D_1' and D_2' are also individually driven to zero.

The combination of the volumetric pressure equation (2.45) and the implicit volume fraction equation (2.52) in the 2 fluid extension of the 2D TEACH code was designated TOFFEA for Two Fluid Flow Equation Analysis and is documented in Carver(1983,1984). The two-dimensional equations may be extracted readily from table 2.1 following note (v).

2.3.6 An Implicit Version of IPSA

Later versions of IPSA used in PHEONICS, Spalding(1980), contain a more implicit formulation. This is developed by solving equation (2.48) for α_1, its equivalent for α_2, and using the resulting expression to replace $\sum\limits_{o} m$ in (2.48).

$$\alpha_1 = \frac{\sum\limits_{I} \alpha_1 m_1 \sum\limits_{o} m_2}{\sum\limits_{I} \alpha_1 m_1 \sum\limits_{o} m_2 + \sum\limits_{I} \alpha_2 m_2 \sum\limits_{o} m_1} \tag{2.53}$$

As noted in Carver(1981), differentiating this gives

$$\begin{aligned} d\alpha_1 = \; & (\sum_{I} \alpha_1 m_1 \sum_{o} dm_2 + \sum_{I} \alpha_1 dm_1 \sum_{o} m_2)\, \alpha_1 \\ & -(\sum_{I} \alpha_2 m_2 \sum_{o} dm_1 + \sum_{I} \alpha_2 dm_2 \sum_{o} m_1)\, \alpha_2 \\ & /(\sum_{I} \alpha_1 m_1 \sum_{o} m_2 + \sum_{I} \alpha_2 m_2 \sum_{o} m_1) \end{aligned} \tag{2.54}$$

Clearly, now α_1 responds correctly to changes in inlet and outlet flows of of each fluid, so the fluids are now implicitly coupled. Equally clearly however, equation (2.54) is cumbersome to handle, and its complexity could easily lead to errors in programming.

It is instructive to check the response of equation (2.52) to pressure change. First, we put it in upwind form.

$$\alpha_1 \sum_{O} (Q_1 + Q_2) - \sum_{I} \alpha_1 (Q_1 + Q_2) = (Q_O - Q_I)_2 \tag{2.55}$$

thence

$$d\alpha_1 = \frac{\sum_{I} \alpha_1 (dQ_1 + dQ_2) + \sum_{O} dQ_2 - \sum_{I} dQ_2 - \alpha_1 \sum_{O} (dQ_1 + dQ_2)}{\sum_{O} (Q_1 + Q_2)} \tag{2.56}$$

This equation also responds correctly to changes in incoming and outgoing flow for each fluid and is considerably less cumbersome than (2.54). Hence, the equations (2.45) and (2.52) are superior to the original IPSA algorithm, and produce the same characteristics as the later IPSA algorithm in a more straightforward fashion. They also have a further advantage over IPSA which will be discussed in section 2.3.8.

2.3.7 Two Dimensional Two-Fluid Convergence Studies

Convergence of the various algorithms was tested by investigating separation of fluids due to centrifugal force in an ideal two-dimensional large radius elbow. The TOFFEA code was extended to solve the conservation equations in polar coordinates for this problem. Various velocities and density ratios were used and various constant values were used for interphase drag.

Converged results were obtained for flows at low Reynolds number and low density ratios using either the Shah scheme of chapter 2.3.2 or the IPSA scheme of chapter 2.3.6. However, for density ratios exceeding 10 these schemes failed to converge, and only the new TOFFEA scheme converged for all density ratios except for conditions which caused complete separation. A modification was developed to successfully address the case of full separation, and is discussed below. Typical computed distributions of mass flow and volume profile, and parametric studies showing the effect on void distribution of inlet velocity and interphase drag constant are given in chapter 3.

2.3.8 Limiting Intermediate Values of Void Fraction

As noted in the previous chapter, the TOFFEA algorithm of volumetric pressure equation and implicit volume fraction equation was by far the most successful scheme tested; however, it broke down under conditions causing complete separation of the fluids. Further study revealed that equation (2.52) would occasionally generate values of α which violated the constraint $\alpha\varepsilon(0,1)$. If the solution returns illegal values, integrity of the iteration process is damaged and conservation can no longer be sustained. It is not sufficient merely to correct stray values back into range subsequent to calculation as (2.52) is a matrix equation, and the remaining values which would be affected by such a correction cannot be adjusted appropriately to reflect the correction. Instead, a means of imposing the bounds implicitly within the matrix calculation is required.

A method was developed, and published as A Method of Limiting Intermediate Values of Volume Fraction in Iterative Two-Fluid Computations in the Journal of Mechanical Engineering Science, Carver(1982).

The positivity constraint is imposed by following Patankar(1970). Equation (2.16) is rewritten

$$A_p\phi_p = \sum_n A_n\phi_n + S_p\phi_p + S_c \qquad (2.57)$$

or

$$(A_p - S_p)\,\phi_p = \sum_n A_n\phi_n + S_c \tag{2.58}$$

The constraint for positivity is that both $-S_p$ and S_c remain positive. Thus, if the source term S_c has a positive component S_1, and a negative component S_2, ($S_c = S_1 - S_2$, $S_1 \geq 0$, $S_2 > 0$), then equation (2.58) is used with $S_c = S_1$ and $S_p = S_p - S_2/\phi_p^0$ where ϕ_p^0 is the previous value of ϕ_p. Thus the new ϕ_p will be computed positive, provided only that ϕ_p^0 is positive. Patankar also suggests a means of ensuring that $\phi_p \leq 1$. Unfortunately, this applies only to equations in which the source term is dominant. His method is to monitor ϕ_p^0 when a particular ϕ_p^0 approaches unity, to write $S_c = S_p = S/(1-\phi_p^0)$, which will return $\phi_p = 1$ providing the source terms are dominant. However, this is not the case in the two-fluid volume fraction equation (2.52). A method based on under-relaxation was developed and this proved satisfactory.

The standard under-relaxation procedure is as follows. In order to promote stability, a certain proportion of the original value is retained in the solution. Instead of solving (2.57) directly, to produce ϕ_p^c, one prefers to compute a relaxed value

$$\phi_p^r = \beta\phi_p^c + (1-\beta)\phi_p^o, \ \beta\varepsilon(0,1). \tag{54}$$

Relaxation may be imposed after the solution but again this is a post correction and may detract from the integrity of the matrix solution. It is preferable to pre-relax, making the relaxation implicit in the matrix solution. Equation (2.57) is thus rewritten in terms of ϕ_p^r and ϕ_p^0 by substituting equation (2.59) for ϕ_p^c

$$A_p' \phi_p^r = \sum_n A_n \phi_n + S'$$

$$A_p' = A_p/\beta, \quad S' = S-(1-\beta)A_p' \phi_p^0 \tag{2.60}$$

The new procedure, developed to sustain the upper constraint, is to again monitor current values of ϕ_p^0, but to approach unity by means of under-relaxation. Equation 2.57 is first solved in point Jacobi form

$$\phi_p = (\Sigma a_n \phi_n + S)/A_p \tag{2.61}$$

Although (2.57) is to be solved in matrix form, the point form (2.61) will give a good prediction of the matrix solution. Thus, if $\phi_p' > (1-\varepsilon)$, individual point relaxation is applied in the form $\beta = \max\,(1-\phi_p^0, \gamma)$. The parameters ε and γ are arbitrary and small, values of 0.05 and 10^{-5} have proved satisfactory. Equation (2.57) is solved in matrix form of (2.60) with individually assigned relaxation parameters.

The method permits the void calculation to proceed smoothly toward unity or depart smoothly from unity if necessary, meanwhile ensuring that continuity is maintained throughout. This algorithm does not require the source terms to be dominant or even significant, and does not conflict in any way with the lower bound constraint.

Finally, it is of interest to note that it is very difficult to impose similar and upper and lower bound constraints to the IPSA algorithm of section 2.3.6. This would require doubly constraining $d\phi$ such that $(\phi+d\phi)\varepsilon(0,1)$ and would therefore be a much more complicated procedure. The decision was therefore made not to continue investigation of IPSA, but to concentrate on the TOFFEA algorithm with implicit constraints on α.

CHAPTER 3. TWO-DIMENSIONAL PROOF OF CONCEPT STUDIES

Flow of fluids in elbows is known to be three dimensional in nature, similarily, although single phase flow through obstructions such as orifice plates in pipes can be regarded as axi-symmetric, two-phase flow in a horizontal pipe is clearly three-dimensional.

However, three-dimensional computation is too detailed and expensive,for use in proof of concept studies, so in order to investigate the characteristics of various numerical schemes, and to verify whether the two fluid model had the propensity to duplicate experimentally observed trends, a number of exploratory studies were completed using the two dimensional code TOFFEA, and are discussed in this chapter.

3.1 Parametric Studies

In order to verify that the new algorithm was working consistently, a number of parametric studies were completed. In these studies, various density ratios were used and no attempt was made to model any experiment; the intent was to demonstrate that the computed results would reproduce known experimental trends. As mentioned in chapter 2, early parametric studies were done using several of the published algorithms. Converged results were obtained only for flows with low density ratios. However for high density ratios, or for any condition promoting pronounced separation, convergence problems occurred in all the methods tested. This led to the development of the Toffea scheme which was outlined in chapter 2 and in a paper published in Advances in Numerical Solution of Partial Differential Equations (Carver 1982).

The new method was used to simulate phase distribution in straight horizontal pipes and in elbows in the horizontal and vertical plane.

3.1.1 Two Fluid Flow in a Horizontal Duct

In a horizontal straight duct the tendency towards separation is entirely due to the gravity term in the momentum equations. Assuming an initial uniform distribution, the v momentum equations for a straight rectangular duct simplify to

$$0 = -\alpha_1 \frac{\partial p}{\partial y} + \psi\,(v_g - v_1) - \alpha_1 \rho_1 g \tag{3.1}$$

$$0 = -\alpha_g \frac{\partial p}{\partial y} + \psi\,(v_1 - v_g) - \alpha_g \rho_g g \tag{3.2}$$

Adding gives the initial static pressure gradient

$$\frac{\partial p}{\partial y} = -\,(\alpha_1 \rho_1 + \alpha_g \rho_g) g = -\,\tilde{\rho} g \tag{3.3}$$

Whereas normalizing by α and subtracting, shows that the initial force promoting a separative velocity is proportional to density difference.

$$(v_g - v_1) = \alpha_1 \alpha_g\,(\rho_1 - \rho_g) g/\psi \tag{3.4}$$

Clearly the light fluid will rise, and this separation tendency increases with density difference, and decreases with interphase drag. These terms will dominate the computation although their relationship becomes more complex, once conditions depart from uniformity and the terms neglected become significant.

A number of exploratory parametric studies were performed to confirm that the solution method would exhibit the appropriate trends.

In these studies, only molecular viscosity was used, no attempt was made to model turbulence by means of effective viscosity, and no artificially high viscosities were used to stabilize the computation. The interphase drag function was implemented as a constant multiple of relative velocity between phases, thus drag will increase with both velocity magnitude, and relative velocity.

Typical results are illustrated in Figure 3.1, which shows vector plots of the velocity field of the heavier phase for four uniform inlet velocities, namely 0,1,10,100 units, with a drag function ψ=1, and a uniform initial value of volume fraction of 0.5 and a density ratio of 100. In order to promote convergence, all values were initialized to entry values, hence the w=0 case simulates a settling problem. Vectors are shown in this case, as although the computed velocities are effectively zero, they have direction. The settling case Figure 3.1a, is quite a rigourous test of the numerical procedure, as it yields full separation. The remaining cases show decreasing amounts of separation with increasing velocity.

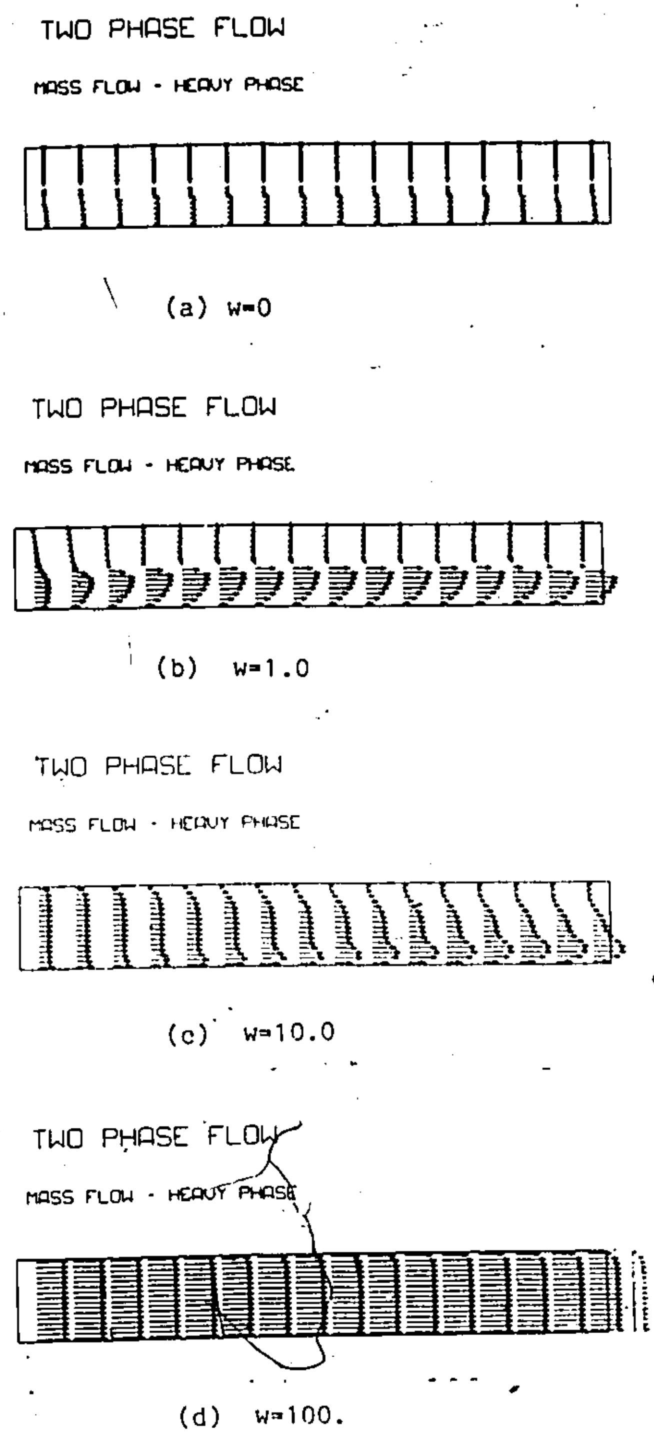

Fig. 3.1 Computed Mass Flux Profiles for Two-Fluid Flow in a Horizontal Duct for Various Velocities. The fluids enter uniformly mixed, α=0.5. (2-D test Calculation)

3.1.2 Two Fluid Flow in Radial Elbows

The situation for radial elbows is more complex, as in the general case there are two forces which may promote separating, the gravitational force and the centrifugal force. Their influence on separation tendencies may be obtained, as in the previous section, by subtracting the v equations for an initially uniform distribution to give the initial relative velocity

$$(v_g - v_1) = \alpha_1 \alpha_g (\rho_1 - \rho_g) (g_y - \frac{\tilde{w}^2}{R}) \tag{3.5}$$

For simplicity, the above assumed $w_1 \sim w_2 \sim \tilde{w}$, and used $g_y = g\sin\phi$, $\theta=0$. In this case it is clear that for a bend in the horizontal plane in the absence of the gravity term, the heavy fluid will always be driven to the outside of the bend, and the separation rate will be proportional to $w^2/_R$. For a bend in the vertical plane, this separation tendency may be increased or decreased by gravity depending on the angular position ϕ. For $\phi=0,180^0$ gravity has no effect, for $\phi=90^0$ gravity counteracts the centrifugal force, and for $\phi=270$, it augments the centrifugal force. These relative effects may be expressed by means of a modified Froude number.

$$Fr = w^2/Rg\sin\phi \tag{3.6}$$

If Fr exceeds unity, centrifugal forces will dominate, otherwise gravity will dominate.

Several parametric studies were completed for elbows in a horizontal plane, to separately examine the effects of radius, velocity and interfacial drag. The effect of gravity was studied subsequently. Figure 3.2 shows mass flux profiles for three inlet velocities for a given radius R. Note that separation clearly increases with w. Figure 3.3 shows that increasing the bend radius decreases separation. Finally, Figure 3.4 shows the effect on the distribution of the heavy phase of three values of inlet velocity, and three values of interphase drag.

A case of special interest is the settling problem (w=0) in a vertical elbow. This turns out to be a far more severe test than settling in a straight duct, as circulation currents must be established during the calculation to permit the fluids to migrate. This case would converge only with considerable relaxation using the SIMPLE based procedure, but converged quite readily using SIMPLER. (See chapter 4 for these procedures).

3.1.3 Discussion of Parametric Studies

These studies were intended to demonstrate that the computational algorithm would produce the appropriate trends and would converge satisfactorily while doing so. Once the method of incorporating the bounding constraints on the volume fraction discussed in chapter 2.3.7 were implemented, no problems were encountered with convergence. The computed trends were correct.

Attention was then turned to modelling experiments in which phase distribution effects had been measured.

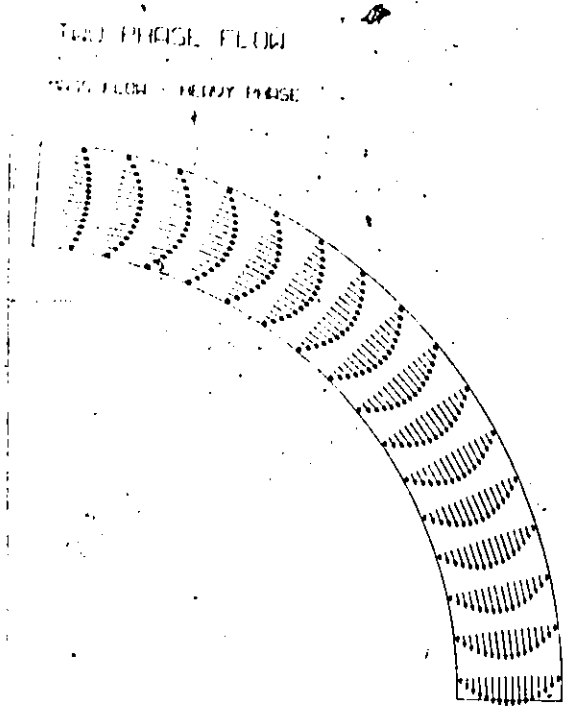

(a) w = 0.1

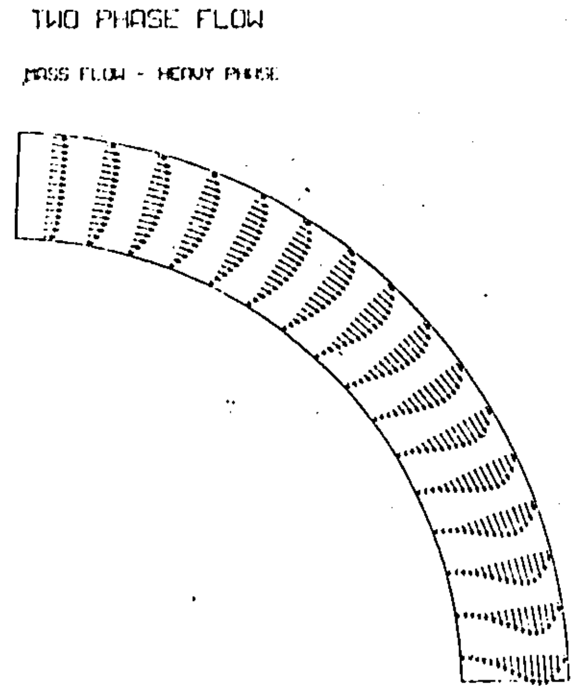

(b) w=1.0

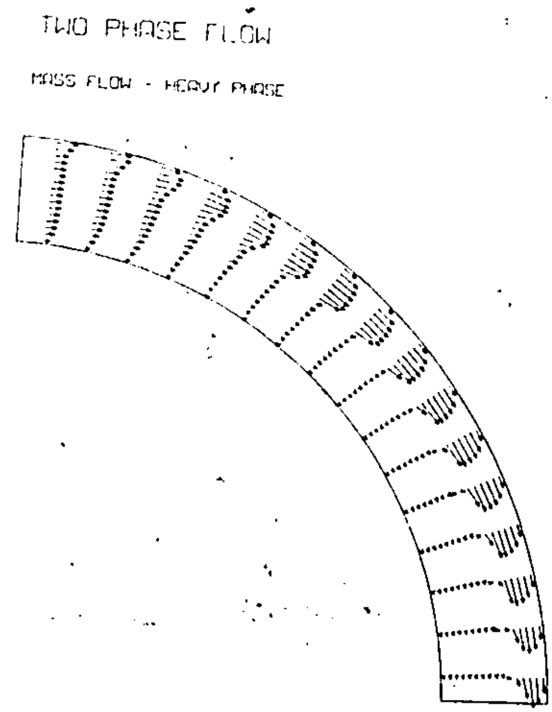

(c) w=10.0

Fig. 3.2 Computed Mass Flux Profiles for Two-Fluid Flow in a Horizontal Radial Elbow: Effect of Velocity. The fluids enter uniformly mixed, α=0.5. (2-D test Calculation)

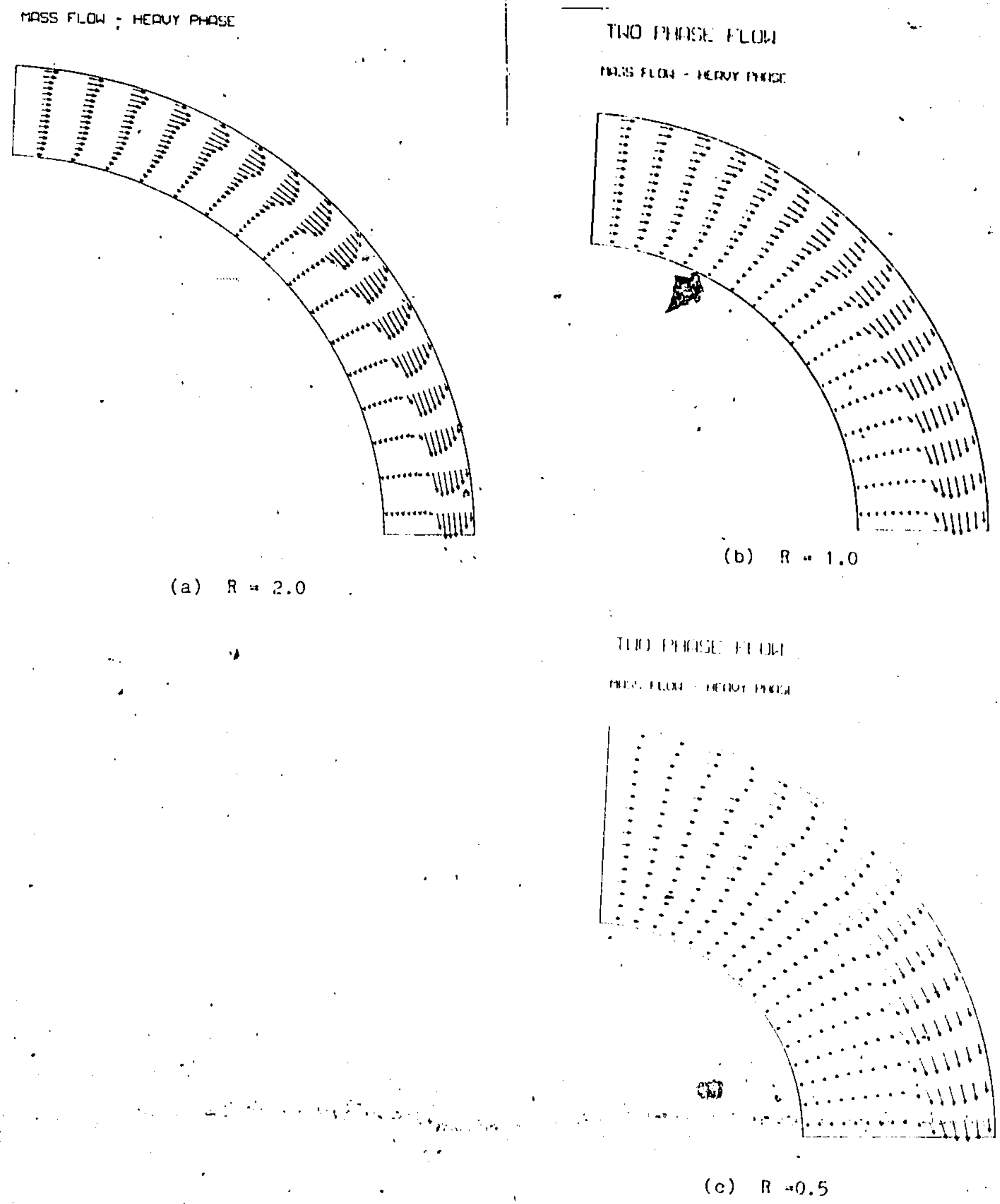

Fig. 3.3 Computed Mass Flux Profiles for Two-Fluid Flow in a Horizontal Radial Elbow: Effect of Bend Radius The fluids enter uniformly mixed, α=0.5. w=1.0 (2-D test Calculation)

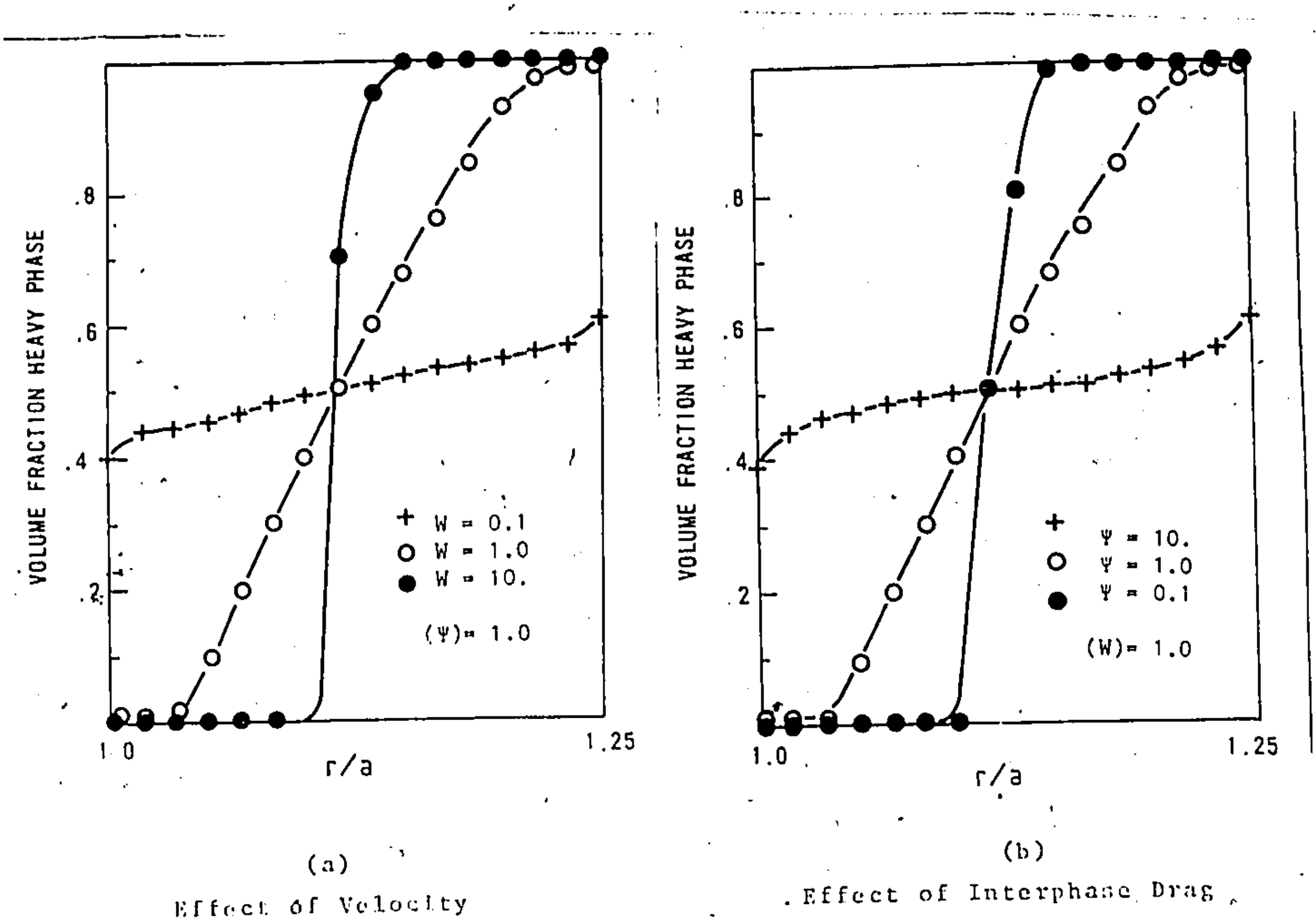

Fig. 3.4 Computed Volume Fraction Profiles in the Exit Plane
for Two-Fluid Flow in a Horizontal Radial Elbow:
The fluids enter uniformly mixed, α=0.5.
Effect of Velocity and Interphase Drag
(2-D test Calculation)

3.2 Two Dimensional Simulation of Flow Around Bends

As the parametric studies illustrate that the numerical procedure performed adequately, the predictions of the two dimensional code were then compared with experiments in bends. This comparison can be regarded only as preliminary, as the flow in bends is known to be three dimensional in nature; single phase flow is known to set up secondary flows rotating in the cross-sectional plane.

3.2.1 The Experiments of Gardner and Neller

Gardner and Neller (1979) measured distribution of air and water in elbows, giving void fraction profiles at several stations in the bend. In the experiments, the rig consisted of a vertical of 6 mm ID pipe followed by a 90^0 elbow and then by a horizontal pipe as shown in Figure 3.5. Measurements were taken at stations A through G. This is a particularly interesting problem to analyse, as the effect of gravity appears first axially, then in opposition to the centrifugal force, then finally perpendicular to the axis.

The experimenters reported that phase distribution was substantially symmetric and fairly uniform in the plane normal to the bend. Thus a two dimensional analysis can be expected to capture the relevant trends in the plane of the bend. The intent of performing comparisons with this experiment was to demonstrate in two dimensions that the two fluid code was capable of simulating experimental trends before launching a more expensive three dimensional simulation.

Gardner and Neller actually used two different bend radii, however only one radius was used in this preliminary comparison. Further comparisons with both radii were made subsequently with the three dimensional program. These are discussed in chapter 5 together with a number of other bend experiments.

Before attempting comparison however it was necessary to replace the constant values for interphase drag used in the parametric studies, with a more realistic model.

3.2.2 Preliminary Interphase Drag Model

A detailed model of interphase drag, and also of effective viscosity due to turbulence is considered later in chapter 5. For these preliminary studies the interphase drag formulation for bubbly flow is taken following a recommendation given in a recent survey by Lahey (1979).

interphase drag $\quad \Psi_{lg} V_r = 3/8\ C_d\ \alpha\ \rho_l\ |V_r| V_r / r_b$ (3.7)

coefficient $\quad C_d = 6.3\ Re_b^{(-.385)}$ (3.8)

bubble Reynolds no. $\quad Re_b = (\rho/\mu)_l\ V_r d_b$ (3.9)

bubble diameter $\quad d_b = .003$ (3.10)

bubble concentration $\quad = 3\alpha/4\pi r_b^3$ (3.11)

These formulae, and appropriate extensions will be discussed in more detail in chapter 5.

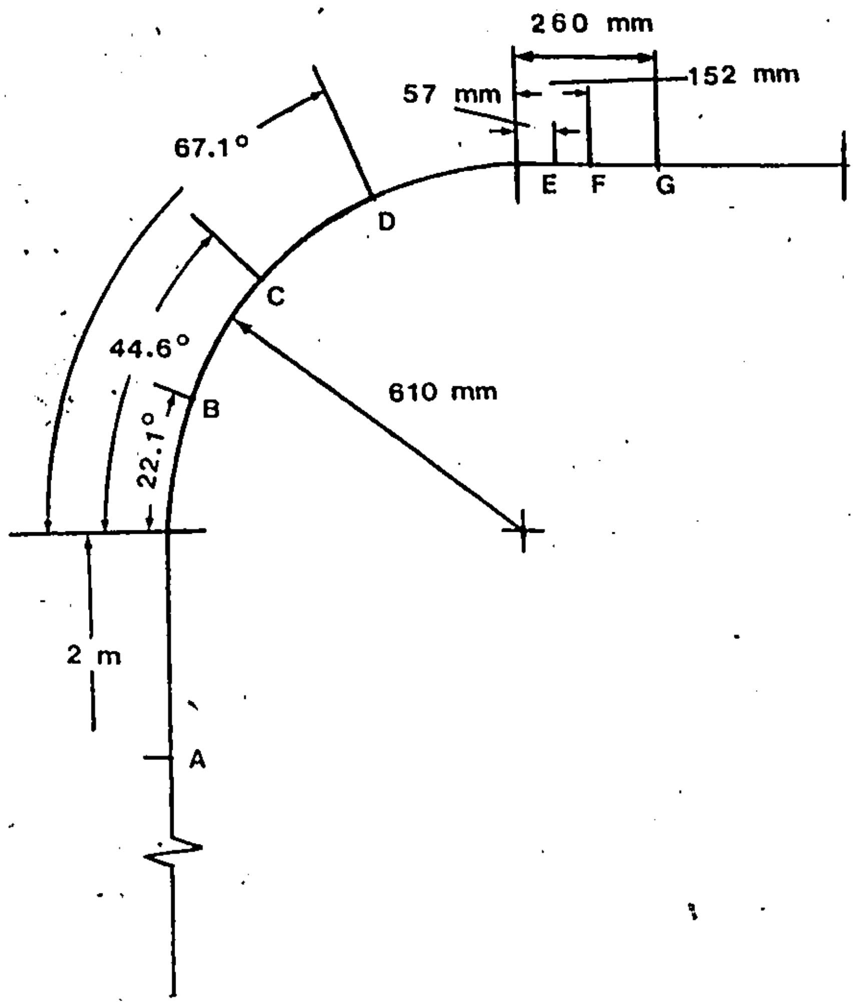

Fig. 3.5 Geometrical Specifications for Bend Experiments of Gardner and Neller (1979)

3.2.3 Comparisons with Gardner and Neller

Typical volume fraction profiles computed by the code are shown in Figure 3.6. In the riser, the air does not change much from the imposed distribution. In the bend the centrifugal force drives the water outward, displacing the air inward, until the increasing influence of gravity starts to reverse this trend. Finally in the horizontal pipe, the distribution is fully reversed and the air returns to the outer surface. Note that this computation is a severe test on the integrity of the algorithm as both fluids cross the pipe during the transition of void fraction on the outer surface from effectively zero, to effectively unity.

Two particular cases were used to compare with results from the TOFFEA code. Case (a) has an inlet velocity of 2.44 m/s, and an average inlet void fraction of 0.375, Case (b) has an inlet velocity of 1.77 m/s and an inlet void of 0.13. Measurements showed that void distribution in the planes normal to the bend was relatively unaffected by position, so the results taken by traverses in the plane of the bend characterize the distribution.

Computed and experimental void profiles for the two cases are shown in Figure 3.7. Note that the trends in void fraction variation are followed approximately by the code. The 40% increase in velocity between the two cases is sufficient to displace the point at which gravity overcomes the centrifugal force from station C in case (a) to between stations D and E in case (b).

The computation appears to reproduce this shift reasonably well, although the air is computed to shift to the top of the horizontal pipe rather less rapidly than in the experiment in case (a) and more rapidly in case (b). Also a rather odd kink in the computed void fraction profile occurs in both cases.

Some of these discrepancies may well be due to three dimensionality or flow regime difference, neither of which can be resolved by this model. However agreement was sufficiently good to motivate further investigation, which is pursued in Chapter 7.

This study was published, together with a description of the numerical method in an ASME paper, Carver (1982) and subsequently revised and published in the Journal of Fluids Engineering, Carver (1983).

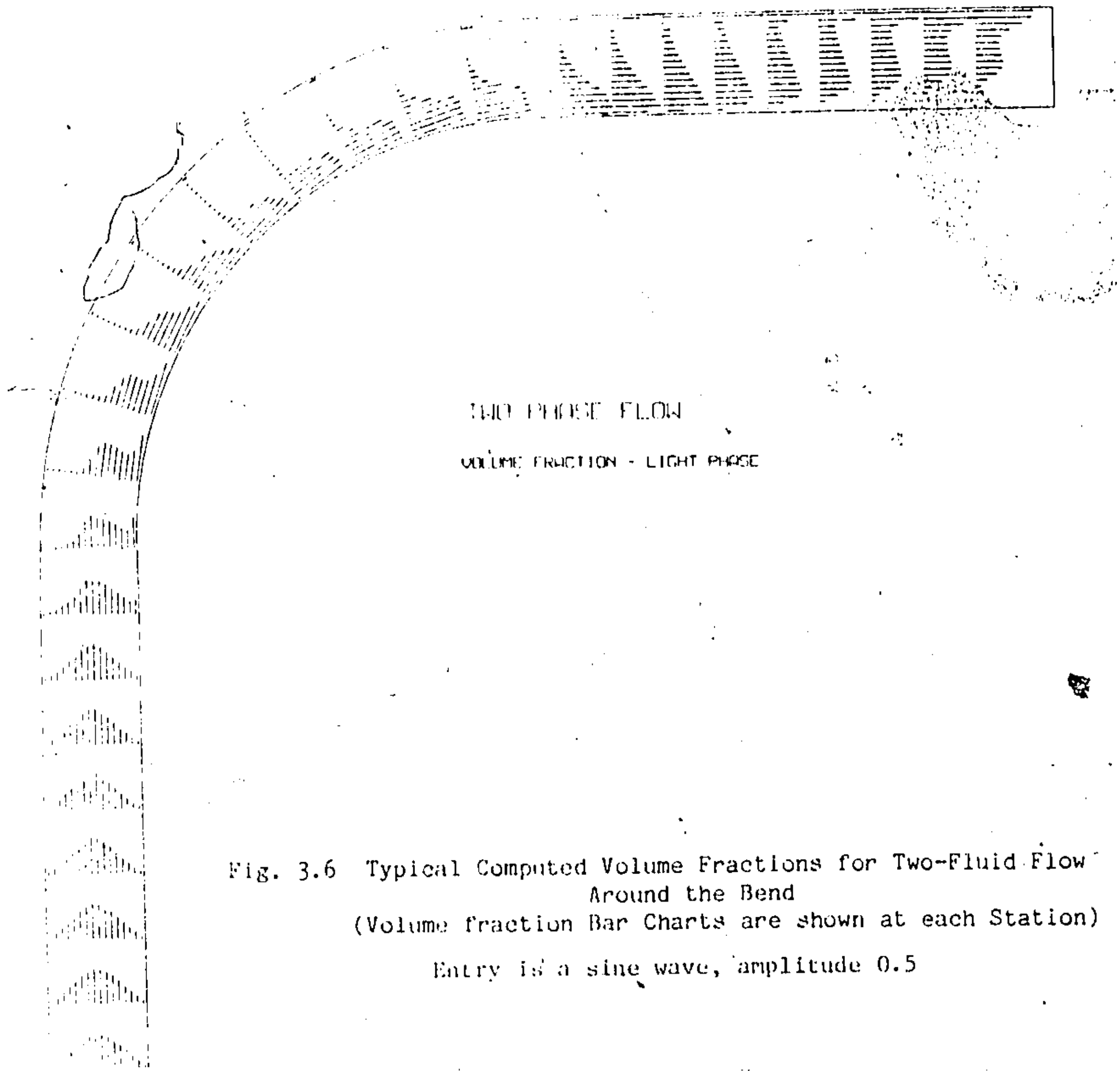

Fig. 3.6 Typical Computed Volume Fractions for Two-Fluid Flow Around the Bend
(Volume fraction Bar Charts are shown at each Station)

Entry is a sine wave, amplitude 0.5

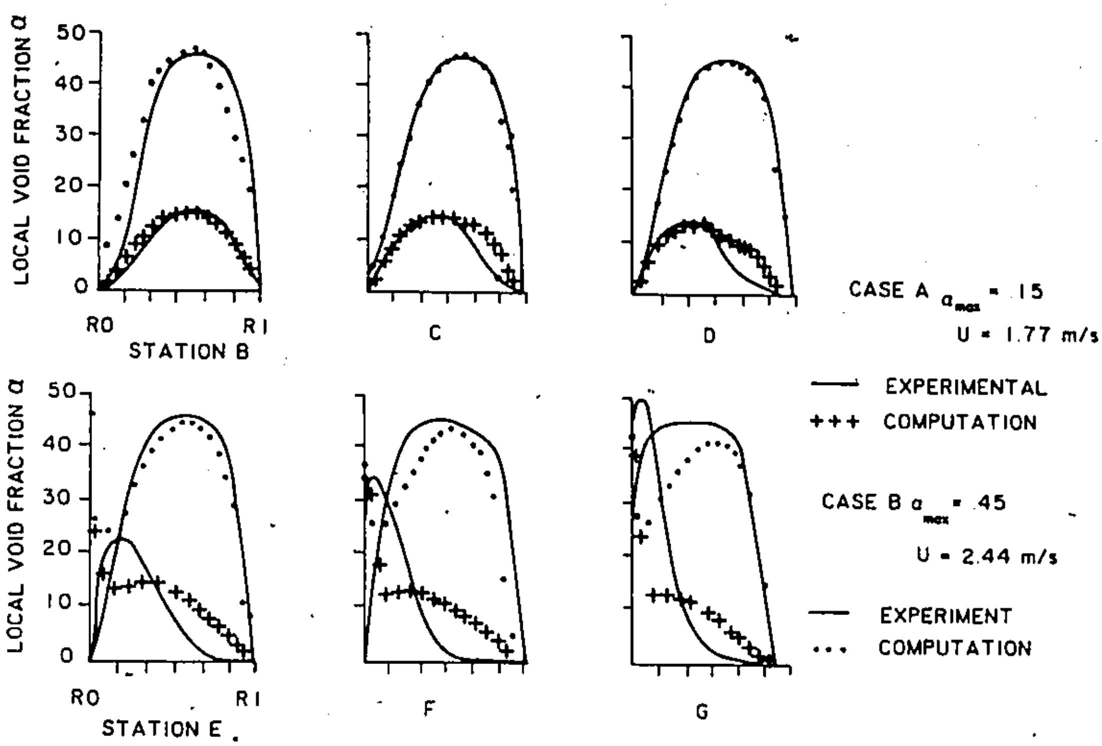

Fig. 3.7 Computed Volume Fraction Profiles in the Bend Compared to Experimental Measurements for Two Cases

3.3 Two Dimensional Simulation of Flow Around Obstructions

It is well known that an obstruction in a two phase flow stream tends to redistribute flow and promotes mixing of the phases. However studies are needed to quantify these effects in more detail. Gardner and Neller also studied flow obstructions, but in this case their data was not sufficient to warrant detailed comparison. However, Salcudean et al (1982) reported some detailed phase distributions.

3.3.1 The Experiments of Salcudean et al

These experiments studied the effect of flow obstructions on pressure drop and void distribution in horizontal air-water flow,. They confirmed that a flow obstruction causes several separately identifiable but related local phenomena: (i) a pressure drop, (ii) a mixing of two fluids (iii) an attendant decrease in local air velocity resulting in (iv) an increase in local void fraction, and (v) an eventual return to stratified flow together with (vi) partial recovery of pressure.

The test section was a 25.4 mm ID horizontal plexiglass tube 3 m long. Air and water flowed at selected rates through a mixer and a 3 m long approach to establish flow prior to the test section. Void fraction was measured at three stations using an optical probe. Two obstructions were used separately, a central disc and a peripheral ring.

Typical results for peripheral and central flow obstructions each blocking 25% of the flow area are shown in Figure 3.8 and illustrate the phenomena mentioned above.

It was clear that the mixing caused by the central flow blockage was far greater than that caused by the peripheral ring.

3.3.2 Comparison with the Experiments

It was of interest to know whether the two fluid model contains the basic mechanisms to simulate these phenomena. Again these effects are clearly of a three-dimensional nature but can be sufficiently characterized in a two dimensional model to provide an adequate proof of concept. A two dimensional model was used with the height equal to the pipe diameter. Similar water and air flow rates and volume fractions were used, and the code computed subsequent pressure drops and phase and velocity distribution. To simulate the mixer, uniformly distributed velocity and void was assumed at entry.

In order to illustrate the features of the flow, demonstration problems at 50% entry void fraction were computed as this yields easily interpreted flow field graphs. Examples are shown in figures 3.9 and 3.10 for both the peripheral and central obstructions. Each figure shows vector fields of volumetric flow ($w\alpha$) for each fluid, and a bar chart of void fraction α. Specific computed values of void fraction and slip ratio are shown in Figure 3.11 for local centre-line conditions and overall cross-sectional average conditions.

As the initial void fraction was uniform, the tendency to stratification can be observed in Figures 3.9 and 10, but only the test section was modelled in the computation, so fully developed stratified flow was not established.

An overall impression of the nature of velocity and phase distribution can be gleaned from the flow fields depicted in Figures 3.9 and 10, particular details can be extracted from the graphs of slip ratio and void fraction in Figure 3.11. Note that the trends in void fraction and slip are also in agreement with the experiment. In particular, the slip can be seen to increase in the plane of the obstruction and decrease markedly just downstream, such that both local and average void increase well above the upstream values. This is also compatible with the experiment. Further downstream, pressure recovery generates an increase in slip and decrease in void. This is computed to occur faster for the peripheral obstruction than for the central one, again as in the experiment.

Because this was a feasibility study in which no attempt was made to simulate the three dimensional nature of the flow, no attempt was made to precisely reproduce experimental conditions. In spite of these approximations, it is clear that the numerical simulation reproduces the main phenomena of interest, and that this agreement is sufficient to encourage proceeding with a three dimensional simulation. This will be discussed in chapter 5.

This study was presented at the 5th IMACS meeting on Numerical Methods for Horizontal Differential Equations, and subsequently reviewed and published in Mathematics and Computers in Simulation (Carver and Salcudean, 1984).

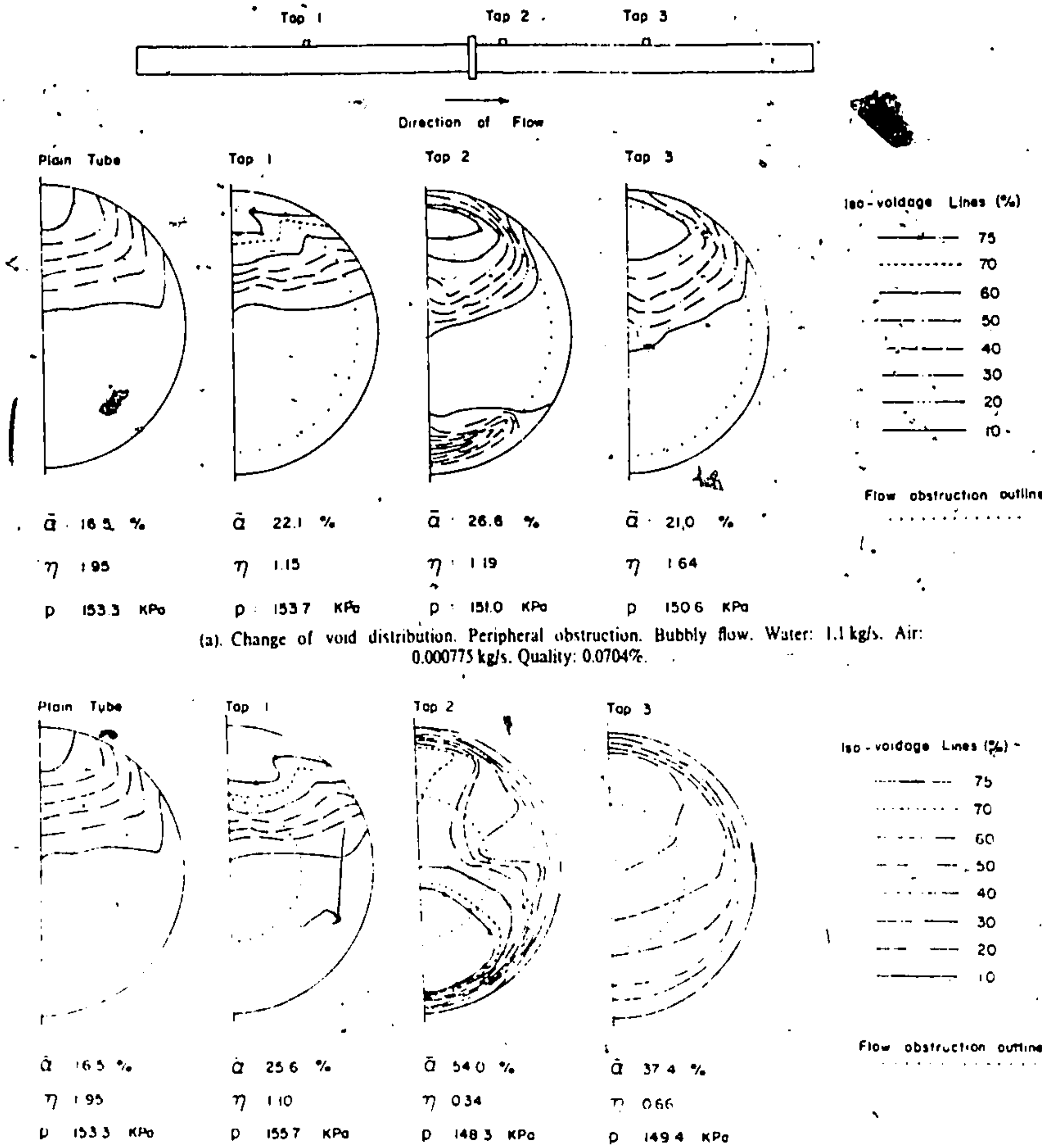

(a). Change of void distribution. Peripheral obstruction. Bubbly flow. Water: 1.1 kg/s. Air: 0.000775 kg/s. Quality: 0.0704%.

(b) Change of void distribution. Central obstruction. Bubbly flow. Water: 1.1 kg/s. Air: 0.000775 kg/s. Quality: 0.0704%.

Fig. 3.8 The Test Section of Salcudean et. al. and Measured Void Fractions for Horizontal Two-fluid flow Past Obstructions.

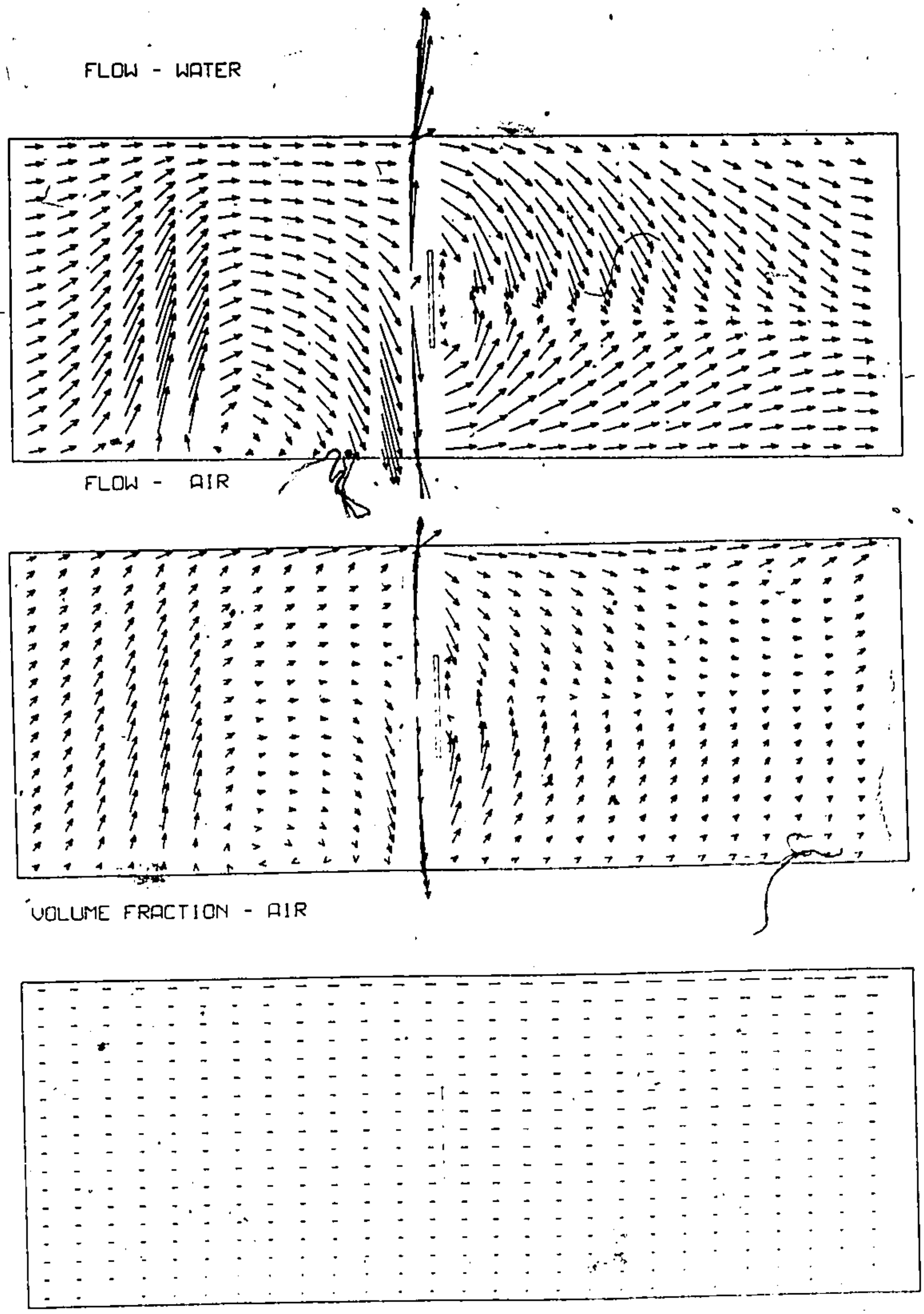

Fig. 3.9 Computed Mass Flux and Volume Fraction Profiles for a Central Obstruction (2-D test Calculation)

Uniform entry with w=2.0 m/s, 50% void

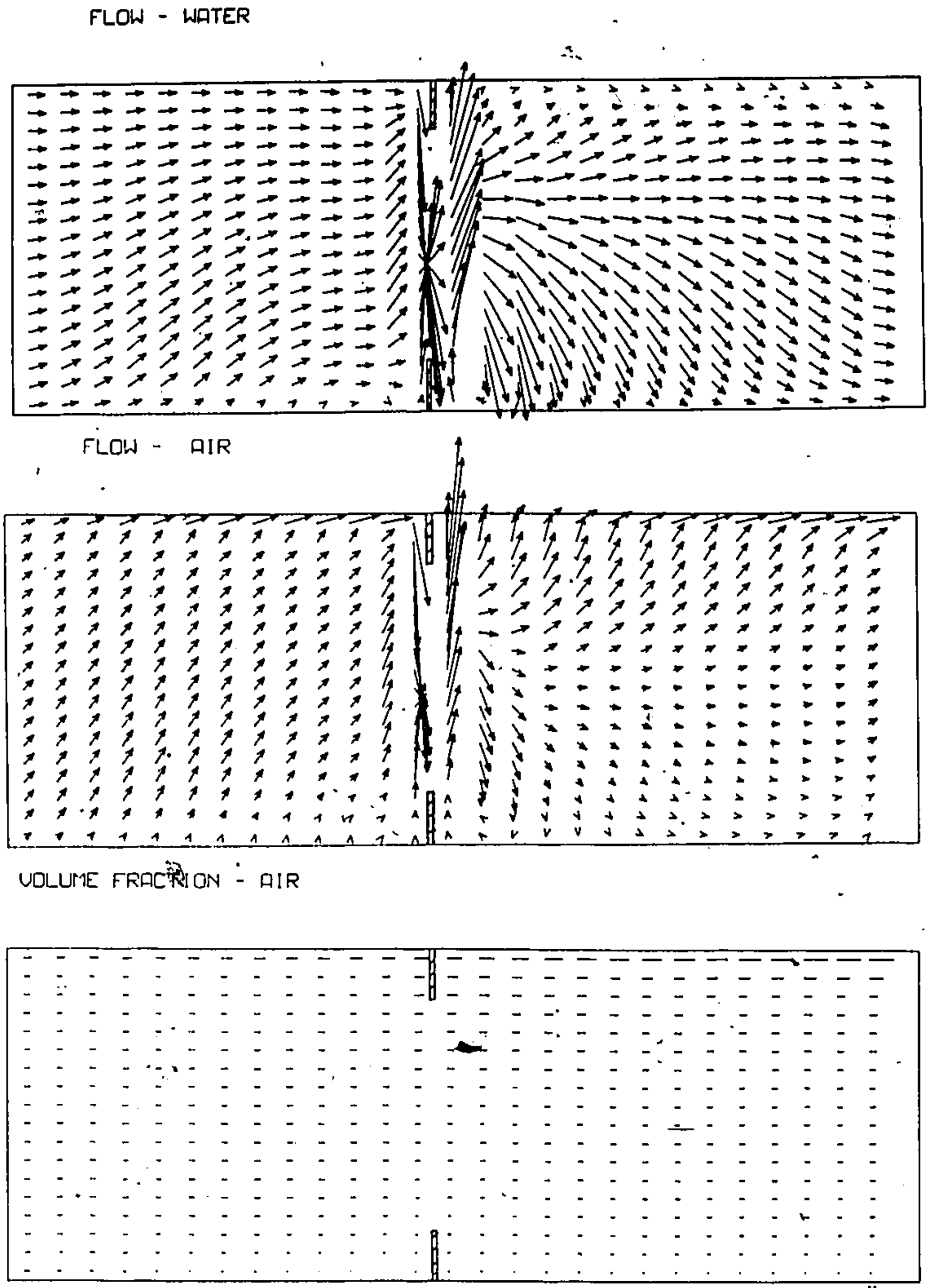

Fig. 3.10 Computed Mass Flux and Volume Fraction Profiles for a Peripheral Obstruction (2-D test Calculation)

Uniform entry with w=2.0 m/s, 50% void

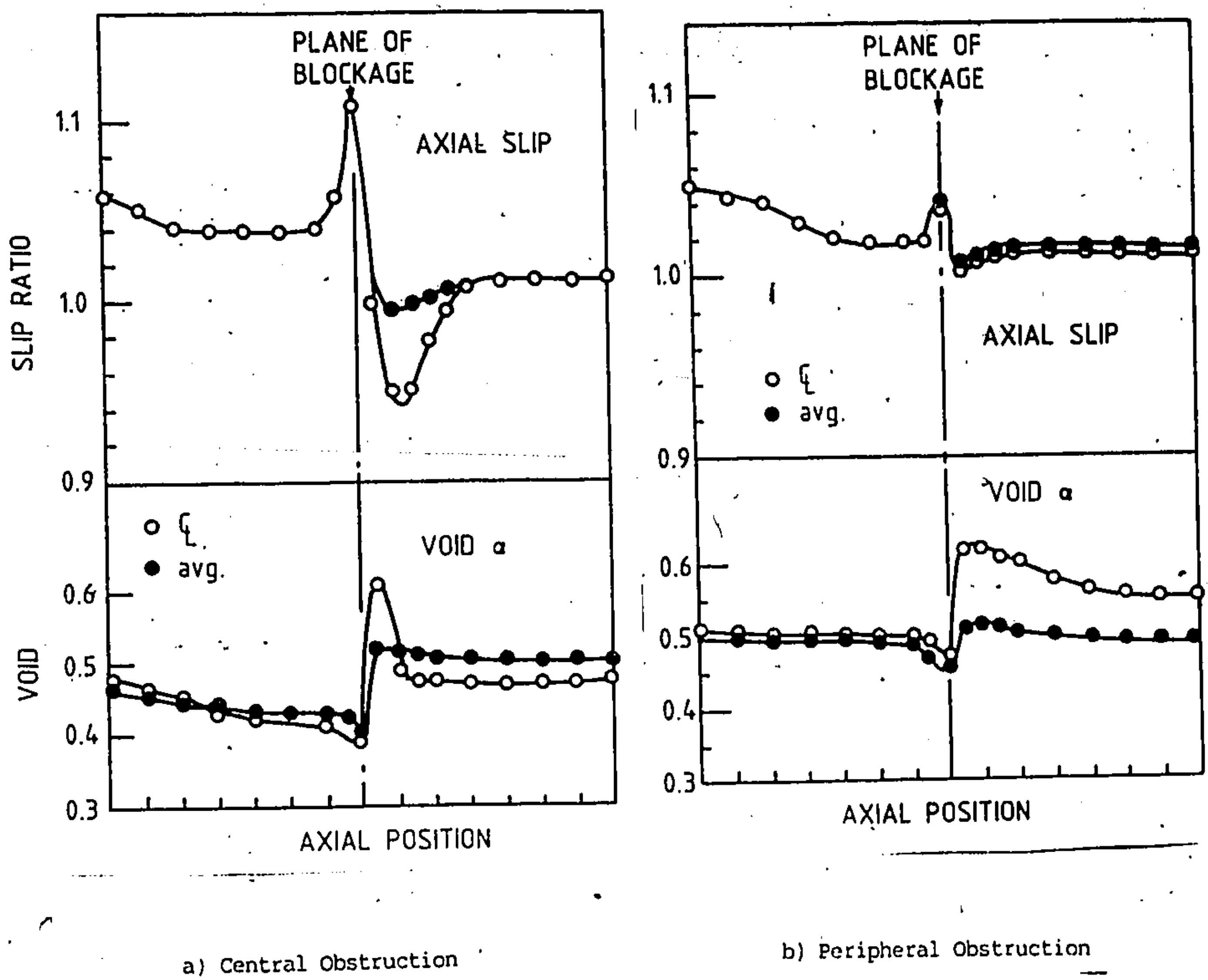

Fig. 3.11 Computed Variation of Volume Fraction and Slip

Shown are average and centreline values

3.4. The Twin Subchannel Experiments of Tapucu

The Experiments of Tapucu et al(1980) also characterize phase redistribution for air and water flowing in geometrically similar horizontal communicating channels. Experiments were run at the same mass flux for each channel but with different inlet void fractions. An interesting feature of the experiments is that the exchange between the channels can be either co-current or counter-current depending on the pressure drop and position. In the particular case of horizontal flow, with one channel above the other, when the lower one has the higher void, both forms of cross-flow occur. Because of the increase in pressure drop in the high void channel, pressure forces both air and water from the high void channel to the low void upper channel initially. However, further downstream, pressure equalises, gravity becomes dominant, and the air then flows up and liquid flows down.

These experiments have been simulated in some detail using the ASSERT subchannel code, and the comparisons are reported by Carver et al(1984). The redistribution of void and mass flux are illustrated in figure 3.12, along with the results predicted by ASSERT. ASSERT computes the longitudinal variations in the channels but cannot estimate any lateral distribution in the cross-section of the channels, and in fact this was not measured in the experiments.

However, as the Toffea code can model lateral distribution, it is of interest to know whether it will predict the same type of cross-over from co-current exchange initially to eventual counter-current exchange. Figure 3.13 shows the computed liquid and gas mass flux vector fields and void profiles for the two channels. Note that indeed, liquid does flow upwards into the upper channel co-current with the air initially, and that the counter-current exchange is established further downstream just as in the experiments. Fig. 3.14 shows computed fields for the case in which the two-phase channel ,is above. In this case, as in the experiment, there is very little phase exchange.

No further comparisons were made because of the lack of data on lateral distribution.

These results were published in a paper in Transactions of the Society for Computer Simulation, Carver(1984).

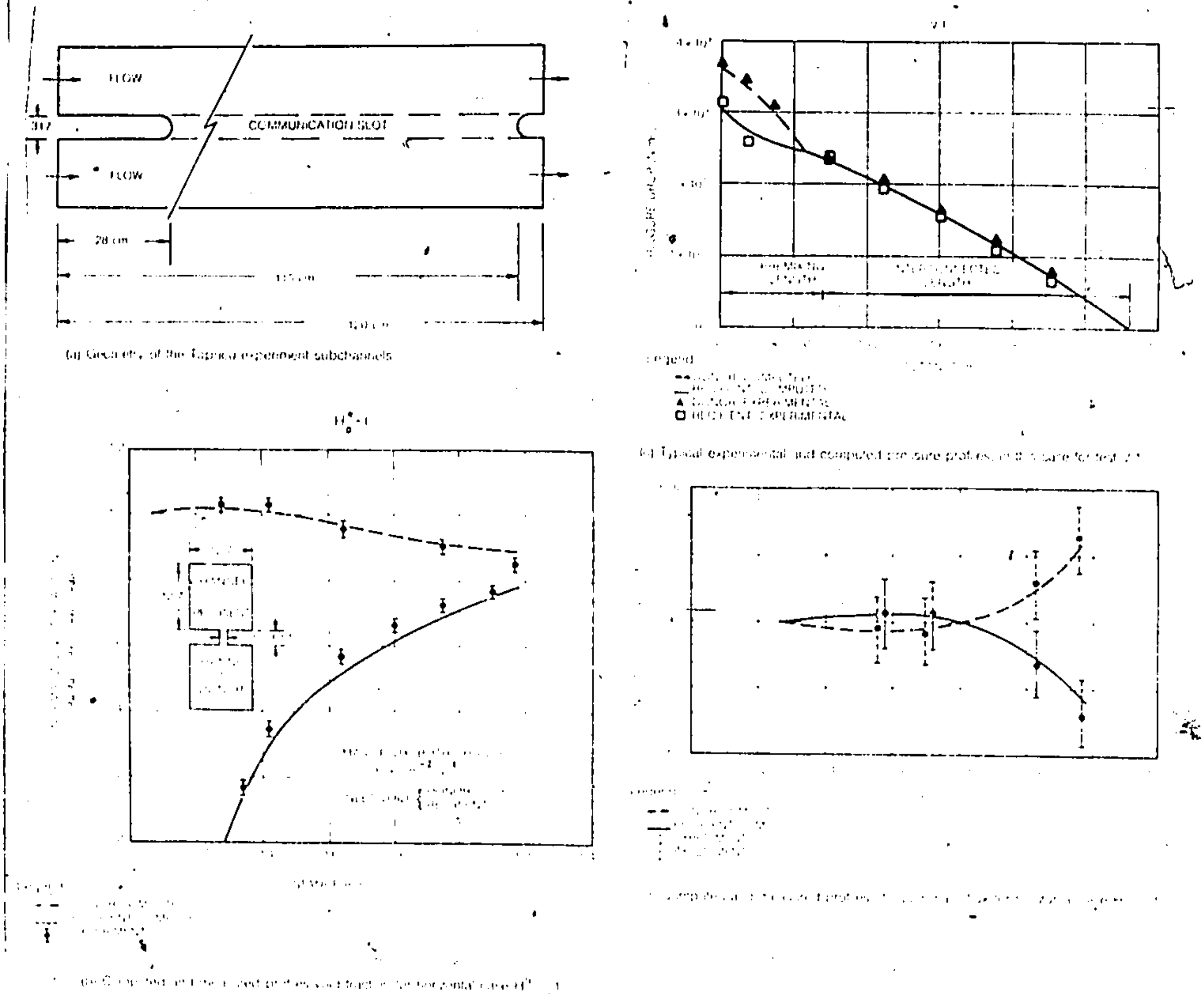

Fig. 3.12 Simulation of The Twin Subchannel Experiments of Tapucu

Using the ASSERT Subchannel Code

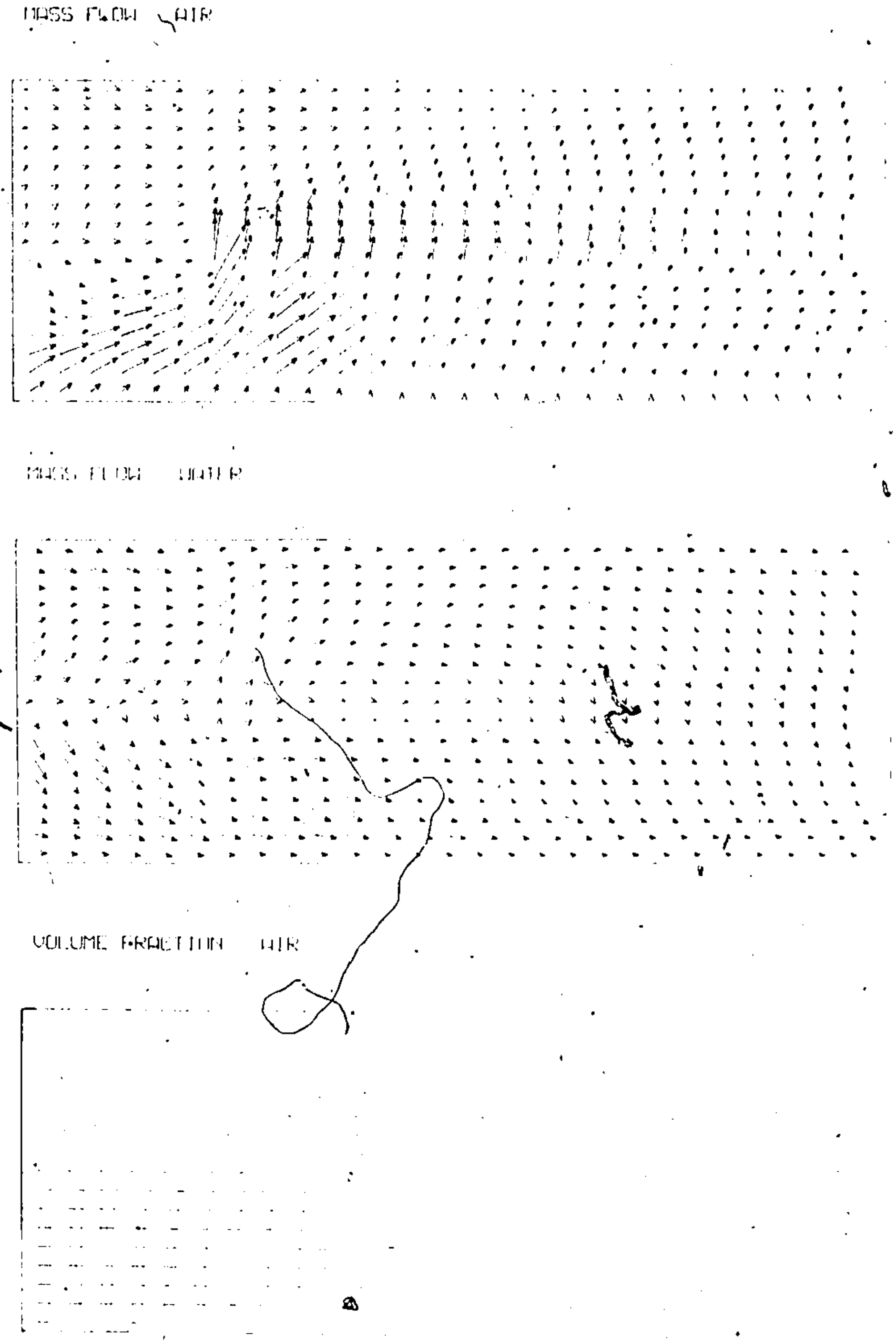

Fig. 3.13 Toffea Simulation of the Tapucu Experiment
Showing fields for Water and Air velocities, and Void Fraction.
Two-phase Channel Below
Entry velocity uniform 3 m/s, void fractions 0.0,0.6

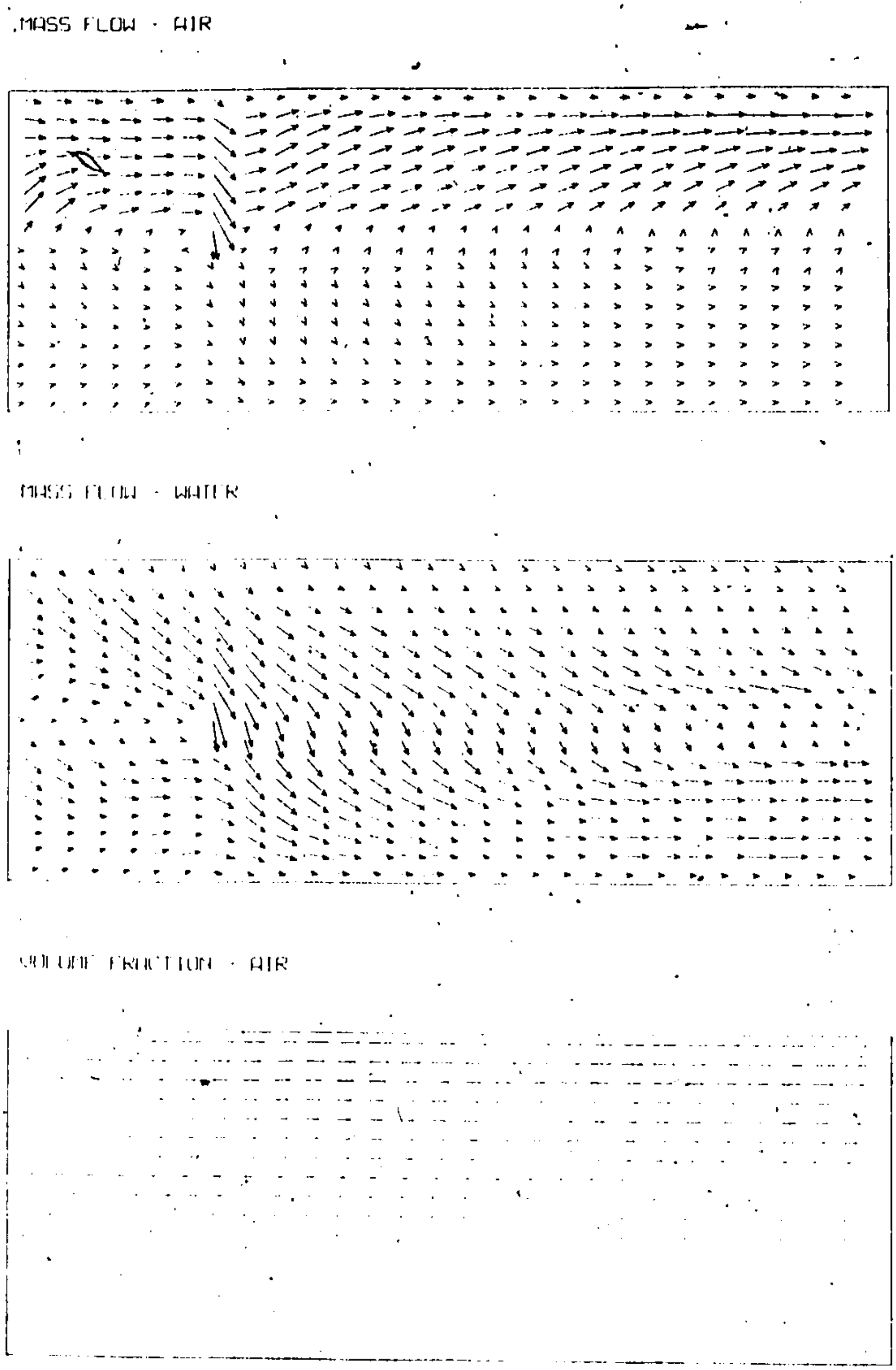

Fig. 3.14 Toffea Simulation of the Tapucu Experiment
Showing fields for Water and Air velocities, and Void Fraction.
Two-phase Channel Above

Entry velocity uniform 3 m/s, void fractions 0.6,0.0

CHAPTER 4.0 THE THREE DIMENSIONAL TWO-FLUID ALGORITHM

The fact that the two-dimensional computations were successful in simulating a number of measured trends in phase redistribution provided encouraging motivation to attempt a three-dimensional simulation. The TOFFEA two-fluid algorithm described in the previous chapters was used in all the preliminary studies, but three-dimensional analysis is required for detailed modelling of phase distribution. The methodology developed for Toffea was extended to three dimensions without requiring any changes in philosophy, although the implementation was considerably more complicated in 3D. The resulting code can be used for single or two-fluid flow. The code was named FAITH for Fluid Flow Analysis In THree dimensions. For single-fluid flow, the overhead required to store variables for the second fluid can be minimized easily by changing parameter statements in the code. This chapter outlines further details of the 3D solution algorithms, and discusses schemes to enhance convergence.

4.1 Iteration Sequence

The two-fluid computation follows the sequence detailed in Table 4.1.

TABLE 4.1

ITERATION SEQUENCE OF FAITH

Step	Purpose	Routine	Equation
1	Executive Routine direct steps 2-12	EXEC	-
2	Initialization of Grid Parameters	INIT	-
3	Computation of viscosity and density	PROPS	2.39
4a	Calculate θ velocities U	CALCU	2.3
4b	Repeat 4a for second fluid if required	CALCU	
5a	Calculate r velocities v	CALCV	2.4
5b	Repeat 5a for second fluid if required	CALCV	
6a	Calculate z velocities w and apply plane by plane flow continuity	CALCW	2.5
6b	Repeat 6a for second fluid if required	CALCW	
7	Compute pressure correction and apply velocity corrections	CALCP	2.51
8	Compute volume fraction if required	CALAB	2.52
9	Compute turbulence energy if required	CALCK	2.40
10	Compute dissipation if required	CALCE	2.41
11	Check convergence and time limits. If required, repeat loop starting at 3.	EXEC	
12	Call for termination output and plots	VECTOR	
	The following are called by all the CALC Routines		
-	Boundary Condition Routine	PROMOD	
	Triagonal Matrix Solver	LINEQN	

4.2 3D Matrix Solution

Having outlined the method of reducing the equations to standard form and how the solutions are combined into an overall iterative scheme, the matter of how the standard matrix equations are solved must be addressed. As the equations are three dimensional, direct solution is costly, so an iterative scheme must be used. For one dimension, equation (2.16) can be solved by tridiagonal Gaussian elimination. A two dimensional iteration can be solved by successively cycling a tridiagonal several times through the second dimension, or alternating direction methods can be used in which first the x, then y direction is used in the tridiagonal algorithm. Finally, in three dimensions, various cyclic plane by plane or alternating schemes can be used. These are discussed by Von Rosenburg (1969). Single and double direction alternating schemes were examined in the two dimensional prototype two-fluid code TOFFEA, preparatory to launching a 3D calculation. The standard tridiagonal algorithm was found to be quite satisfactory, particularly in view of the fact that an exact solution of the inner equations is not required during the overall iteration.

The three-dimensional 2-fluid FAITH program is based primarily on a version of the single-fluid code 3DTEACH, obtained from Dr. Gosman at Imperial College, Restivo et al(1980), extended to incorporate work done on the 2D single-fluid version of TEACH, Salcudean and Abdelrehim(1980), and a 3D single-fluid sequel, Salcudean et al(1985), both obtained from the University of Ottawa. The 3D TEACH code was cartesian.

In addition to developing the two-fluid option by incorporating the TOFFEA algorithms in FAITH, cylindrical and toroidal coordinate options have been added and verified.

In three dimensional computation, savings in storage may be made by using marching techniques which solve the problem plane by plane in the direction of the flow regimes, however, these are confined to truly parabolic flows in which the effects of downstream conditions are not propagated upstream Patankar(1980). As it is known that bends and significant flow obstructions do influence upstream conditions, parabolic computations cannot be used, and the minimum computational requirement is to use a partially parabolic scheme such as that introduced by Pratap (1976). This again uses a plane by plane solution but uses a more detailed treatment of pressure. However, as pointed out by Pratap, this procedure is not adequate for strongly curved ducts in which recirculation may occur, so an elliptic solution procedure is used in the program. Iterated plane by plane solutions are used in the momentum equations in the lateral plane, a plane by plane solution plus block pressure correction is used in the axial momentum equation and a fully elliptic equation is solved for the pressure fields. Full details of this method for the single-fluid case are given by Restivo, et al (1980).

4.3 Convergence Enhancement

Because of the considerable expense involved in completing a 3D calculation, it was necessary to spend some effort on improving convergence. Some convergence enhancement methods were investigated. In particular, it was found helpful to extend the various procedures recomended by Van Doormaal and Raithby (1984) to three dimensions and to two fluids. These include the SIMPLEC variation, monitoring residuals and overrelaxing the tridiagonal solver. A block correction, as recommended by Latimer and Pollard (1985), was also used. The SIMPLEC variation is effective and can be implemented readily without modification as described in Appendix B, the other devices required some extension as discussed below.

4.3.1 Axial Block Correction

Following computation of the axial velocities w in each of the k planes a block correction is applied to impose axial continuity. The correction is applied by incrementing all the velocities in the plane by an amount computed from the difference between the total inlet flow and the integrated flow through that plane. This accelerates convergence in the single phase case, providing the flow is not strongly recirculatory.

$$\Delta m_k = \Sigma_{ij}[(\alpha\rho w)_k - (\alpha\rho w)_{in}]\, A_{ij} \tag{4.1}$$

$$\delta\bar{w}_k = -\Delta m_k / \Sigma_{ij}(\alpha\rho A)_{ij} \tag{4.2}$$

$$w_{ijk} = w_{ijk} + \delta\bar{w}_k \tag{4.3}$$

$$d(\Delta m_k)/dp = \Sigma_{ij}(\alpha\rho A dw/dp)_{ij} \tag{4.4}$$

whence

$$\overline{d\bar{p}_k} = -\Delta m_k / \Sigma_{ij}(\alpha\rho A(\partial w/\partial p))_{ij} \tag{4.5}$$

For the single phase case the application is straightforward, but for the two-fluid case it was necessary to develop a variant. Initially a scheme was tried in which δw was calculated for each fluid separately followed by a pressure correction for each fluid. This led to poor convergence. Satisfactory convergence was obtained by computing the individual flow corrections, but applying only the pressure correction derived from the water flow correction, using the rationale that the pressure field is dominated by the heavy phase.

Finally a new approach was developed in which a block pressure correction was derived to be compatible with the full pressure equation. Thus the block pressure correction is that required to drive the sum of the volumetric flows to zero.

$$\Delta m_t = \Sigma_\iota \; \Delta m_\iota \tag{4.6}$$

$$\begin{aligned} \partial(\Delta m_t)/\partial p &= \Sigma_\iota(\partial\Delta m_\iota/\partial p) \\ &= \Sigma_\iota\{\; \Sigma_{ij}(\alpha A\partial w/\partial p)_{ij}\} \end{aligned} \tag{4.7}$$

$$\delta\bar{p}_k = (\; -\Sigma_\iota\Delta m_\iota)/\Sigma_\iota(\Sigma_{ij}(\alpha A\partial w/\partial p)_{ij})_\iota \tag{4.8}$$

It was also found more appropriate for two-fluid flow to base the flow correction not on the average axial flow correction obtained from 4.7, but on individual corrections based on the resulting block pressure correction.

$$\partial w_{ijk} = (\partial w/\partial p)_{ijk} \delta \bar{p}_k \tag{4.9}$$

For the single phase case the two corrections converge equally well, but for two-phase cases, 4.9, referred to as DW, always behaved at least slightly better than 4.7, referred to as AW. Figure 4.1 shows the convergence obtained using both corrections, for a vertical flow case, and the bend reference case given in Chapter 7. The two methods perform equally for the former case but for the latter (4.9) is superior.

While convergence is usually fairly smooth, it is sometimes necessary to adjust relaxation factors. The factors usually employed for

$$\{ u , v , w , p , \alpha , k , \varepsilon , \mu \}$$

were

$$\{.7, .7, .7, 1. , .3, .5, .5, .5\}$$

A faster rate of convergence would be more pleasing, but, as shown in the figures, the single phase algorithm is not beyond improvement. As the two fluid option was added incrementally to the single phase framework, any improvement in the latter will also be reflected in the former.

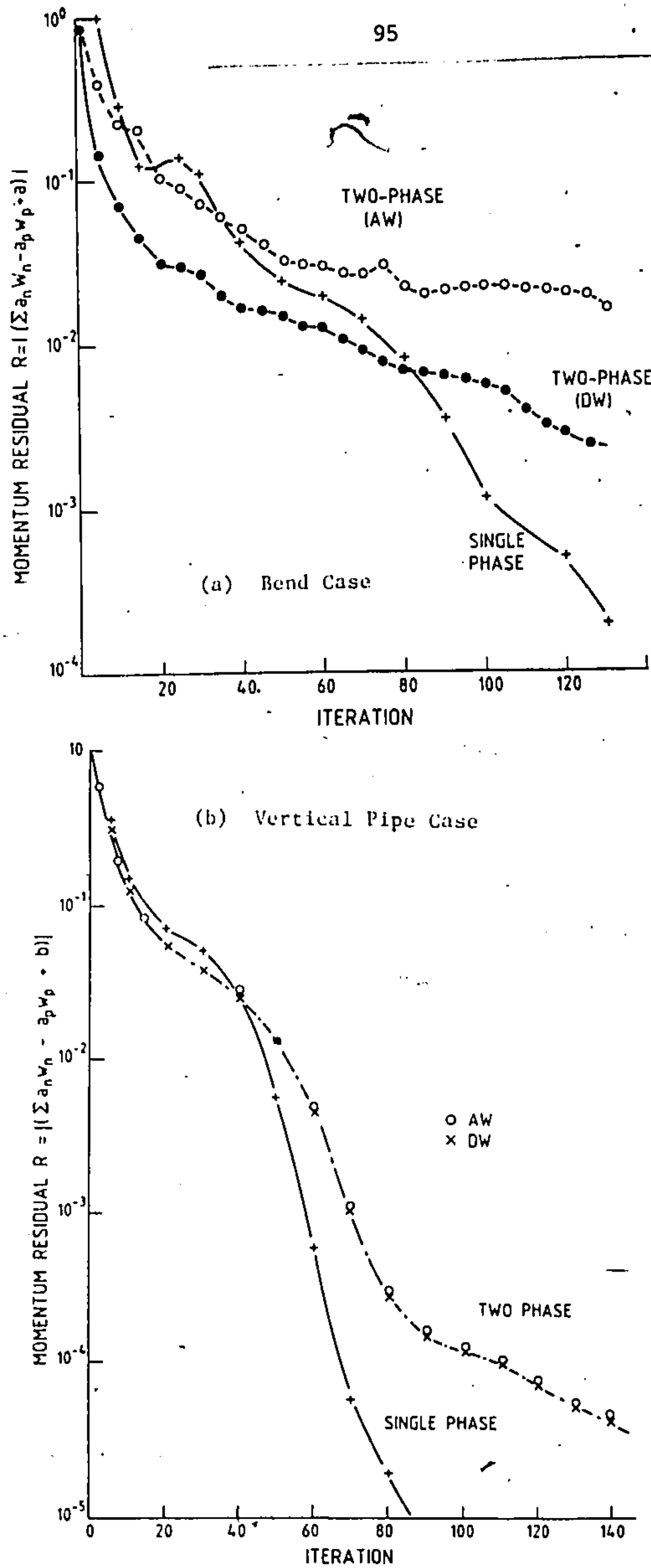

Fig. 4.1 Effect of Block Corrector on Residuals

4.3.2 Over-relaxation in the Pressure Equation

The over-relaxation method was implemented to accelerate convergence in the pressure equation, and residuals were monitored, both as recommended by Van Doormaal and Raithby(1985) in their two-dimensional single fluid studies.

This method attempts to compensate for the fact that during the current sweep of the tridiagonal ADI solver, the terms on the alternate diagonal would also be changing in an amount roughly proportional to those currently being updated. The equation to be solved is :

$$a_p p_p = a_e p_e + a_w p_w + a_n p_n + a_s p_s + b \tag{4.10}$$

This will be solved by sweeping along the i lines implicit in j and then along the j lines implicit in i. Thus while sweeping the j lines, for example, p_p, p_e and p_w are updated, p_s has just been updated, but p_n has not. The assumption is made that p_n will change in a like manner to p_p.

$$\begin{aligned} p_{n,new} &= p_{n,old} + (p_{n,new} - p_{n,old}) \\ &= p_{n,old} + (\beta-1)(p_{p,new} - p_{p,old}) \end{aligned} \tag{4.11}$$

Hence 4.10 becomes :

$$(a_p - a_n(\beta-1))p_p = a_e p_e + a_w p_w + a_s p_s + a_n(p_n - (\beta-1)p_p)_{old} \tag{4.12}$$

A value of β=1.8 is recommended. The mirror image of (4.12) is applied in the i sweep.

For this study, a three dimensional equivalent was derived, and it was found useful to use two β factors one for the inner and outer loops. The extension to incorporate k sweeps is self evident:

$$(a_p-(\beta_j-1)a_n+(\beta_k-1)a_d)p_p = a_e p_e + a_w p_w + a_s p_s + a_u p_u + a_n(p_n-(\beta_j-1)p_p)_{old} + a_d(p_d-(\beta_k-1)p_p)_{old} \qquad (4.13)$$

Again the equivalent expressions follow ~~by~~ analogy. As the outer loop is less closely coupled than the inner loop in the sequence, it was found that a smaller value of β_k was necessary. The set β_j=1.75, β_k=1.35 was found to give good convergence while larger values of β_k occassionally diverged.

Convergence was assessed by monitoring the residuals :

$$R_{sum} = \Sigma_{ijk} \mid \Sigma_n(a_n p_n + b - a_p p_p) \mid \qquad (4.14)$$

The pressure equation was set up to complete a maximum of 8 sets of three ADI sweeps, residuals were checked, and the sweeping was terminated if for the m'th sweep :

$$R_{sum} < 0.1\ R_1 \qquad (4.15)$$

Usually for the β values above , only 2-3 sweeps were required , however for β=0, the criterion was rarely met with 8 sweeps. This is illustrated in figure 4.2.

Appendix B outlines further details of the solution algorithms required.

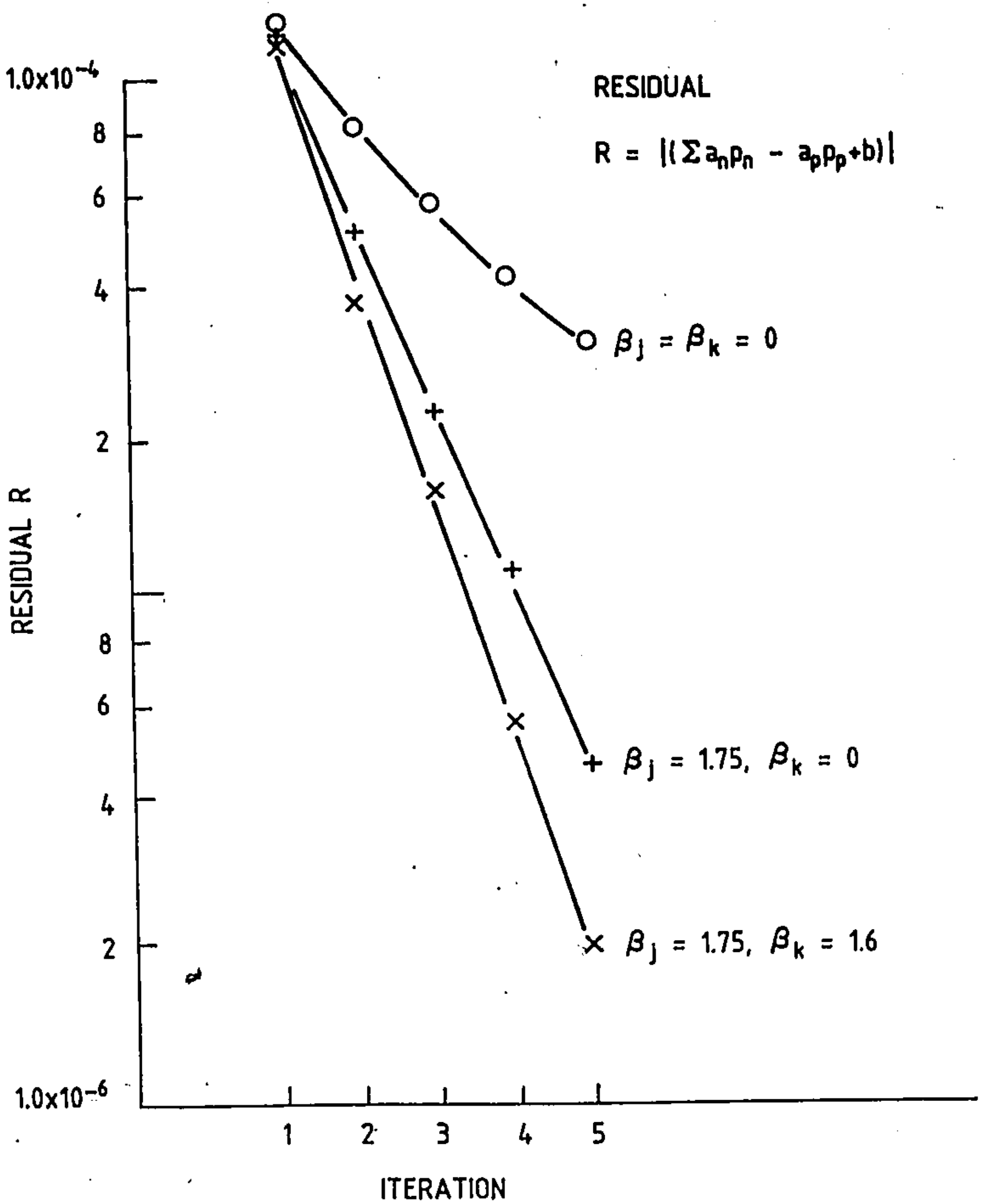

Fig. 4.2 Effect on Residuals of Over-Relaxing the Pressure Equation

4.4 Numerical Diffusion

The formulae used to interpolate variable values at the control volume faces are discussed in Appendix A . Unfortunately there are two considerations in the choice of formulae which conflict, stability and accuracy. In the Appendix, it is shown that the low order upwind formulae preferred for stability, introduce an excess diffusion into the equations. Work on minimising false diffusion by using higher order upwind formulae has been restricted to date to two dimensions. While it is often possible to mimimise false diffusion in 2-D by choosing a very small grid spacing, this is rarely possible in 3-D, particularly when available computer memory is limited or relatively unlimited but expensive.(One complete run costs about $600 on the CDC 175 computer in prime time). False diffusion thus remains a significant impediment in 3-D calculations, however if the current 2-D methods of minimising the problem are extended to 3-D, there is no reason why they could not be used in the current algorithms. The topic has been reviewed recently by Galpin, Huget and Raithby(1986), and is discussed further with reference to the current study in Appendix B, where it is concluded that the obstruction cases of chapter 6 are prone to more severe numerical diffusion than the bend cases of chapter 7.

CHAPTER 5. DETAILED MODELLING OF PHASE DISTRIBUTION IN VERTICAL PIPES

In chapter 3, the two-fluid model was used in simplified form to demonstrate that the mechanisms controlling phase redistribution due to bends and obstructions could be simulated. In order to undertake more detailed comparisons with experimental data it is necessary to review the equations in detail and incorporate more realistic models of interfacial momentum exchange and effective viscosity. Although detailed measurements of velocities and phase distributions in bends and obstructions are rare, a considerable number of studies have been reported on vertical flow of two phase mixtures in vertical pipe in the bubbly regime, and these have revealed important characteristics of bubbly flow which are now discussed.

5.1 Overview

Phase distributions in two-phase flow are rarely uniform. For calculational purposes the gaseous phase, or void, is commonly considered in vertical flow to be distributed in a power law distribution analagous to a velocity profile. This distribution was noted by Zuber (1960) and led to the well known Zuber-Findlay (1965) distribution parameter analysis. At the lower void fractions characteristic of bubbly flows however, a concentration of bubbles close to the wall has been noted by a number of investigators, and it has been established that this phenomenon is not a product of the method of bubble injection, but is in fact an intrinsic property of the flow which develops even for uniform bubble injection.

The phenomenon was first reported in detail in Malnes (1966), and has been confirmed by a number of investigators including Inoue et al. (1976), Serizawa et al. (1975) and Sato and Sekoguchi (1975). It was also noted by Usui et al. (1983) in their measurements of void distribution in vertical inverted U-bends. Very recently the subject was reviewed by Beyerlein et al. (1985). The review by Beyerlein does not mention the data of Malnes or Usui et al., however otherwise it is quite comprehensive, so previous work will be discussed only briefly here and the reader is referred to Beyerlein et al for further details and references.

In particular, several of the theories mentioned, such as Zun et al. (1975) and Rouhani (1976) concentrated on rotation of the bubbles which, in non-uniform velocity field, can be related to the radial gradient of axial velocity, which in turn is a function of effective viscosity. Serizawa et al. (1975) and Sato and Sekoguchi (1975) proposed that, in bubbly flow, the turbulent structure of the liquid dictates the phase distribution. They developed an expression for effective two-phase turbulent viscosity which is dictated primarily by the liquid viscosity, but is also modified by a term introduced to simulate the effects of bubble agitation. Sato et al. (1980) extended this effective viscosity concept to calculate velocity profiles of the liquid phase from given profiles of void distribution. The calculated profiles show good agreement with their measurements and with those reported by Serizawa, and Inoue. They also demonstrated that bubbles introduced into glycerine caused departure from laminar flow towards turbulent velocity characteristics and distributed in the same wall peaking pattern.

Drew and Lahey (1981) reduced the adiabatic two-fluid continuity and momentum equations established by Ishii (1975) to the case of fully developed flow (zero transverse velocities), and were able to arrive at an expression for the radial profile of void fraction in terms of the components of the Reynolds stress tensor in the liquid. By using optimization techniques to adjust the free parameters, they were able to fit the data of Serizawa, but found that it was not possible to obtain a good fit under the constraint of isotropic turbulence structure; it was necessary to permit anisotropy. No predictions of velocity profile were made.

Most recently, Beyerlein et al. extended the analysis of Sato and Sekoguchi to establish a diffusivity for the form of the void transport equations derived by Zun et al. Using an assumed form of the liquid velocity profile, they were able to calculate developing and fully developed void profiles which they matched with measurements from their own experiments, again by adjusting empirical constants.

Clearly these previous works have contributed greatly to the understanding of the phenomena, but all the analyses suffer from three deficiencies which limit their versatility and render them inappropriate for use in general engineering calculations. First, each has been obtained by parameter fitting, specific to the data under consideration, and second, they calculate either void profile or liquid velocity but not both. Finally, they apply only to vertical pipes and cannot be applied to bubbly flow in other topographies. In particular, for bubbly flow in horizontal pipes or in bends, the gravitational and centrifugal forces overwhelm the delicate balance of lateral forces which exists in vertical flow.

For generally applicable 3D two-fluid calculations it is necessary to invoke a turbulent model to obtain reasonable agreement with the velocity distribution data. In this study, velocity and void profiles in vertical bubbly flow computed using a modification of the k-ε model are compared to reported data. Although the results are perforce not so accurate as those obtained by fitting free parameters to the data, both void and velocity distributions are computed simultaneously, and agree quite well with observed data for vertical pipes. The technique is not restricted to vertical pipes, but also can be applied in bends and horizontal pipes.

5.2 Interphase Momentum Exchange

The conservation equations for steady two-fluid flow are written using the principle of interpenetrating continua introduced by Harlow and Amsden (1971), and discussed at length by Ishii(1975). Hence the equations for each fluid are analagous to the single phase equations, except for the terms involving phase interaction. Ishii(1975) and Drew and Lahey(1979) state the equations as follows:

Continuity

$$\nabla.(\alpha\rho U)_\iota = \Gamma_\iota \qquad \iota=g,l \qquad \Gamma_l = -\Gamma_g \tag{5.1}$$

For adiabatic flow , the mass exchange $\Gamma=0$.

Momentum

$$\nabla.(\alpha\rho UU)_\iota = -\nabla(\alpha p)_\iota + (\alpha\rho)_\iota g + \nabla.\alpha_\iota(\tau_L + \tau_T) + M_{\iota\iota}, \tag{5.2}$$

As discussed in chapter 2.2.4, in the equations, the turbulent fluctuations have been extracted by the usual averaging practice for single-phase flow to incorporate the resulting Reynolds stresses in the effective stress tensor such that

$$\tau_E = \tau_L + \tau_T \tag{5.3}$$

According to the above authors, the interphase momentum exchange is a resultant of a number of components : momentum exchange due to phase change the difference in phasic pressures, drag, virtual mass, lift, and components due to the Basset and Faxen forces.

$$M_{ll'} = M_{\Gamma} + p\nabla\alpha + M_{dp} + M_{d} + M_{vm} + M_{L} + M_{B} + M_{F} \tag{5.4}$$

For the case of separated flows the difference in phasic pressure is important, but for dispersed flows, Drew and Lahey argue that the momentum exchange due to phasic pressure difference is insignificant. For adiabatic flow there is no momentum exchange due to phase change. The lift force on a sphere is due to the interaction on the dispersed phase of the relative velocity and the shear in the continuous phase.

$$M_L = C_L(u_c - u_d).\nabla u_c \tag{5.5}$$

This force is important in slow viscous flow, but according to Drew and Lahey, is of no significance in air-water flows.

The virtual mass term is of considerable importance in transient analysis as it represents the force required for one fluid to accelerate the other. A number of different forms have been postulated to simulate virtual mass effects , and in one dimensional analyses, the most prevalent approach is to choose a form which ensures hyperbolicity of the conservation equation set, Hancox and Banerjee(1971). In general the term is a function of volume fraction and the velocities.

$$M_{vm} = C_{vm}(\alpha, v_c, v_d) \tag{5.6}$$

The effect of the history up to time t of the relative motion of a sphere in liquid is expressed in terms of the Basset force. Soo(1967), points out that this is significant for creeping flows.

$$F_B = -1.5 r_d \sqrt{(\pi \rho_c u_c)} \int_{-\infty}^{t} (dv_r/dt)/\sqrt{(t-t')}\,dt' \quad (5.7)$$

Another influence is the Faxen force

$$F_F = \pi r_d^3 \mu_c d^2 u/dy^2 \quad (5.8)$$

This expresses the influence of fluid velocity gradient on the sphere. Drew and Lahey recommend against attempting to specifically incorporate the Basset and Faxen forces in two-fluid flow analyses, because there is insufficient knowledge of their effect in groups of bubbles in gas-liquid systems, hence M_B and M_F are omitted. The most significant term in interphase momentum exchange is the classical drag force. This is usually expressed in terms of a drag coefficient.

$$M_d = 3/8\, \alpha_d \rho_c C_D (u_c - u_d)^2 / r_d \quad (5.9)$$

Finally although virtual mass is a transient force, its effect in steady state is not necessarily zero, as the fluctuating components probably will result in a net residual effect as in the Reynolds stresses. In this study, rather than attempting such a residual term by averaging the various formulations of virtual mass suggested in the literature, the term has been treated as included in the turbulent stresses in a manner which is discussed below.

With the above assumptions the conservation equations now reduce to the simpler form used by Drew and Lahey (1981), and Apizadis (1985).

$$\nabla \cdot (\alpha\rho U)_\iota = 0 \tag{5.10}$$

$$\nabla \cdot (\alpha\rho UU)_\iota = -\alpha_\iota \nabla P + (\alpha\rho)_\iota g + \nabla \cdot (\alpha\tau_E)_\iota + M_{d,\iota\iota'} \tag{5.11}$$

In one dimensional analysis the effective stresses are usually incorporated in a friction factor, and two-phase multiplier. In multidimensional analysis a model of the effective turbulent stresses is required, together with a method of incorporating two phase effects.

By assuming fully developed flow, u=v=0, $\nabla\cdot u=0$, Drew and Lahey showed that equations (5.11)in the transverse plane only, reduced to:

$$-\alpha_\iota \nabla P = \nabla P + \nabla \cdot (\alpha\rho\tau_E)_\iota = 0 \tag{5.12}$$

Clearly, equations (5.12) can be manipulated to eliminate the pressure gradient terms, leaving an expression which relates the gradients in void fraction profile to the gradients of the stress vector. For incompressible fluids, this is:

$$\Sigma_\iota\ (1 - \alpha)_\iota\ \nabla \cdot (\alpha\tau_E)_\iota\ (-1)^\iota = 0 \tag{5.13}$$

Drew and Lahey then simplified further by assuming that the stress vector in the vapour phase was proportional to that in the liquid phase, and by making fairly standard assumptions about the form of the elements of the liquid stress vector. As noted above, they were then able to fit the data of Serizawa by permitting the stress field to be anisotropic.

Sato and Sekoguchi also worked on the assumption that the liquid phase turbulence determined bubbly flow characteristics, but instead of expressing vapour phase turbulence stresses as a multiple of those in the liquid phase, they merely modified the liquid phase stress vector to allow for the presence of bubbles.

$$\begin{aligned}\tau_E &= \tau_L + \tau_T + \tau_B \\ &= (1 - \alpha)\ (\mu_L + \mu_T + \mu_B)\ \frac{dw}{dr}\end{aligned} \qquad (5.14)$$

$$\mu_B = k_B \alpha d_b W_\infty \rho_1 \qquad (5.15)$$

$$\mu_T = k_T \frac{R}{6} \left(\frac{\tau_w}{\rho_1}\right)^{1/2} \left[1 - \left(\frac{r}{R}\right)^2\right] \left[1 + 2 \left(\frac{r}{R}\right)^2\right] \rho_1 \qquad (5.16)$$

τ_w can be obtained using the usual one dimensional friction factor analysis.

If the void profile is known as a function of r, then the velocity profile may be obtained by integrating (5.14). In a subsequent paper, Sato et al. (1980) devised a more complex form of (5.15) and (5.16), introducing a standard exponential multiplier in both equations. This led to better agreement with the data close to the wall.

Beyerlein et al. developed a void propagation equation from (5.9). For axisymmetric coordinates, (5.9) becomes for the vapour phase:

$$\frac{1}{r} \frac{\partial}{\partial r} (r\alpha\rho v)_g + \frac{\partial}{\partial z} (\alpha\rho w)_g = 0 \qquad (5.17)$$

Assuming constant density, and that the relative velocity in the vertical direction is the bubble rise velocity gives:

$$w_g = w_l + w_\infty \qquad (5.18)$$

$$\frac{\partial\alpha}{\partial z} = - \frac{1}{w_l + w_\infty} \frac{1}{r} \frac{\partial}{\partial r} (r\alpha v_g) \qquad (5.19)$$

They further propose that the effective bubble flux is composed of two components, a convection flux due to the rotation of bubbles down the velocity gradient and a diffusion flux related to the void gradient.

$$\alpha\, v_g = \alpha\, v_r - \varepsilon_B \frac{\partial\alpha}{\partial r} \qquad (5.20)$$

$$v_r = - \frac{C w_\infty^2}{g} \left(\frac{\partial v_l}{\partial r}\right) \qquad (5.21)$$

Equations (5.18) to (5.21) can be solved for the developing void profile if a liquid profile is given and assumed to be fully developed.

In summary, the previous analyses are all limited by assumptions such as fully developed flow, or require a known void or velocity profile, primarily because the analyses are based on simplified subsets of the governing equations. A more generally applicable approach would be to solve the full set of equations (5.9) and (5.10), using a more general model of the turbulent stresses.

5.3 Modelling the Turbulent Stresses in Two-Fluid Flow

The previous studies described have established that for bubbly flow, the liquid phase turbulence field determines the distribution of the gaseous phase. This is not a surprising conclusion as it is evident that in the bubbly flow region the inertia of the liquid is clearly dominant, a typical weight fraction for atmospheric air water flow at 20% void being approximately 0.0005. In this analysis, we will follow the previous authors in assuming that the liquid stress is predominant, and in particular will follow Drew and Lahey in assuming that the vapour stress field is a simple multiple of the liquid stress field. In the theory of particulate suspensions, see for example Apizadis (1985), it is common to assume that for the particulate phase this multiple is zero, and this assumption is often used for bubbly flow, Biesheuvel and Van Wijngaarden (1984). However, it is also logical to assume that the multiplier is the void fraction, Rietema and Van Den Akker (1983), this having the additional advantage that the two momentum equations sum to the appropriate single-fluid equation if the fluids are identical.

Both of these possibilities have been considered in the current study, however results were always very similar. An assessment of the magnitude of the terms in the momentum equations reveals that for the gaseous phase the only important terms are those due to pressure gradient, gravity and momentum exchange; the others are insignificant by comparison. It would be quite possible to obtain a good solution of the two fluid equations using only these terms in the gaseous momentum equation providing the density ratio ρ_l/ρ_g was very large as for water and air, and that full separation of the air never occurred. However the full equation has been retained in the current study to maintain generality. See Appendix B for further comments on this.

Although a number of length scale models have been proposed to compute the effective turbulent viscosity in single fluid flow, Schlichting(1979), these are not regarded as general. A two equation model of turbulence, the k-ε model, Launder and Spalding (1974), has gained widespread acceptance by giving reasonable predictions for a number of flow situations.

Cook and Harlow (1984) have used a length scale model in their two dimensional equations, however, they recommend use of the k-ε model for future studies. Ellul and Issa (1986) also use the k-ε model for two-fluid flow. Neither publication offers any quantitative justification for this choice.

The k-ε model was developed for single phase flow, and is not directly applicable to two phase conditions. Modifications to the k and ε equations to incorporate the effects of momentum interaction between dispersed and continuous phases are discussed by Sun and Faeth (1985). Unfortunately these involve further empirical constants yet to be determined. Furthermore, as discussed above, the momentum interaction between phases is not confined to the drag force, but also includes virtual mass forces and the Bassett history force. Both of these latter forces are difficult to evaluate with force. Both of these latter forces are difficult to evaluate with confidence, and as they are also transient in nature, they are usually omitted from steady state analyses. However they are probably active in two-phase turbulent flow and may play a significant role in increasing the effective turbulence above that expected for the liquid flow.

In one dimensional analyses, this increase in effective turbulence is commonly catered for by introducing a two-phase multiplier to compute frictional pressure drop in two phase flow, and correlations for two phase multipliers are well established.

In the current study, the increase in effective turbulence due to the phase interaction has been related to this established method instead of the more unusual method of Sato et al, who add the term involving bubble rise velocity equation (5.14), particularly as this equation was found in the current study to introduce excessive viscosity.

Among the numerous methods of evaluating the two phase multiplier, the method of Chisolm and Sutherland (1969) was developed to permit a more straight-forward analytical sequence than earlier methods.

In this method the two phase multiplier ϕ^2_{LO} is formulated as follows:

$$\phi^2_{LO} = 1 + \frac{C}{x} + \frac{1}{x^2} = \frac{\Delta P_{TP}}{\Delta P_{FL}} \qquad (5.22)$$

$$C = \eta\sqrt{(\rho_g/\rho_1)} + \sqrt{(\rho_1/\rho_g)}/\eta \tag{5.23}$$

$$X = \sqrt{(\Delta P_{FL}/\Delta P_{FG})} \tag{5.24}$$

$$\eta = U_g/U_1 \tag{5.25}$$

The parameter X, Lockhart and Martinelli (1949), can be evaluated using standard equations for friction factors. The usual impediment to using this sequence is the evaluation of the slip ratio η. However in a two fluid analysis, η is available, so the evaluation can be completed readily. For the conditions of interest in the current study ϕ^2_{LO} is calculated to be approximately 3, which is the same as obtained by Sato et al for $(\mu_B+\mu_T)/\mu_T$, equations (5.15) and (5.16). Hence this method can be applied to equation (5.9) instead of using equation (5.16).

However equation (5.16) is not general, and was also found to give excess viscosity in the current study even for the liquid, so the k-ε equation was applied to the liquid field, by applying equations 2.40 to 2.44, replacing ρ with $(1-\alpha)\rho$, and μ with $(1-\alpha)\mu$. This is equivalent to applying the homogeneous two-phase multiplier

$$\phi^2_{LOH} = \rho_L/\rho_M = 1/(1-\alpha) \cdot \tag{5.26}$$

Hence a further multiplier ϕ^2_{NE} must be applied to incorporate non-equilibrium effects,

$$\phi_{LO}^2 = \phi_{LOH}^2 \, \phi_{NE}^2 . \tag{5.27}$$

The use of the k-ε equation has the further advantage that the wall model is already incorporated in the standard exponential manner. The net effect of this model is that equation (5.14) becomes:

$$\tau_E = (\tau_L + \tau_T)(1 + \tau_b/(\tau_L + \tau_T)) = (\tau_L + \tau_T)\phi_{NE}^2 \tag{5.28}$$

5.4 Computed Results for Vertical Flow

Vertical flow can be regarded as effectively axisymmetric, and ~~so can~~ be simulated using only two dimensions. However, the following computations were completed using the 3D FAITH code with three circumferential divisions. This is the minimum that the code logic handles without further modification, and also served to confirm symmetry of computation.

Comparison to the Velocity Profiles of Malnes (1966)

Velocity and void profiles were measured by Malnes for a number of different void fractions at two different velocities in a vertical pipe 46 mm in diameter. In addition to the peaking of the void profiles near the wall, he noticed that the velocity profiles were flattened considerably in comparison to the profiles in single-phase flow. Profiles as given by Malnes are shown in Figure 5.1, together with results computed in the present study. Note that the computed results clearly duplicate the flattening of the velocity profiles, and agree well with the measurements. Flow conditions for each case are given in table 5.1 for reference purposes. Void and velocity profiles were measured in separate experiments, but as the flow conditions were not exactly the same for each, discussion of the void profiles is left to the following section.

Comparison with the Analysis and Data of Sato, et al. (1981)

Sato et al. compare their analysis to their own data and the data of several other experimenters including Malnes, Serizawa et al., and Inoue et al. As noted above, their analysis computes the liquid velocity profile from a known void profile, however both void and velocity profiles are computed in the current study. In Figure 5.2 these computed profiles are compared to the data of the four experimenters and also to the velocity profiles predicted by Sato et al. Note that the velocity profiles computed by the current method are in as good agreement as those computed by Sato et al. from the measured void profile. The void profiles computed by the current method show the characteristic peaking near the walls, and in general the relative magnitude of the peaks for various cases is also reproduced. However, the void peak is computed to be too close to the wall. Beyerlein et al.(1985) hint that they experienced a similar problem, and had to modify their calculation at the wall but do not give details. However the computed velocity profiles were not sensitive to minor changes in the void fraction in the near wall region.

Comparison to the Results of Serizawa et al.(1975)

Only Serizawa et al. reported measured profiles of void, liquid velocity and bubble velocity. Profiles for two cases computed in the current study are compared to these measurements in Figure 5.3. Note that the agreement in velocity profiles is quite good, and that the near wall peak in void fraction is again reproduced, but is too close to the wall.

TABLE 5.1

Flow Parameters for the Experiments

Case	w_{lo} m/s	w_{go} m/s	α	X %	P MPa	T ^{o}C	d_b mm	D mm	Experiment	Remarks
1	1.0	0	0		.14	20	—	46	Malnes (1966)	Case 2 & 3 Omitted
4	1.0	.417	.261		"	"	4	"	"	by Malnes
5	1.0	.707	.366		"	"	"	"	"	
6	1.5	0	0		.16	"	—	"	"	(Brackets) denote
7	1.5	.197	.105		"	"	4	"	"	valves assumed or
8	1.5	.470	.222		"	"	"	"	"	computed by Sato
9	1.5	.591	.260		"	"	"	"	"	
10	0.32	.085	.15		(.15)	(20)	(4)	40	Inoue (1976)	Reported by Sato (1981)
11	1.0	.243	.173		.115	30	4.6	26	Sato (1981)	
12	1.03	.277	(.178)	.034	(.10)	(20)	(4)	60	Serizawa (1975)	
13	0.74	.04	(.040)	.012	(.10)	(20)	(4)	60		
14	1.0	0.02	0.02		.115	20	2.4	51	Beyerlein (1985)	

5.5 Summary of Vertical Flow Modelling

The current analysis solves the full three-dimensional equations of two fluid flow and is able to predict the salient features observed in bubbly flow in vertical pipes. Because previous analyses have used only subsets of these equations, they have been limited in application to vertical flow, and to computing liquid velocity profiles from a known or assumed void profile or vice-versa. The current analysis encompasses these subsets but is not so limited and is able to compute simultaneously the distribution of void and liquid and gaseous phase velocity. The peaking of the void profile near the wall in vertical flow is reproduced in the analysis, but the computed peak is always in closer proximity to the wall than observed in the experiments, showing that a mechanism which causes radial migration of the void in proportion to the radial velocity gradient of the liquid axial velocity is incorporated in the model. However, the mechanism which limits this migration in close proximity to the wall is not, and thus requires further investigation, perhaps by adjusting the existing coefficients, but, more likely by incorporating further empirically based terms. The void peak near the wall could not be reproduced by using a large, constant effective viscosity, a viscosity gradient was required. This is in agreement with the observation by Sato et. el.(1980), that bubbles in glycerine congregated near the wall but also caused departure from laminar flow characteristics.

In general, the liquid and gaseous phase velocity profiles computed by the current analyses were in as good agreement with the data as were the results of a specialized analysis. This gives reasonable assurance that, although the model cannot be regarded as a definitive representation of two-phase turbulence, it can be regarded as a useful approximation tool and be used effectively to simulate flow in the other configurations to be addressed.

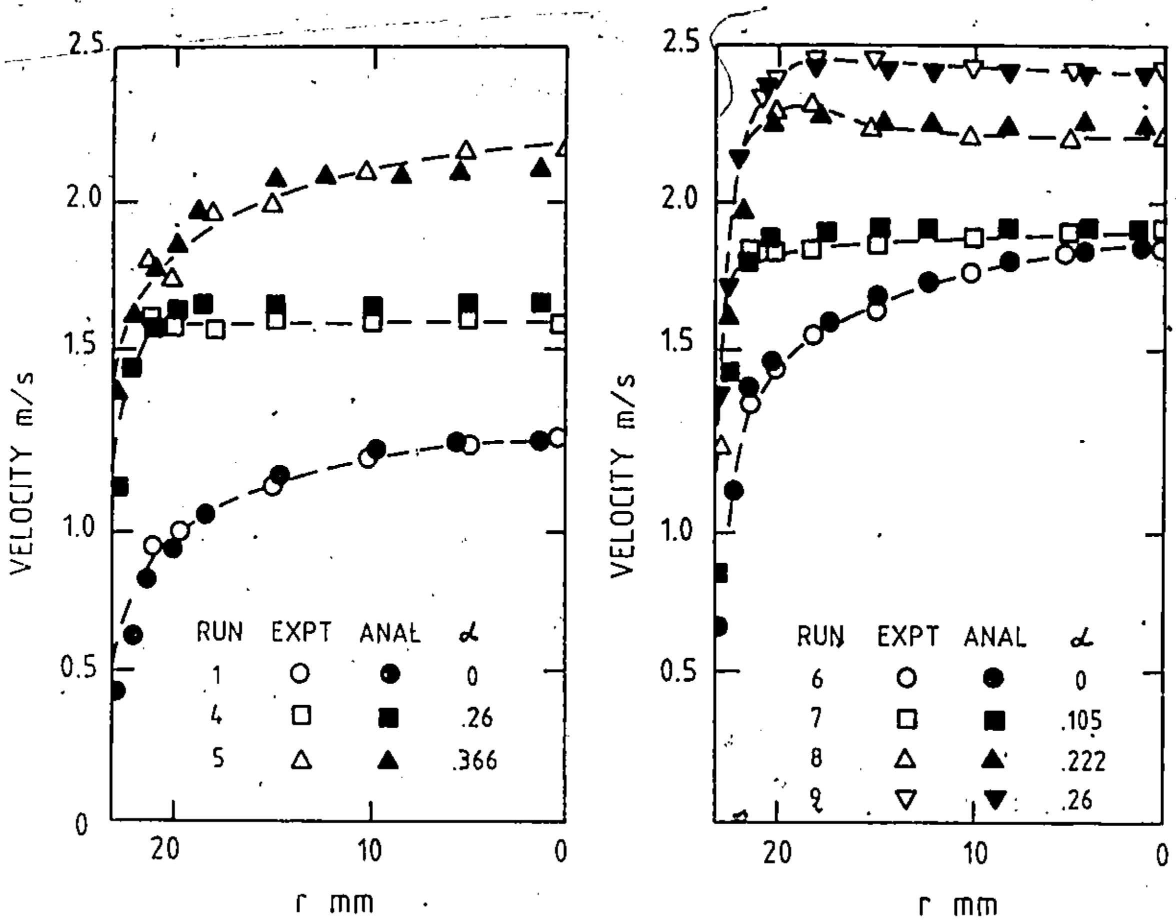

Fig. 5.1 Comparisons of Computed Liquid Velocity Profiles with the Measurements of Malnes (1966)

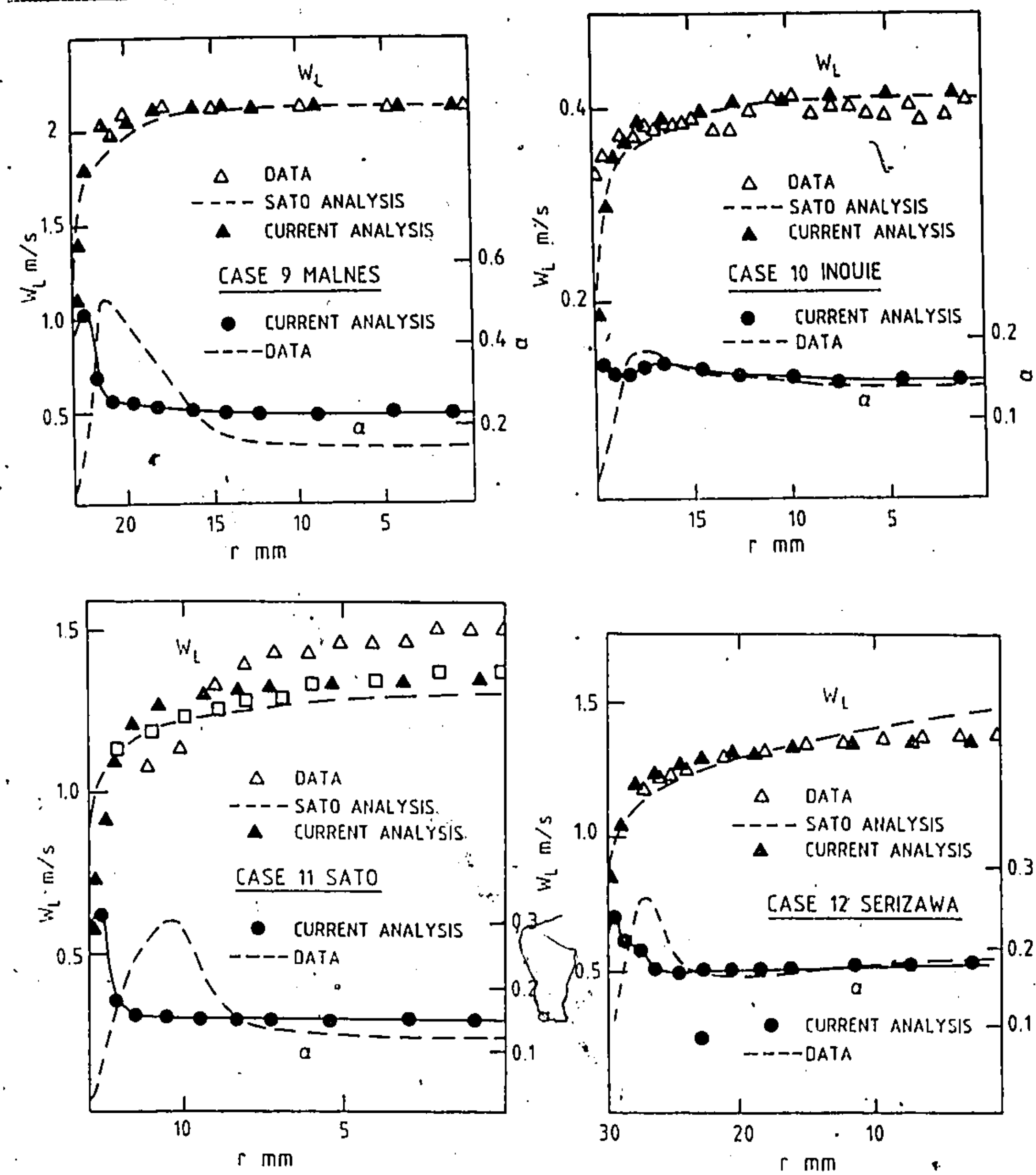

Fig. 5.2 Comparison of Computed Liquid Velocity and Void Profiles to the Various Experiments and Analysis of Sato et al (1981)

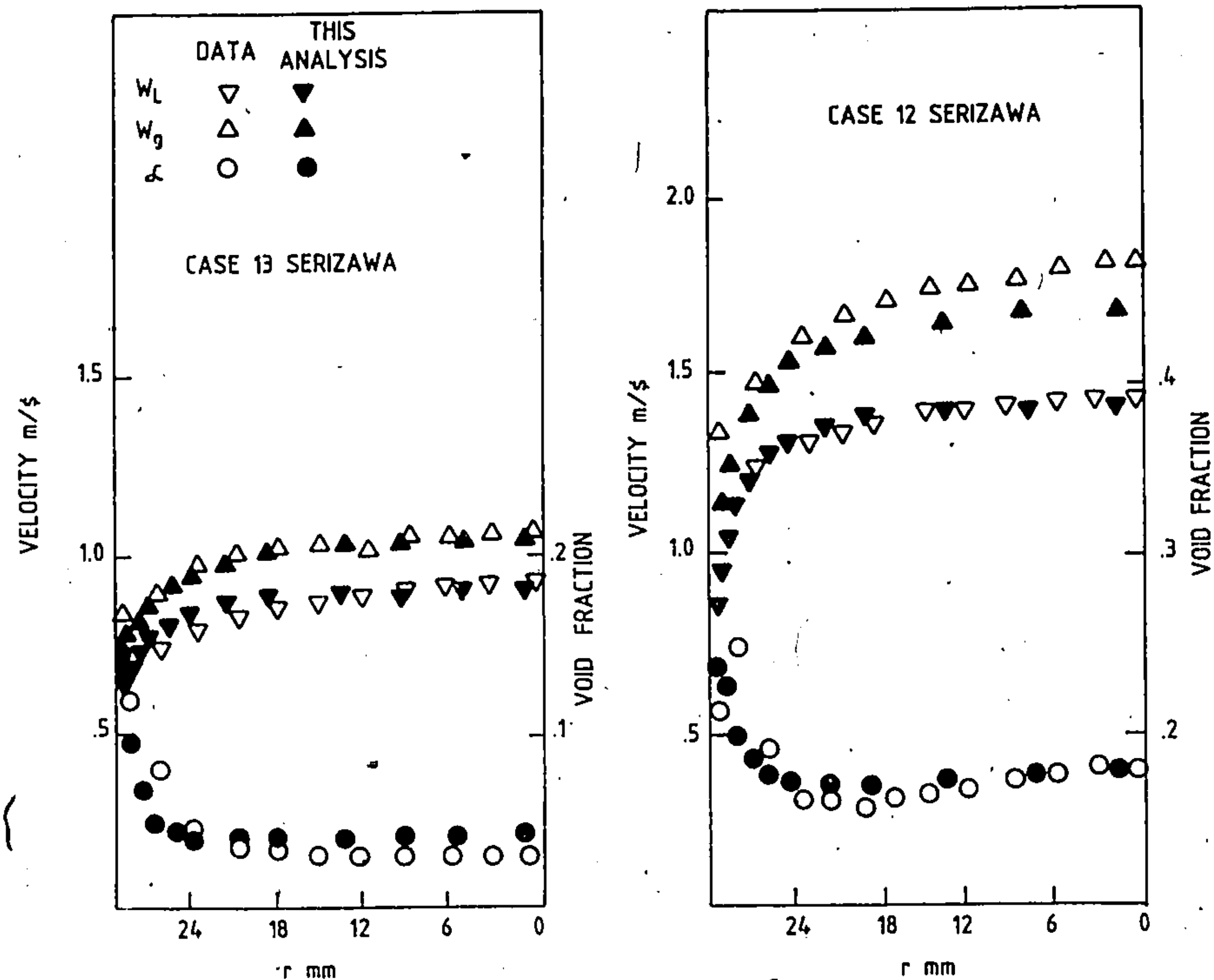

Fig 5.3. Comparison to the Experiments of Serizawa (1975) of Computed Liquid Velocity, W_L Gaseous Velocity W_g and Void Profiles α

CHAPTER 6. DETAILED 3D MODELLING OF PHASE DISTRIBUTION AROUND OBSTRUCTIONS IN HORIZONTAL PIPES

Having demonstrated in chapter 3 that the two-fluid model can reproduce the trends observed in two-fluid flow around obstructions, and in chapter 5 that the model can also be used to simulate velocity and phase distribution in bubbly pipes, attention is now turned to detailed modelling of flow in horizontal pipes with obstructions.

Recent experiments reported by Salcudean, et al (1983) studied the effect of flow obstructions and pressure drop in horizontal flow of air and water. These experiments showed that a flow obstruction causes a sequence of inter-related phenomena:

(i) sudden pressure drop

(ii) subsequent partial recovery

(iii) significant mixing of the two fluids in the recovery zone

(iv) significant reduction of the air velocity in the recovery zone

(v) an eventual return toward stratification.

Similar observations were reported by Gardner and Neller (1970) and Salcudean and Leung (1984), but detailed measurements of void distribution were taken in neither case.

It is of interest to know whether a two-fluid model can simulate these phenomena. The study, discussed in Section 3 showed that all these phenomena could be simulated in concept using the two-dimensional two-fluid computer program. No attempt was then made to simulate specific experimental conditions, as the problem is clearly three-dimensional in nature. However, the two-dimensional analysis did reproduce the appropriate trends, and the results were sufficiently successful to suggest that a three-dimensional analysis would reproduce quantitative comparisons. The following describes the extension of the previous study to three dimensions and compares computed results to those obtained by Salcudean et al (1983).

It is apparent from the experiments of Salcudean et al (1983) that even when the flow approaching an obstruction is in the bubbly regime, considerable increases in void fraction occur downstream of the obstruction, often to higher voids than those normally associated with bubbly flow. It is therefore necessary to extend the model of interphase drag to address these conditions.

6.1 Extension of the Interphase Momentum Model

This study was restricted primarily to bubbly flow as interphase forces can be simulated from an approximation based on the drag of bubbles. Conditions for bubbly flow can be established from flow regime maps for vertical or horizontal flows and correspond roughly to fairly high liquid superficial velocities and fairly low gaseous superficial velocities, hence low void fractions.

The formulae for interphase drag have been introduced in chapter 3, equations (3.7) to (3.11). It is now necessary to elaborate further.

The relative velocity V_r is given by

$$|V_r| = \left[\Sigma \, (U_l - U_g)_i^2 \right]^{1/2} \tag{6.1}$$

The bubble size diameter is discussed in Appendix B, as are some recommended formulae for drag coefficient $\bar{C}_d$. The recommended formulae are:

$$d_b = 2 \, \{\sigma/g(\rho_f - \rho_g)\}^{1/2} \tag{6.2}$$

$$C_d = 6.3 \, Re_b^{(-.385)} \tag{6.3}$$

These equations apply only in the bubbly flow range. The distribution pattern departs from bubbly flow when gaseous flow is increased, and bubbles coalesce. The sequence of flow regimes is different for horizontal and vertical orientation, and is quite complex in each case. Both horizontal and vertical flow incorporated the feature of transition from bubbly through mixed bubble and slug region to annular flow. In our model, for $\alpha<\alpha_{bs}$ all the gaseous flow is in bubbles, for $\alpha>\alpha_{sa}$ all the gaseous flow is in one large slug of diameter $d_s = d\sqrt{\alpha}$ which approximates annular flow. For $\alpha_{bs}<\alpha<\alpha_{sa}$ the gaseous flow is contained in slugs each accompanied by trailing bubbles.

The void fraction is thus composed of bubbles and slugs, such that $\alpha = \alpha_b + \alpha_s$, and it follows that

$$\alpha_b = \alpha_{bs}(\alpha_{sa} - \alpha)/(\alpha_{sa} - \alpha_{bs}) \tag{6.4}$$

$$\alpha_s = \alpha_{sa}(\alpha - \alpha_{bs})/(\alpha_{sa} - \alpha_{bs}) \tag{6.5}$$

The interfacial area for each component follows, and the drag force per unit volume is the sum of the bubble and slug components

$$\psi V_r = F_b A_b N_b + F_s A_s N_s \tag{6.6}$$

A more complex drag model is used in the TRAC system code, Rohatgi and Saha (1980); however, Kelly and Kazimi (1982) have recommended simplifications to this model for the THERMIT subchannel code. The current model is closer to that used in the RELAP5 system code, Ransom et al (1981), where the drag coefficient of the slug is taken to be constant, and is also similar to that used by Egely and Saha(1984). However, in each of these cases, the models are applied to cross-sectional averaged values in a channel. In the FAITH code, however, relationships are used locally throughout a three-dimensional grid. Although the local values of void fraction vary widely, the cross-sectional variation is much smaller. It is not clear therefore whether the local flow pattern is determined by local or overall flows. Quite probably the overall flow is more important, and bubbly flows can exist even when the local void fraction is quite high due to separation forces, providing the overall flow ratios are characteristic of bubbly flow.

Equations (3.7-3.11,6.1-6.6) were used to simulate interphase drag in the FAITH code, and the transition voids, α_{bs} and α_{sa}, were left as parameters to permit the use of local or overall criteria for transition.

Finally, the use of molecular viscosity alone in the viscous terms was not satisfactory, as it led to anomalous velocity and void profiles, so an effective turbulent viscosity as discussed in chapter 5 was used.

As most of the models reported are one dimensional, the use of effective viscosity does not usually arise, neither does its possible interaction with the interphase drag function. Clearly the two should interact, and in these studies,the results shown had the interphase drag function linked to effective viscosity by using the latter in the Reynolds number in the drag formula. This increased the interphase friction in the vicinity of the walls and gave more realistic void profiles than when the interaction was neglected. Neglection caused excessive migration of void to the walls.

6.2 The Flow Blockage Experiments

The experiments reported by Salcudean et al (1983) are recorded in greater detail by Chun (1983). The test section was a 25.4 mm i.d., 3 m long plexiglass tube. Air and water entered at selected flow rates through a mixer and a further 3 m approach length, to ensure established horizontal flow at the test section.. Peripheral and central obstructions each blocking 25% of the flow area, were used separately. Pressure was measured at 23 stations, shown in Figure 6.1.

Distribution of void fraction was measured at the three axial stations shown by taking measurements at 99 points over the cross-section using an optical probe. The void profiles measured for bubbly flow are shown in Figure 3.8, along with the derived average values of void fraction and slip ratio ($\eta = w_{air}/w_{water}$).
Note that the central blockage causes a greater disturbance to the flow distribution than does the peripheral obstruction, and that the obstruction causes a local increase in void and decrease in slip.

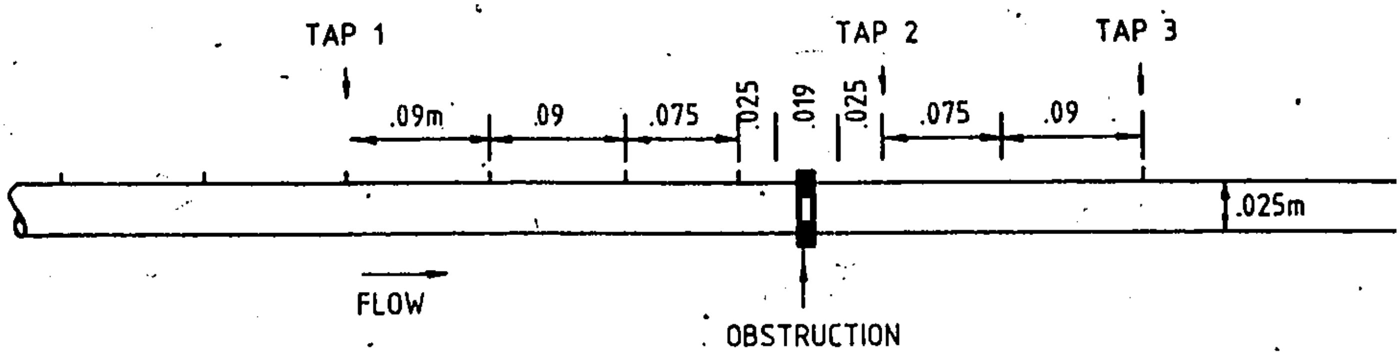

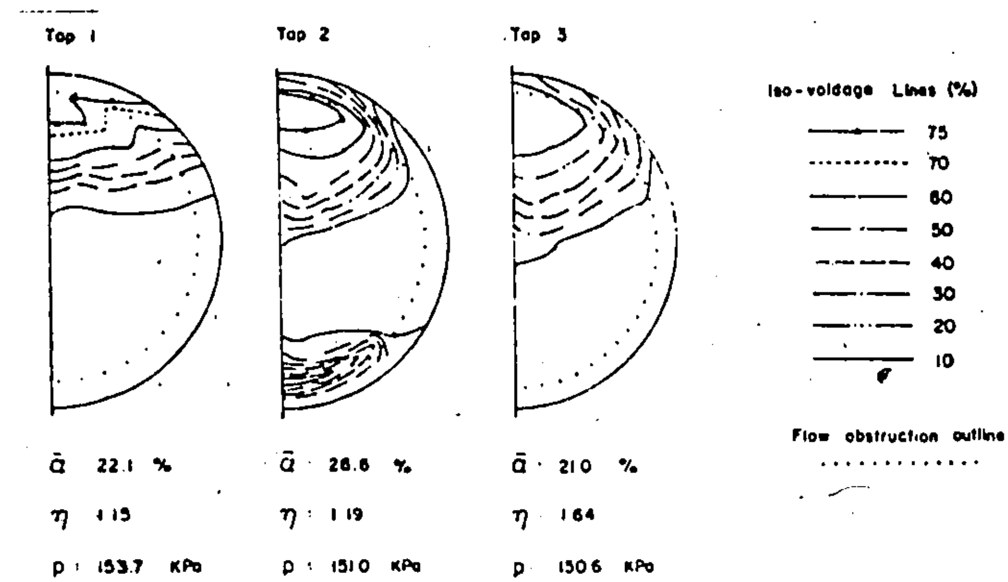

(a). Change of void distribution. Peripheral obstruction. Bubbly flow. Water: 1.1 kg/s. Air: 0.000775 kg/s. Quality: 0.0704%.

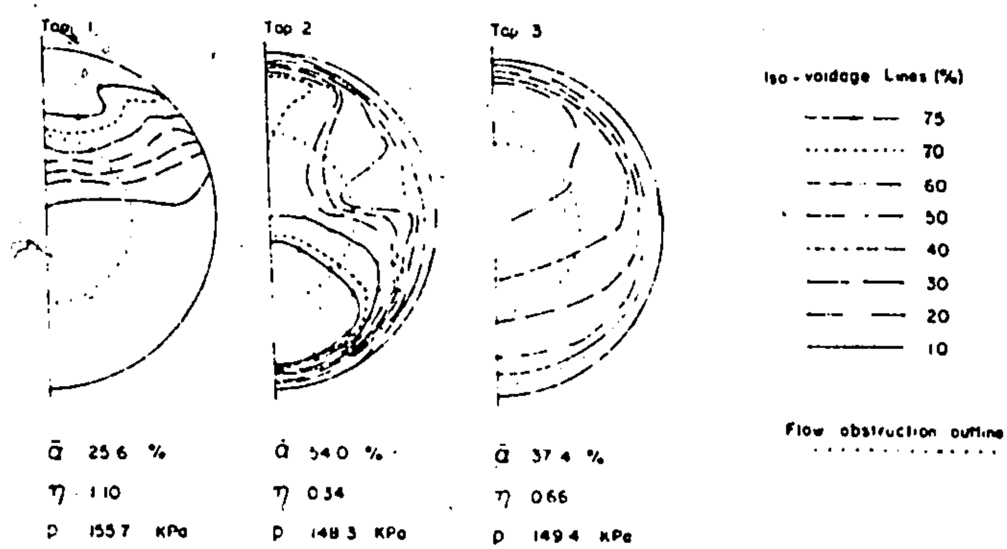

(b) Change of void distribution. Central obstruction. Bubbly flow. Water: 1.1 kg/s. Air: 0.000775 kg/s. Quality: 0.0704%.

Fig. 6.1 Test Section and Measured Void Profiles For the Obstruction Experiments of Salcudean et.al.(1983)

6.3 Simulation Results

The calculations were completed on a r,θ,z grid of 13x11x25 grid which taxes the memory capacity of the CRNL CDC 175 computer. Because of this, only minor changes in grid division could be made, however the flow redistribution caused by the orifices is quite pronounced, and the overall features did not seem sensitive to these grid changes. However in detail the recirculation fields did change, and in particular, in order to simulate the establishment of flow upstream of the test section, it was necessary to compute the approach flow pattern in a separate calculation involving no flow blockage. As this upstream portion is a parabolic flow field, these computed conditions could be used as input to the test chapter containing the obstruction. The latter clearly requires an elliptic calculation due to the recirculation effects.

6.3.1 Pressure Profiles

In the simulation of the experiments, it was first necessary to examine whether the multidimensional model adequately reproduced the measured pressure profiles. Computed values using the k-ε model are compared to the experimental data in Figures 6.2 and 6.3.

For the central block single-phase case, Figure 6.2a, the pressure profile appears to be calculated reasonably well, however the experimental pressure recovers slightly faster than is computed. For the two phase case, Figure 6.2b, it is apparent that the pressure gradients in the undisturbed flow are computed quite accurately, but that the obstruction pressure drop is overestimated, and the recovery length is underestimated. However these discrepancies are minor. Varying the parameters in the drag model d_b and α_{bs} did not greatly change the pressure drop or recovery length, but did slightly change the rate of convergence of the calculation.

For the case of the peripheral blockage however, the agreement is not quite as good. Figure 6.3a shows that the pressure drop associated with the peripheral blockage is slightly overpredicted in single phase. In two phase, Figure 6.3b, the computation over-predicts both the drop and the recovery length. Grid refinement in the radial direction did not improve the agreement. Although somewhat worse than the central block case, these discrepancies are not gross. It is known that for the case for single phase flow over a simple step, the recirculation cannot be simulated accurately unless numerical diffusion is reduced, either by using a very fine grid or by invoking skew differencing schemes, see for example Hackman et. el. (1984). The obstruction cases are more akin to the flow over surface ribs investigated by Benodeckar et. al.(1985), who made similar conclusions. Both these were single phase two-dimensional studies and are discussed further in Appendix B.

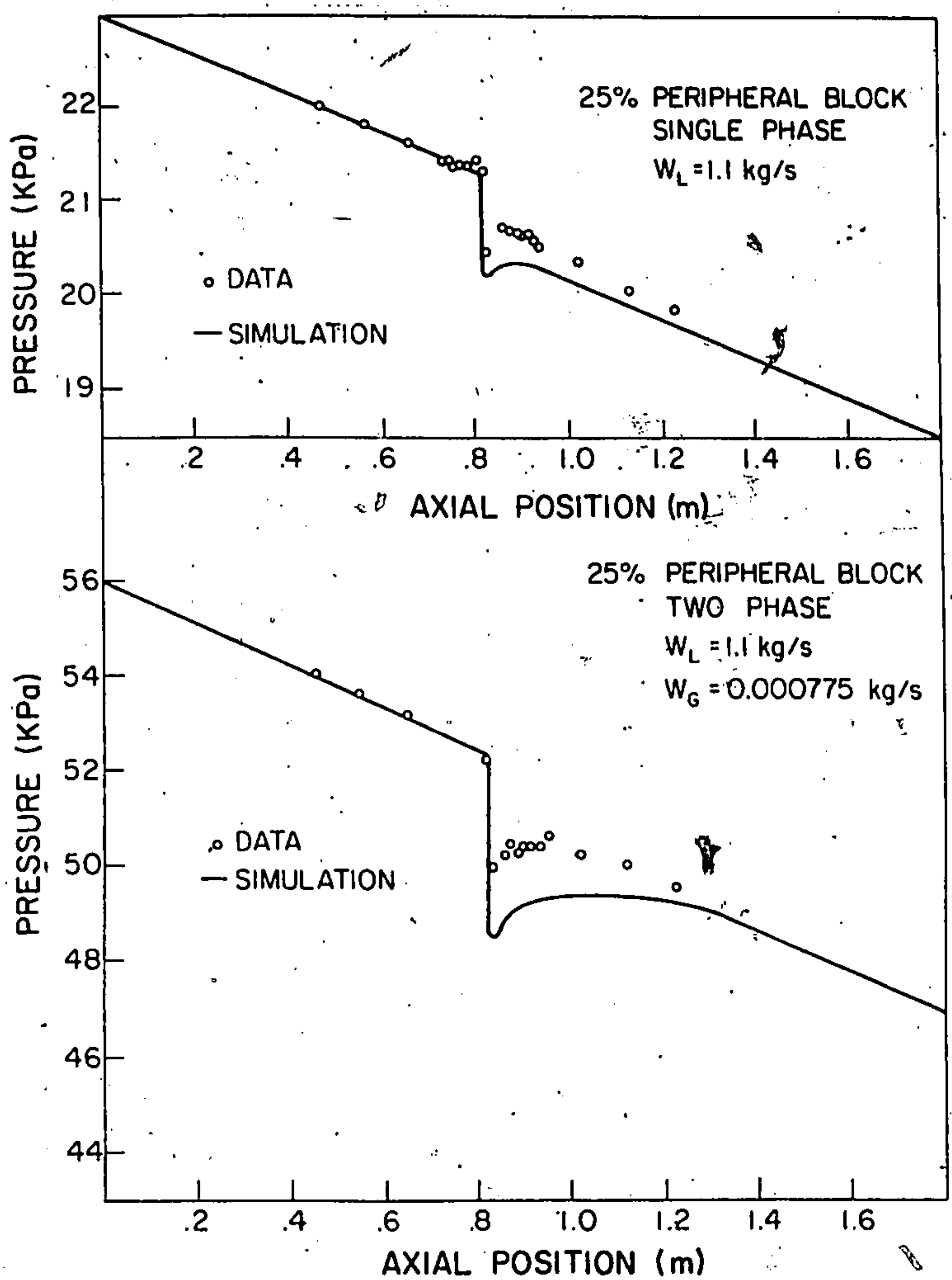

Fig. 6.2 Computed and Measured Pressure Profiles for Peripheral Obstruction

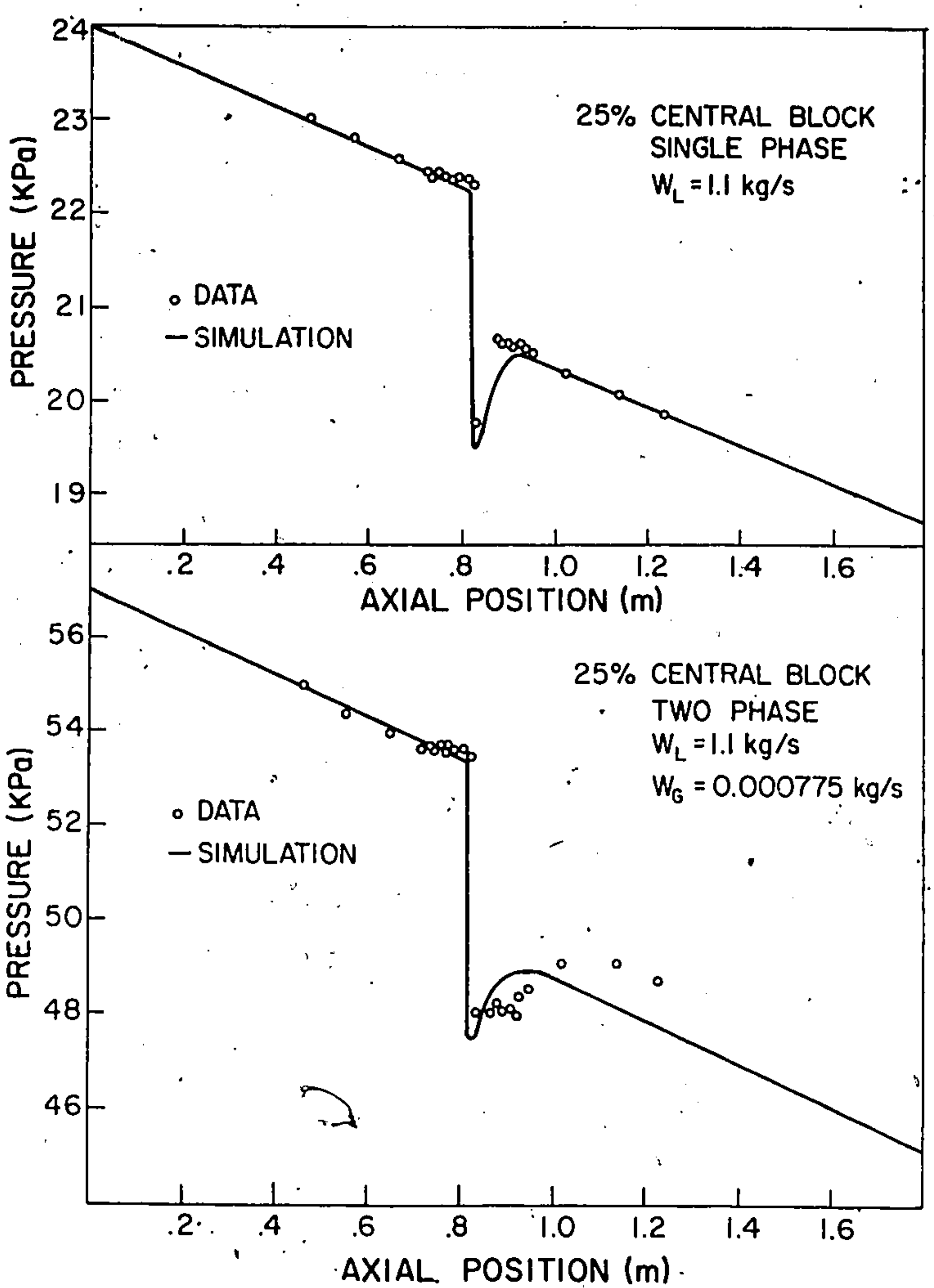

Fig. 6.3 Computed and Measured Pressure Profiles for Central Obstruction

6.3.2 Velocity and Void Distribution

Computed velocity fields in the plane of symmetry are depicted for the central and peripheral obstructions in figures 6.4 and 6.5 respectively. The figures show the vector fields on the plane of symmetry for each fluid. In order to better illustrate the cross flows and the distinctly different velocity fields in the two phases, the radial velocity scale factor is twice that for the axial velocity. The initial void fraction is uniform, so the tendency toward stratification at fully developed flow is observed.

The obstructions only slightly affect the flow patterns upstream. As expected, the central obstruction causes a divergent deflection, while the peripheral obstruction causes a convergent deflection. Downstream, the restoring tendencies are, of course, opposite. For the central obstruction, the downstream restoring velocities are generally downward in the upper half of the channel where most of the air resides, tending to drive this air back towards the centre of the channel and produce the enhanced mixing observed in the experiment. By contrast, the peripheral obstruction generates upward restoring velocities downstream in the upper regions where most of the air resides, and as this is the preferential direction for air, the mixing effect is less pronounced. The diagrams also clearly show that the redistribution effects of the central obstruction persists much further downstream than for the peripheral obstruction, again as observed in the experiment and that the central obstruction creates a larger zone of recirculation. The flow around the obstructions shows that a zone of recirculation is formed in the wake, and air flowing into this zone causes a slow moving air pocket. This accounts for the high void region observed in both experiments and calculation.

Further details of the phase distribution are given in Figure 6.6, which shows computed void profiles for the central, and peripheral obstructions, and may be compared to Figure 6.1. While the individual computed contours do not show a precise match with the experimental contours, their combinations do exhibit a very strong similarity both in trend and detail. For the upstream pipe flow the computed values show a slightly greater amount of stratification and clearly this must also affect downstream results. Computed results show little change between stations just upstream of the obstruction, so flow can be considered to be established.

For the peripheral blockage, at tap position 2, just past the obstruction, both experimental and computed profiles show that air has been deflected outward and displaced downward by the obstruction, and significant void appears near the bottom of the channel. Both experimental and computed results show that by the time the downstream observation point, tap 3, is reached, the distribution has returned considerably but not completely towards the pattern established upstream.

For the central blockage, both experimental and computed profiles show considerably more redistribution at tap position 2. Again, there is a significant displacement of air downward, but this involves considerably more air. The computed values reproduce the larger concentration of air in the centre of the pipe, and do show an air pocket near the bottom of the pipe, but the latter is much less concentrated than in the experiment. At tap position 3, both computed and experimental plots show that the distribution has not re-established nearly as much towards the upstream condition as in the peripheral case.

Finally, the computed values of cross-sectional averaged void fraction and slip also show the same variation as reported in the experiment, with the slip ratio well below unity in the central blockage case. The computed increase in void for the peripheral obstructon is very close to that in the experiment. For the central obstruction the change in void and slip is computed to be somewhat less than the experiment. In view of the numerical and experimental uncertainties, the agreement between the computed and experimental values is quite good.

In order to illustrate the axial variation of average void and slip more completely, graphs of computed cross sectional average void fraction and axial velocity ratio (air/water) are given for the peripheral and central obstruction cases in Figures 6.7a and 6.7b. Note that the trends in void fraction and slip are again in agreement with the experiments in Figure 6.1. In particular, the slip can be seen to decrease markedly just downstream of the obstruction, with the overall void fractions varying inversely as expected. Again as in the experiment, the central obstruction causes a significantly greater disturbance than does the peripheral one.

Further downstream, recovery occurs with an associated increase in slip and decrease in void. The recovery is computed to be faster for the peripheral obstruction than for the central one, again as observed in experiment.

6.4 Summary of Results for Obstructions

The effects of two types of flow obstruction on the redistribution of the phases in horizontal flow of air and water have been simulated using a three dimensional two-fluid computer program. The program simulates all the following phenomena observed in experiments:

(i) the sudden pressure drop

(ii) the subsequent pressure recovery

(iii) the homogenization of the phases

(iv) the reduction of air velocity and increase in void fraction

(v) the eventual return towards stratification

(vi) the greater effect of the central obstruction compared to the peripheral one of equivalent area.

The quantitative agreement between the computed results and experiments is not precise, but is reasonable in view of the necessarily simple models used in the computer program, and the fact, as mentioned, that the high cross-flows induced by the blockage probably give rise to significant numerical diffusion, as discussed further in Appendix B.

This study is published in a paper accepted by Mathematics and Computers in Simulation, Carver and Salcudean(1987).

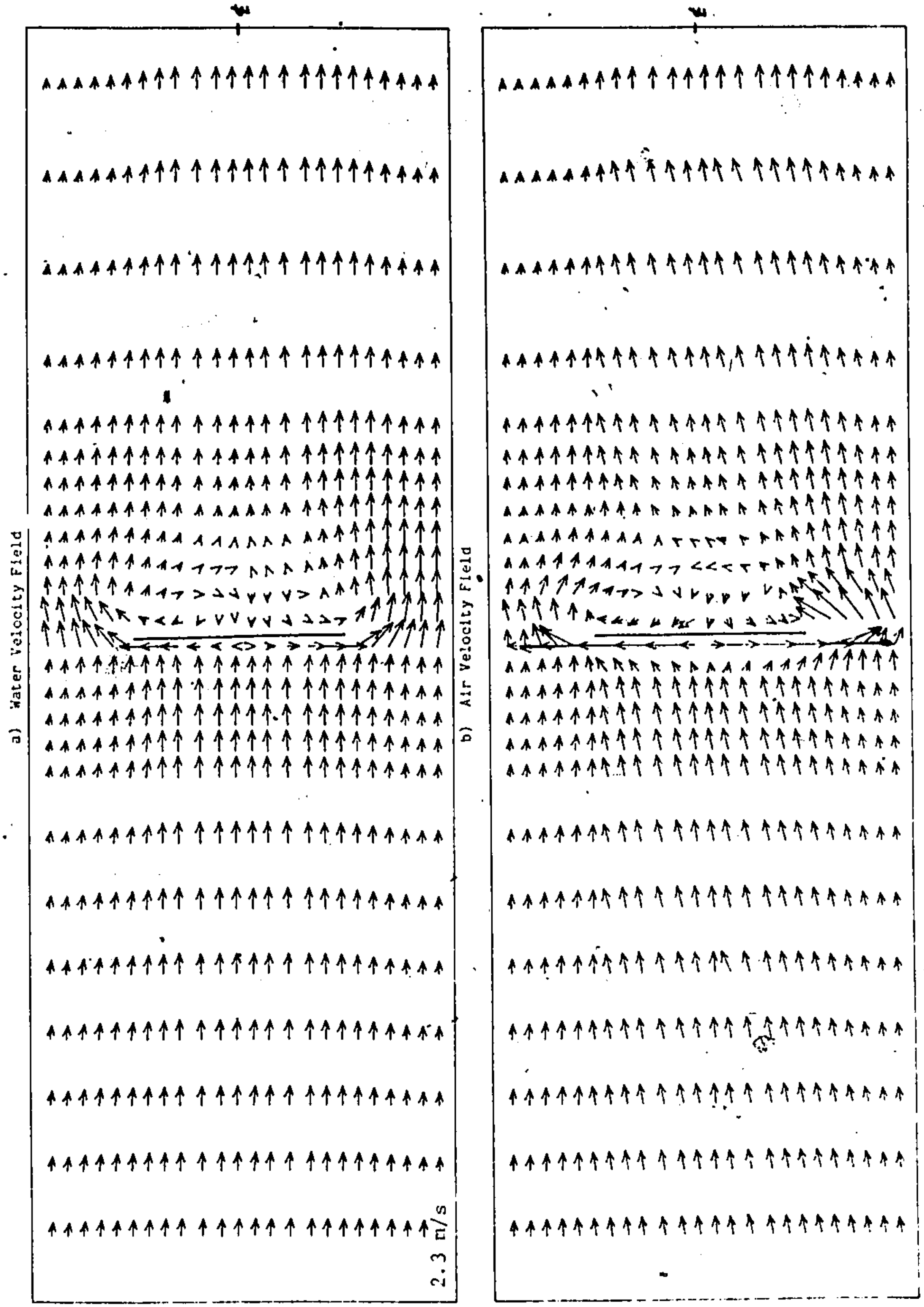

Fig. 6.4 Computed Velocity Fields in the Plane of Symmetry for Central Obstruction

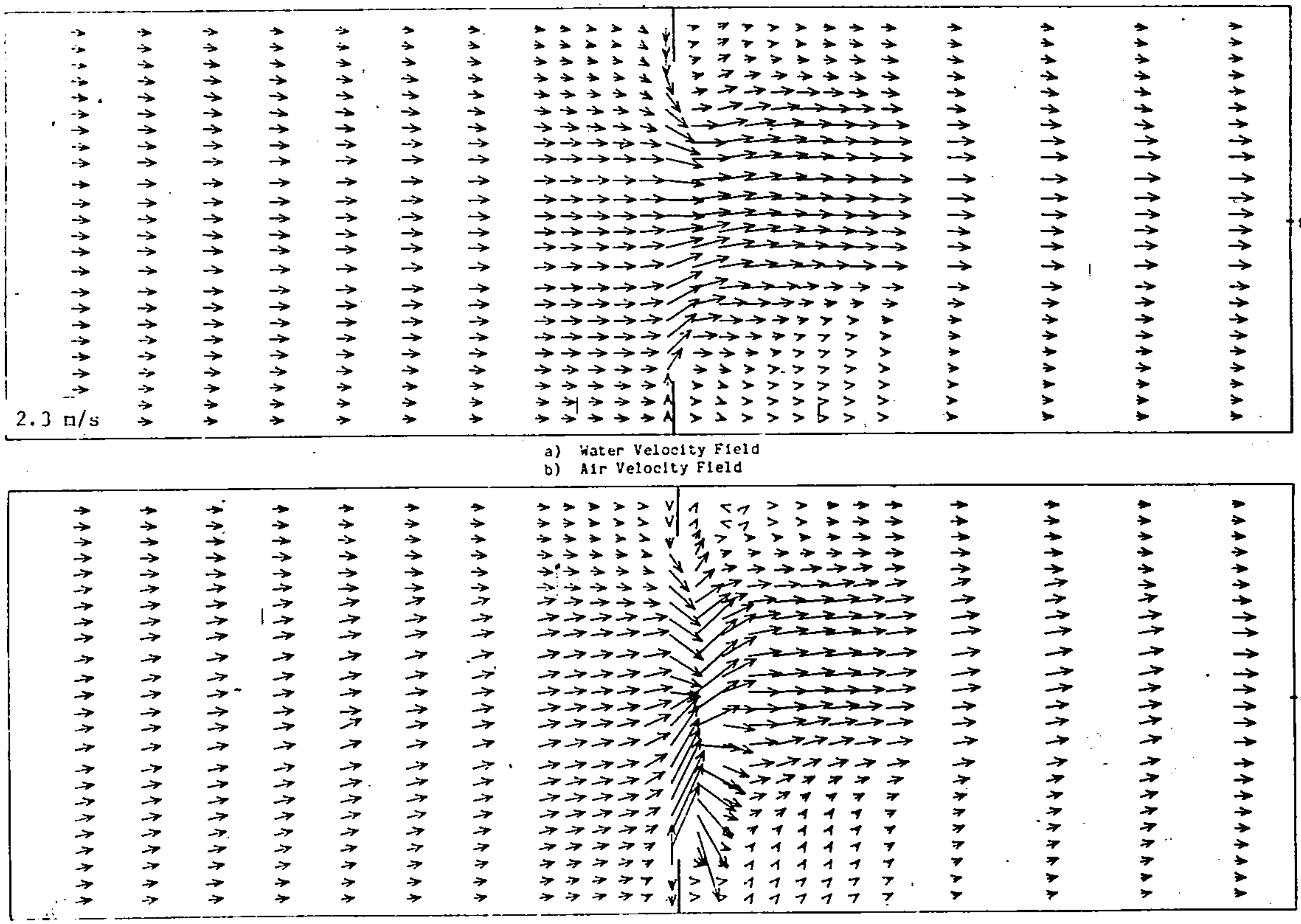

Fig. 6.5 Computed Velocity Fields in the Plane of Symmetry for Peripheral Obstruction

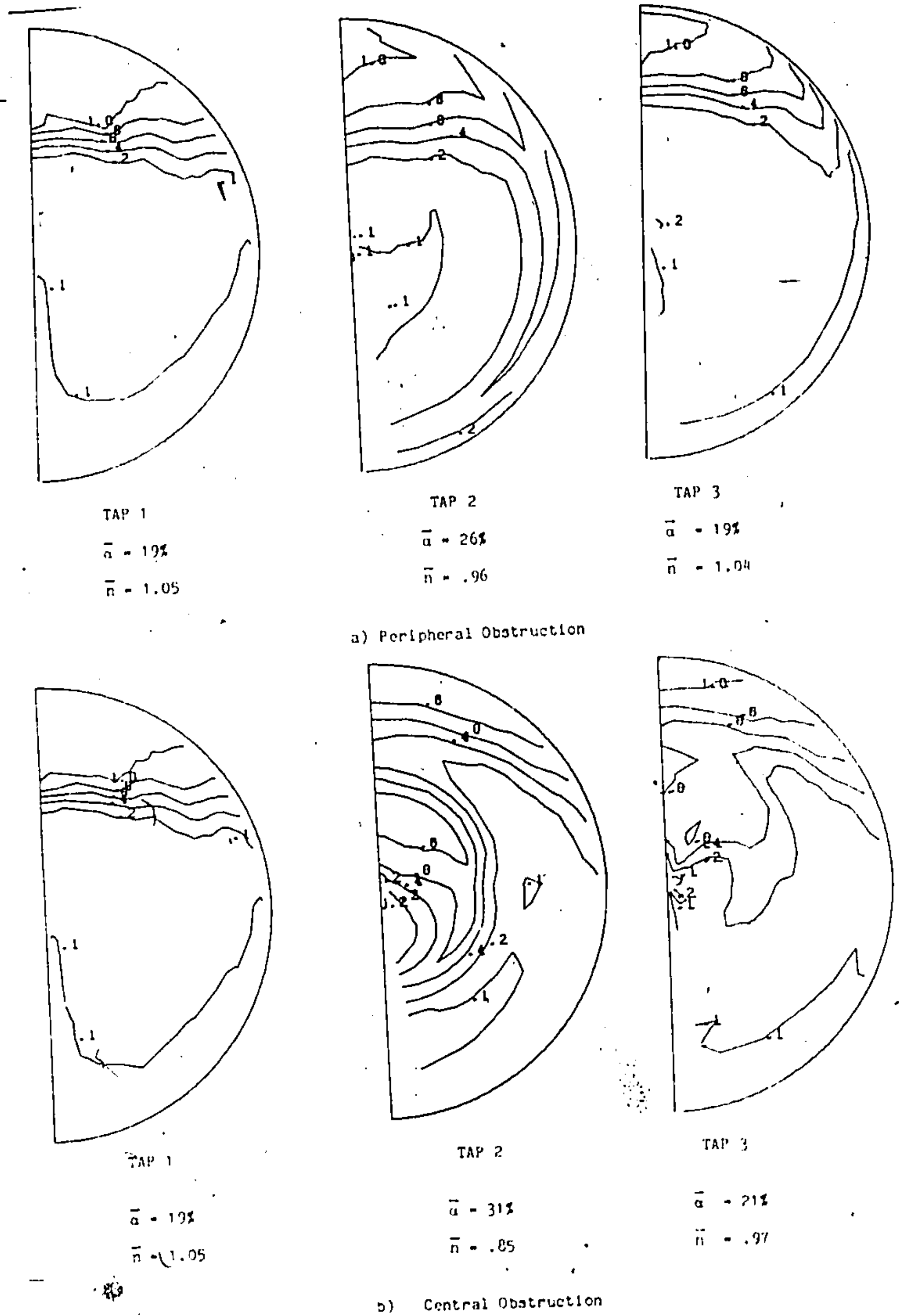

Fig. 6.6 Computed Void Distribution Contours

at Tap Positions 1 to 3

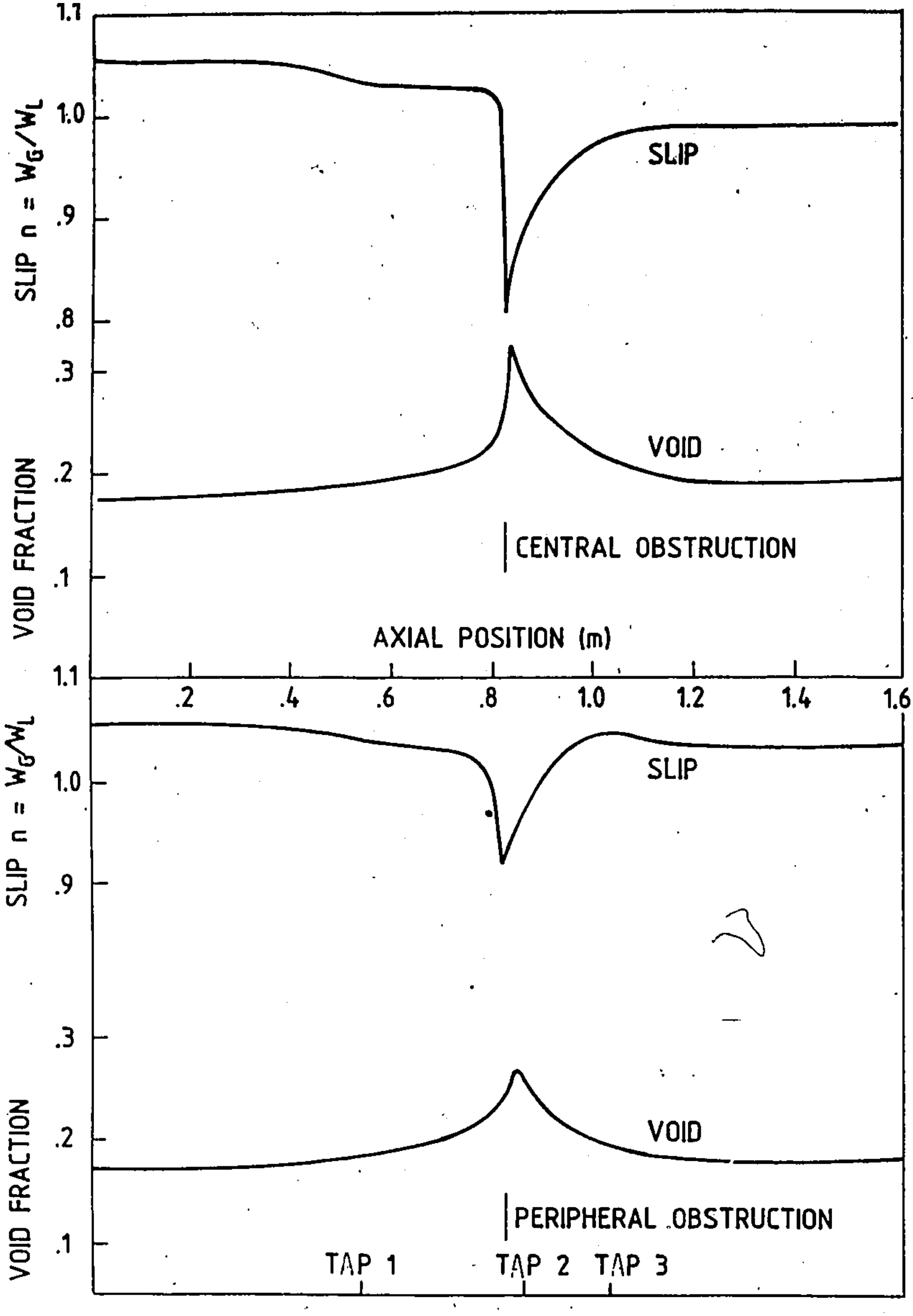

Fig. 6.7 Computed Variation of Average Void and Slip in the Neighbourhood of Obstructions

CHAPTER 7. DETAILED 3D MODELLING OF PHASE DISTRIBUTION IN BENDS

In chapter 3 a two-dimensional two-fluid simulation of phase distribution was presented as proof of concept, and in chapters 4 and 5 detailed modelling of bubbly flow in vertical pipes and horizontal pipes with obstructions was presented. Clearly in a bend, the flow undergoes continuous transition from horizontal through vertical stages, so reasonable results in simulations of both horizontal and vertical flows are prerequisite to a meaningful simulation of flow around a bend. This chapter reviews experiments in several types of bends, and gives results of detailed simulations.

7.1 Overview

Clearly the net effect of a bend in two-fluid flow is determined by the interaction of the centrifugal force with gravity and interphase friction. The change in flow distribution around a bend will therefore be a complex function of pipe and bend geometry, orientation, fluid densities and upstream flow conditions.

A literature survey reveals that although many experimenters have studied single phase flow and heat transfer in bends, relatively few have studied two fluid flow and phase distribution in bends, and only three experiments with detailed measurements have been reported. Gardner and Neller (1970) measured phase distributions in each of two 90° bends, Usui et al., (1980,1983) have reported phase distributions and limited data on slip in return elbows in horizontal and vertical positions, and Hoang and Davis (1984) have reported limited data on velocity profiles. None of these authors were able to suggest any correlation to predict phase distribution details, so it is necessary to use numerical simulation to obtain such predictions. Two dimensional calculations are incapable of reproducing the secondary flow pattern of circulation normal to the main flow direction, which is a well-known characteristic of single phase flow in bends, and has also been noted by Gardner and Neller in two-phase flow. This study extends the methods used in the two dimensional numerical simulation reported in chapter 3 to three dimensions, and shows that not only are the secondary flow patterns predicted, but that observed relationships between slip and void in bends are also reproduced, and that computed phase distributions agree reasonably well with measured data from the different configurations.

7.2 Single Phase Results

In order to check that the equations had been correctly implemented and solved, standard single phase problems, such as flow on a flat plate and developing flow in a duct were solved and the solutions verified. Finally solutions for single phase flow around bends were obtained and compared to results reported by Pratap et. al (1976).

Single phase flow in bends is characterized by the Dean number $K_d = R_e \sqrt{a/R}$ Dean (1927). Two particular cases were used. Results from the first, a laminar flow case, Mori and Nakayama (1967), are shown in Figure 7.1, and from the second, a turbulent case, Hogg and Seader, (1970) are shown in Figure 7.1. In each case the results are fully developed velocity profiles, and agreement is comparable to that reported by Pratap (1976) who used a similar cross-sectional coordinate grid, calculating only half the field by invoking symmetry about the bend radius. Also of interest are the classic secondary flow patterns set up in the cross-section. The computed cross-section flow vectors shown in the figures illustrate these secondary flows. Finally, the correct velocity profiles for turbulent flow cases cannot be obtained using molecular viscosity in the stress terms. An effective turbulent viscosity must be used. In these studies this was computed using the k-ε model of Launder and Spalding (1972), already discussed.

Figure 7.1 and 7.2 illustrate the axial flow velocity, normalized by the experimenters to average and centreline velocities respectively. The Θ=0 curve is the profile on the bend radius, whereas the Θ=90^0 curve shows the normal profile; only half of the latter is shown by reason of symmetry and to reduce clutter. The fact that the turbulent flow profile appears to be less distorted by the bend is related to both the undisturbed profile and the bend radius. In turbulent flow, the latter cannot be incorporated explicitly in a Dean number as for laminar flow, as an average effective viscosity would have to be used

$$(K_d = wd\rho\sqrt{(a/R)}/\bar{\mu}_c) \tag{7.1}$$

and no means of arriving at this quantity has been established in the literature.

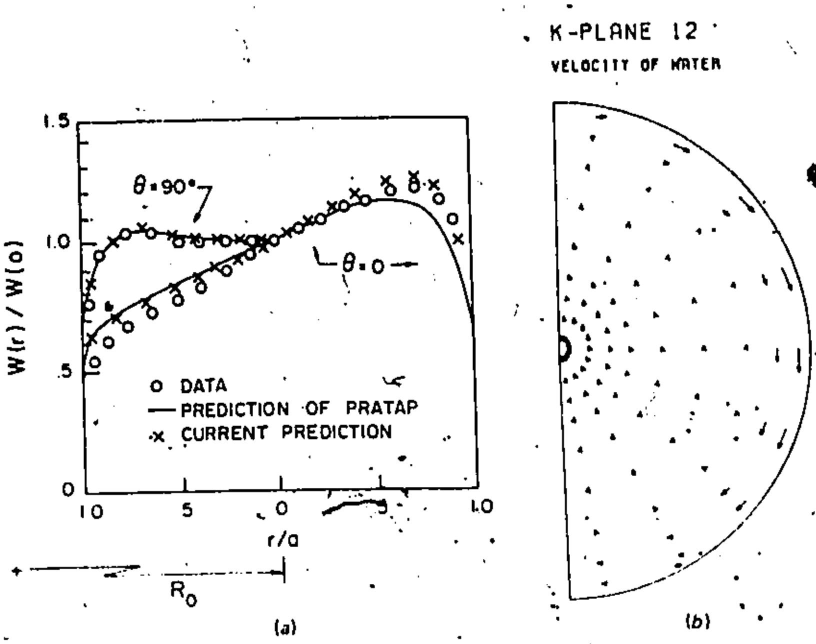

Fig. 7.1 Computed and measured values for fully-developed laminar velocity profiles in single-phase flow in a helix; $K_a = 632$, $R/a = 40$, Re = 4000. Data of Mori and Nakayama. Also shown are computed velocity plots showing secondary circulation.

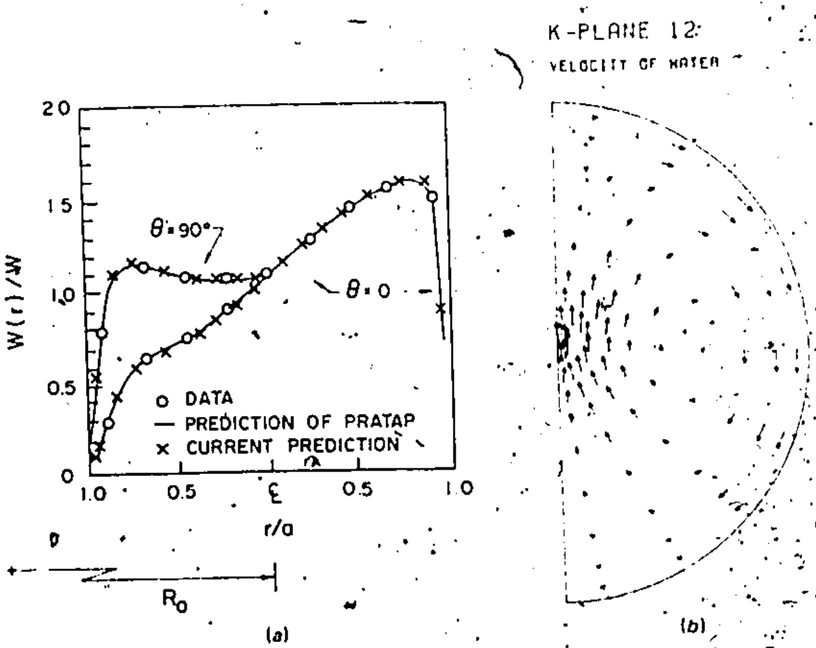

Fig. 7.2 Computed and measured values for fully developed turbulent velocity profiles in single-phase flow in a helix; $R/a = 20$, Re $= 6.8 \times 10^4$. Data of Hogg and Seader. Also shown are computed velocity plots showing secondary circulation.

7.3 Two Fluid Results

7.3.1 Modelling

In this study the turbulent stresses in the continuous liquid field were evaluated using the k–ε model modified as discussed in chapter 4, and the interphase drag model discussed in chapters 5 and 6.

Also for all computations it was necessary to provide sufficient length before and after the bend to ensure that steady profiles were established upstream and downstream.

7.3.2 Phase Distribution in Pipes and Bends

As discussed in chapter 3, in horizontal pipes, there is a tendency for the phases to separate due to gravity. The separation force is a simple function of density difference and gravity, and is resisted by the interphase friction and viscous forces. In a bend of radius R, the centrifugal force also plays a part in separation, thus for a bend in a horizontal plane, one would expect separation tendencies to increase with density difference and axial velocity, and to decrease with bend radius. Finally for a bend in a vertical plane, the separation force depends on the vectorial sum of the gravitational and centrifugal forces, which varies throughout the bend.

When centrifugal and gravitational forces interact, the direction of migration of the heavy fluid is determined by the ratio of the two forces, which can be expressed as a modified Froude number:

$$F_r = \overline{W}^2/gR'\sin\phi \qquad (7.2)$$

When F_r exceeds unity, centrifugal forces will dominate; however, while this simple criterion is useful to predict behaviour in a qualitative sense, it gives no quantitative indication of how much the phase distribution will change. Hitherto, only measurements could determine this information, but the following results show that three-dimensional computation also yields this quantitative information.

7.3.2 Flow in a C Bend in the Vertical Plane

Usui et al. (1980) have conducted experiments on two-fluid (air and water) flow in a C bend for both upward and downward flow. Detailed measurements are not given, but photographs are included for the downward flow case, and a sketch from their photograph of bubbly flow is given in Figure 7.3. In the C bend, gravity alone acts in the horizontal arms, counters the centrifugal force in the first part of the bend and augments it in the second half.

There is considerable stratification in the upstream horizontal arm, and as the flow enters the bend, the centrifugal force accelerates the heavier fluid, displacing the air towards the inside surface. The centrifugal displacement is augmented by gravity in the latter half of the bend. Thus, the bubbles migrate across the pipe prior to entering the downstream horizontal section, where stratification is increased further by gravity alone.

The experimenters also noted that in addition to the air crossing the pipe, the average void fraction increased in the vertical section of the pipe. This is due to the significant reduction of the relative velocity caused by buoyancy of the air.

A numerical simulation of these conditions was completed using the FAITH code. Contour plots of computed void fraction for the same conditions are given in Figure 7.4. Although there are some minor anomalies at the r=0 singularity these clearly show the air crossing the pipe, and the increase of average void fraction in the vertical section. Insufficient measurements were given for a more detailed comparison, however the computed variations of slip and void fraction are also given in Figure 7.4 and show the observed trends. Note the increase in average void fraction in the vertical chapter of the bend and the corresponding decrease in slip. Quantitative comparisons are discussed below for the experiments which had more detailed measurements.

These computations were completed on a 10 x 10 x 25 grid; 25,000 nonlinear algebraic equations are generated to solve the 10 partial differential equations, (8 conservation equations and 2 turbulence equations at each point). Although this grid is quite coarse, it represented the limit of in core solution in the CDC 175 computer. Small variations in grid spacing and in the number of nodes did not greatly affect the behaviour of the solution. It is well known that excess or false diffusion is introduced by a multidimensional numerical scheme which uses locally one-dimensional differencing, and that this is increased when the flow departs significantly from alignment with the coordinate axes. In the cases under consideration, the cross flows, although significant, are small compared to the axial flow. However false diffusion is probably significant, even in comparison to the effective turbulent viscosity, see appendix B.

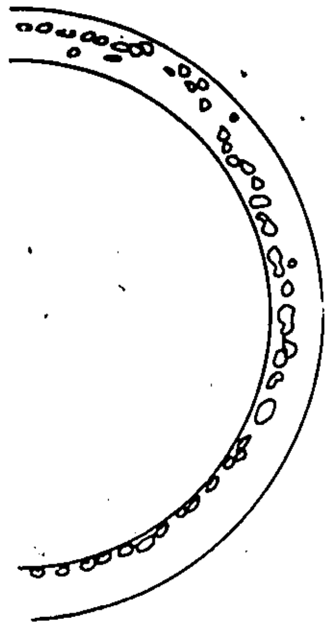

Fig. 7.3 Sketch of bubble path in downward flow of air and water in a C bend; $w = 0.016$ m, $R = 0.09$ m, $V_{LO} = 1.7$ m/s, $V_{GO} = 0.085$ m/s. From Usui et al.

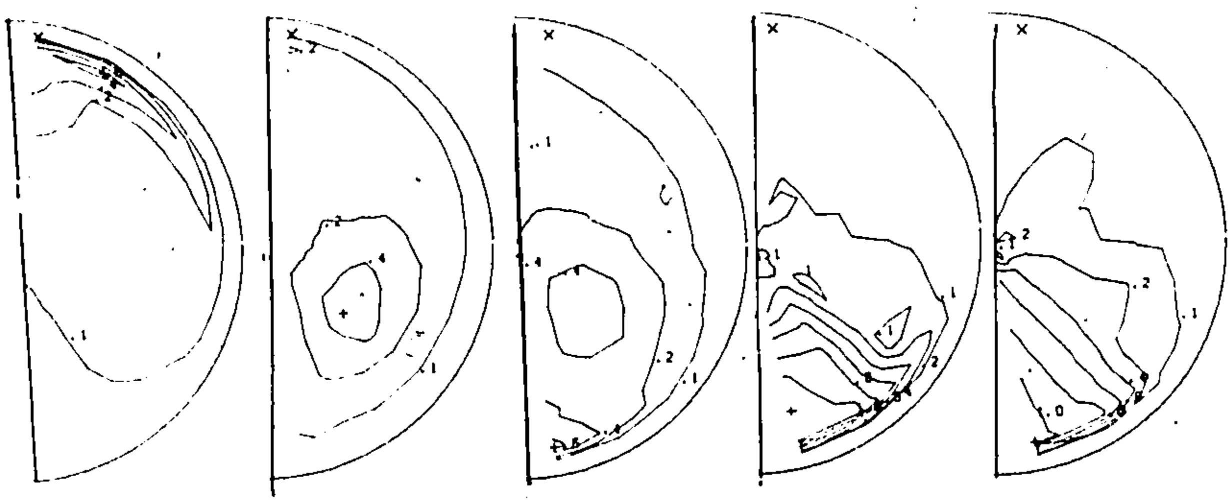

10°	Position	50°	90°	130°	170°
0.08	Average void	0.15	0.22	0.22	0.16
1.09	Average slip	0.91	0.89	0.91	0.92

Fig. 7.4 Computed Contours of Volume Fraction for Downward Flow in a C Bend, Showing Void Migration Across the Channel

7.3.4 Flow in a 90° Bend and the Effect of Bend Radius and Flow Velocity

In the previous experiment, insufficient measurements were taken to examine the separate effects quantitatively. However, void distributions were measured in some detail by Gardner and Neller (1979) using an electrolytic probe in air and water flowing in each of two different bends ($R_1/R_2 = 2.0$) in the apparatus shown in Figure 7.5.

Flow is introduced to the bend through a riser and exhausts through a horizontal pipe. Thus the gravity force acts first axially, then in opposition to the centrifugal force and finally perpendicular to the flow axis. The effects of gravity and centrifugal forces can thus be assessed both in combination and separately.

This experiment has also been simulated using the FAITH code, to demonstrate the effect of gravity and centrifugal force in phase distribution. The entry profile was taken to be sinusoidal, as in the experiment. Once flow enters the bend, centrifugal force drives the water outward, forcing the air inward; however, in the horizontal pipe the air is forced outward again as the water descends. Measured and computed void profiles in the plane of the bend for particular cases are shown in Figure 7.6. Since these attempt to depict two dimensional profiles in the cross-section with a one dimensional variation along the axis of symmetry, one would not expect precise correspondence. However note that in general, the computed results show good agreement with the experimental values, particularly as the void must migrate through the full computational grid, and although the computed values shown are from positions as close as practical to the axis of symmetry, they are not precisely on the axis.

In Figure 7.6, the initial tendency of the centrifugal force to carry the water to the outer radius is seen only at station D(23^0). Gravitational forces then become predominant and the void starts to move upward through the stations E(45^0) and F(67^0) to the outer surface again. Stratification develops rapidly in the horizontal section GH and J, once the centrifugal force is no longer active. The computed profiles show the same response of void movement to the relationship between centrifugal and gravitational forces, and although the computed profiles are not exact, the predominant location of the void is predicted quite well at each individual station.

The effect of bend radius is illustrated by comparing Figures 7.6a and 7.6b, which show measured and computed profiles for the two different bend radii at each of the measuring stations. Note that for the larger bend radius, centrifugal forces are dominant only at station D, whereas for the smaller bend, centrifugal forces dominate through to station F. For the larger bend, the computations follow the measurements quite closely, however in the smaller bend the computed distribution does not separate quite so quickly as the experiment.

The effect of velocity can be seen by comparing Figures 7.6b and 7.6c. In the latter, the velocity is 40% higher, although the void fraction is also higher. This velocity is sufficient to maintain centrifugal dominance through to station F. It is interesting to note that conditions in this particular case are outside the accepted limits of bubbly flow, but the computational model still seems to produce quite acceptable results, although the agreement on profile is not as good as the bubbly flow cases.

The sensitivity of results to the bubble/slug transition in the interface friction model, equation 6.4, was investigated, and the model which assumes that the flow remains bubbly throughout gave the best agreement in each case. Although the experimenters did not discuss this clearly, they infer that the low flow cases remained bubbly in nature and this is consistent with experiments in bubbly flow reported by Salcudean, et al (1983). Invoking the slug/bubble transition in the current model and all the accepted models somewhat lowers the drag per unit volume at high voids, and this gives considerably more distortion of the profile, particularly in case (c), than was observed.

The contours of computed void fraction given in figure 7.7, show a more complete picture of the transitions, and are consistent. The contours show migration of the air consistent with the interaction of centrifugal force and gravity. The stronger centrifugal influence in the smaller radius bend can be seen by comparing the contours of case (b) with case (a); (b) shows more initial migration to the inside of the pipe, and a slower return to the outer wall. The effect of velocity is similar, and can be seen by comparing contours of case (c) with case (a).

Parameters for all the bend cases are given in table 7.1.

TABLE 7.1

FLOW PARAMETERS FOR THE BEND EXPERIMENTS

Authors	Case	d	R	type	$\bar{W}$	$\bar{\alpha}$	w_{lo}	w_{go}
Gardner & Neller (1979)	a	.076	0.61	Γ	1.77	.130	1.54	0.23
	b		0.305		1.77	.130	1.54	0.23
	c		0.61		2.44	.375	1.53	0.92
Usui et al (1980)	a	.016	0.09	C	1.78	.05	1.70	0.09
Usui et. al. (1983)	a	.024	0.10	U	1.26	.21	1.00	0.28
	b				1.13	.12	1.00	0.13
	c				0.83	.32	0.52	0.24
	d				0.65	.19	0.52	0.12
	e				0.36	.36	0.28	0.13

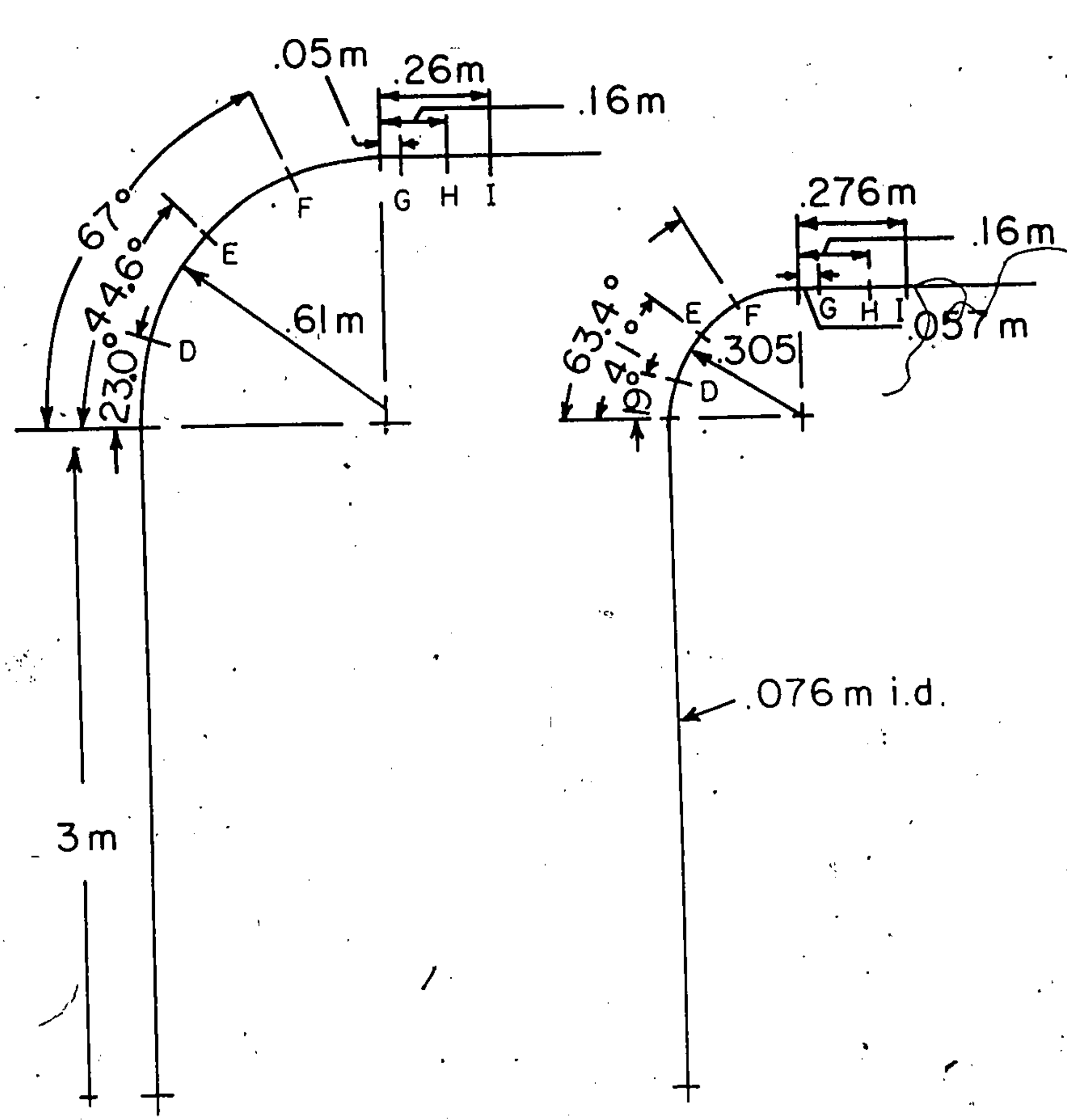

Fig. 7.5 Geometry of the Two Radial Bends

used in the Experiments of Gardner and Neller (1979)

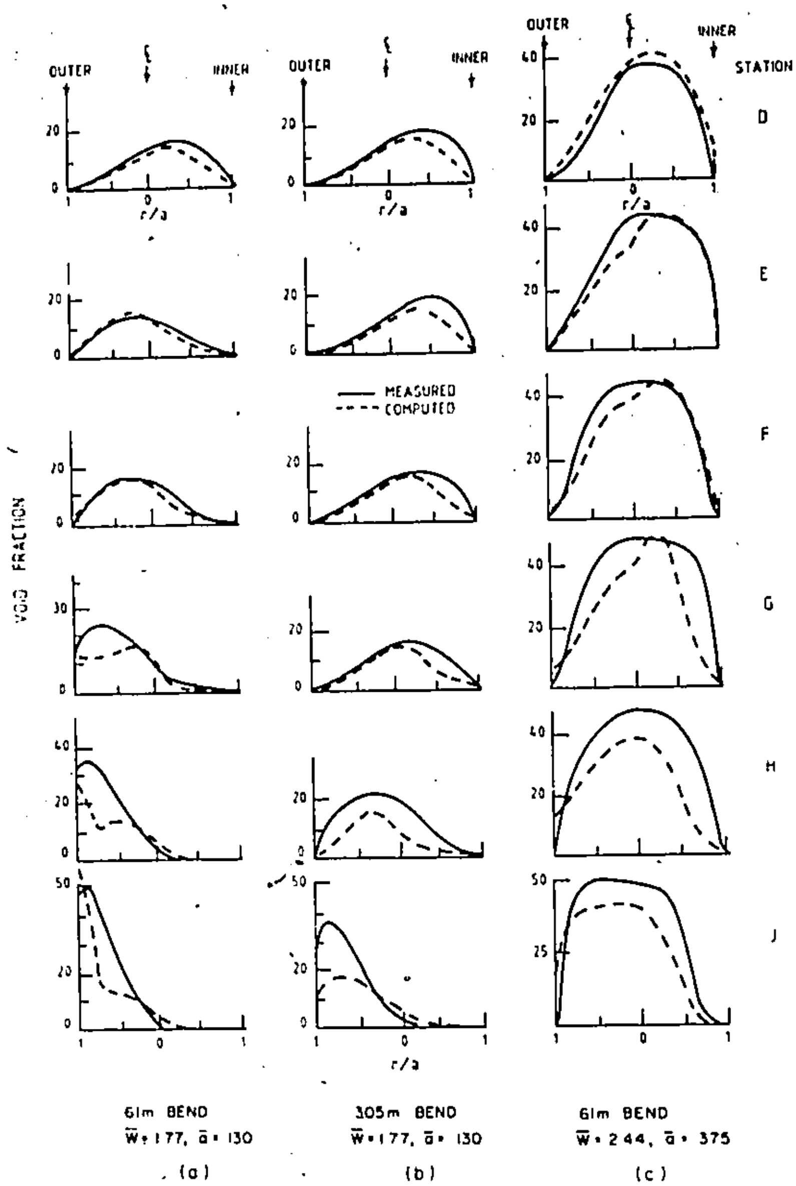

Fig. 7.6 Measured and Computed Volume Fraction Profiles for Particular Cases of Gardner and Neller (1979) Experiments

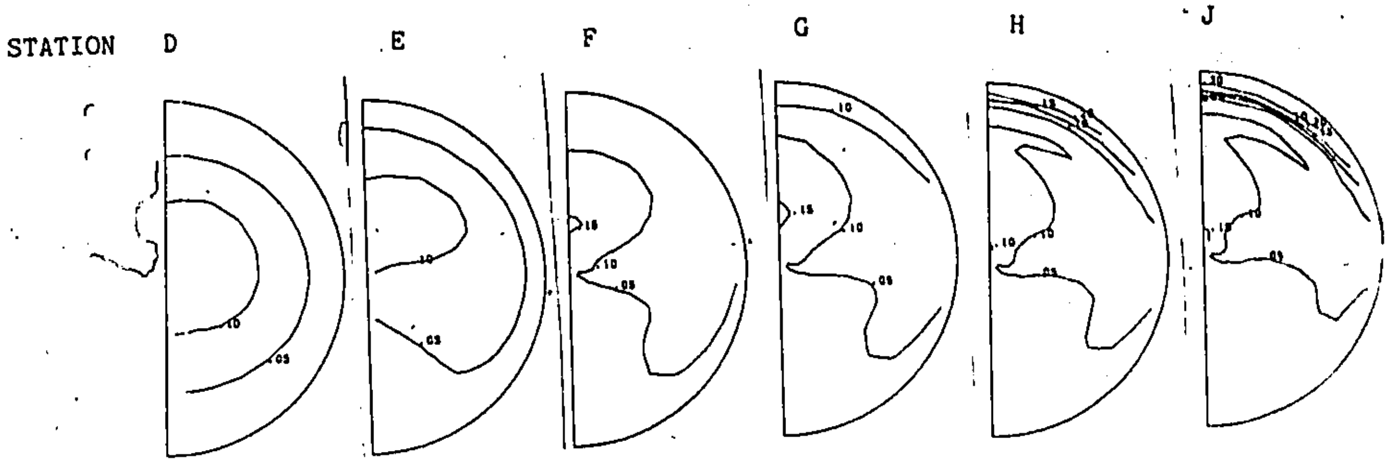

(a) $\overline{W} = 1.77$ m/s $\overline{\alpha} = 0.13$ $R_c = 0.61$m

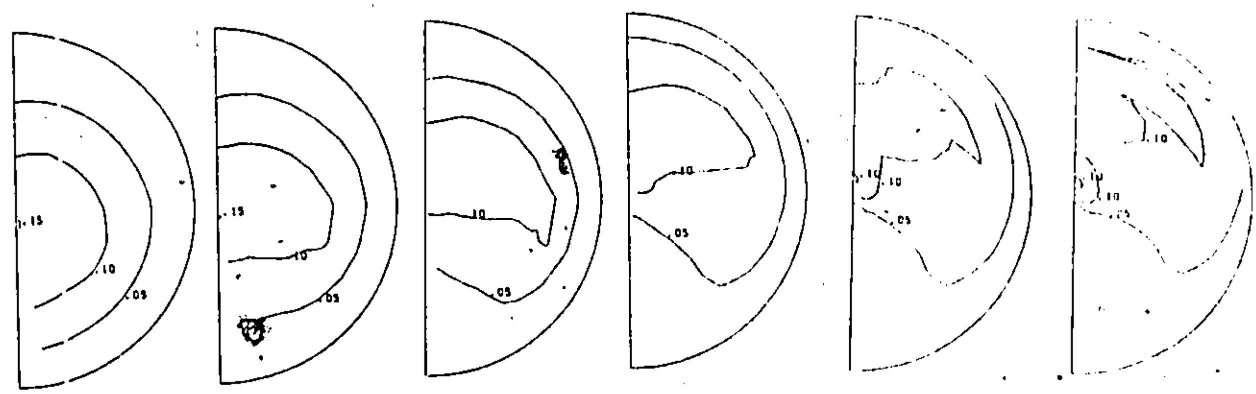

(b) $\overline{W} = 1.77$ m/s $\overline{\alpha} = 0.13$ $R_c = 0.305$m

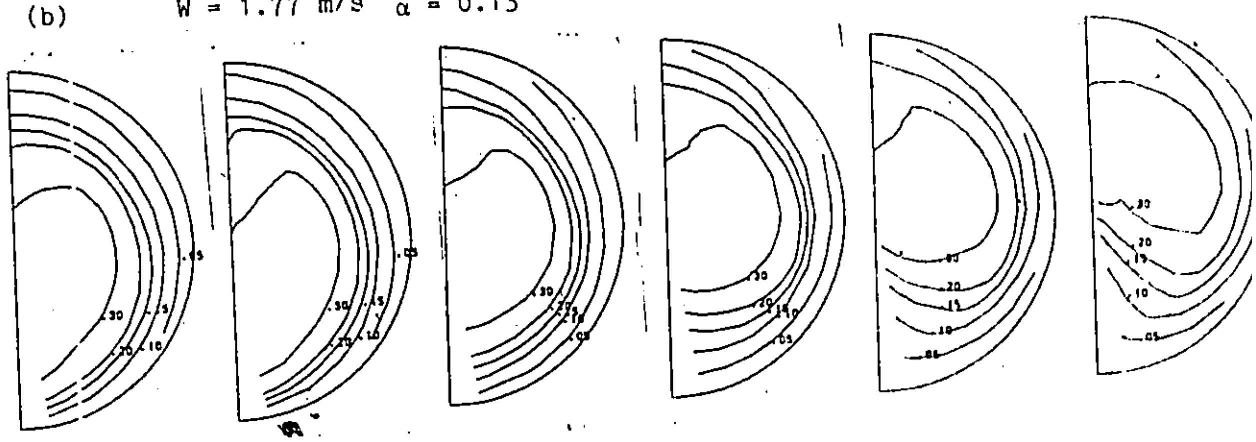

(c) $\overline{W} = 2.44$ m/s $\overline{\alpha} = 0.375$ $R_c = 0.61$m

Fig. 7.7 Computed Contours for the Gardner and Neller(1979) Expts. showing the effect of velocity and Bend radius.

7.3.5 Flow in an Inverted U Bend and the Effect of Velocity

The final examples are of two fluid flow in an inverted U bend, a case of great interest in the design of U tube steam generators. The experiments chosen are the third in the series of experiments by Usui et al., (1983) and thus include their most detailed measurements. Huang and Davis (1979) and Oshinowo and Charles (1974) also studied U-tubes, but the former gave very few measurements and the latter discussed only qualitative observations.

Unlike the previous 90° bend cases, flow leaving a U bend is likely to change distribution only slowly after leaving the bend, as the only disturbing influence is turbulent mixing. Clearly then three classes of events can be identified, one in which centrifugal force is dominant throughout, one in which the relative dominance changes and one in which gravity is dominant throughout. In the former, water will migrate to the outside of the bend and remain there, in the intermediate case water may migrate first outward then inward, while in the last case the velocity is slow enough for the air to migrate upward to the outer edge and stay there.

Typical cases of these three classes were measured and these were simulated using FAITH; computed and measured void profiles are given in Figure 7.8. Note that again the migration of the phases particular to each case is computed reasonably correctly by the computer model. Although more precise agreement could no doubt be obtained by fitting each case individually, it is more informative to use the same parameters for all five cases. The cases a and b, in which centrifugal force is dominant are simulated quite well. The computed results for cases c and d follow the change from centrifugal to gravitational domination quite well, but appear to favour gravity. However for the low flow case, Figure 7.8e, the tendency of the void to expand greatly due to the relative deceleration of the air in the downcomer is not reproduced by the model, when the same bubble diameter was used. However, an increase in bubble diameter to 6 mm did not reduce drag sufficiently to reproduce the expansion effect shown. The previous cases were then repeated to see what the effect of the 6 mm diameter would be. In the two high flow cases (a,b) the effect was small. In the mid-range cases (c,d) excessive premature migration of the void occurred. Invoking the bubble slug transition with $\alpha_{sb} = 0.3$ has less effect than increasing the bubble diameter in all the cases considered. The results in the latter cases are not sufficiently different to warrant inclusion. Further sensitivity studies are discussed in section 7.4.

The computed contour plots for cases (a),(c), and (e), which represent each of the three classes, are given in figure 7.9. The transitions are quite smooth.For the high velocity case, (a), the centrifugal force is seen to be dominant throughout, displacing the air to the inner wall of the pipe, where it remains. For the low velocity case, (e), gravity dominates throughout, and the air rises to the outside of the pipe and remains. The intermediate case, (c), is most interesting, as it clearly shows that, in the riser, centrifugal force initially concentrates air towards the inside of the pipe, but that gravity overcomes this force in the horozontal portion, and air rises to the outside, until centrifugal force again becomes dominant in the downcomer, and the air is forced inward again.

Computed pressure profiles are given in figure 7.10, and these are again consistent with the velocities, but no experimental values are available for comparison.

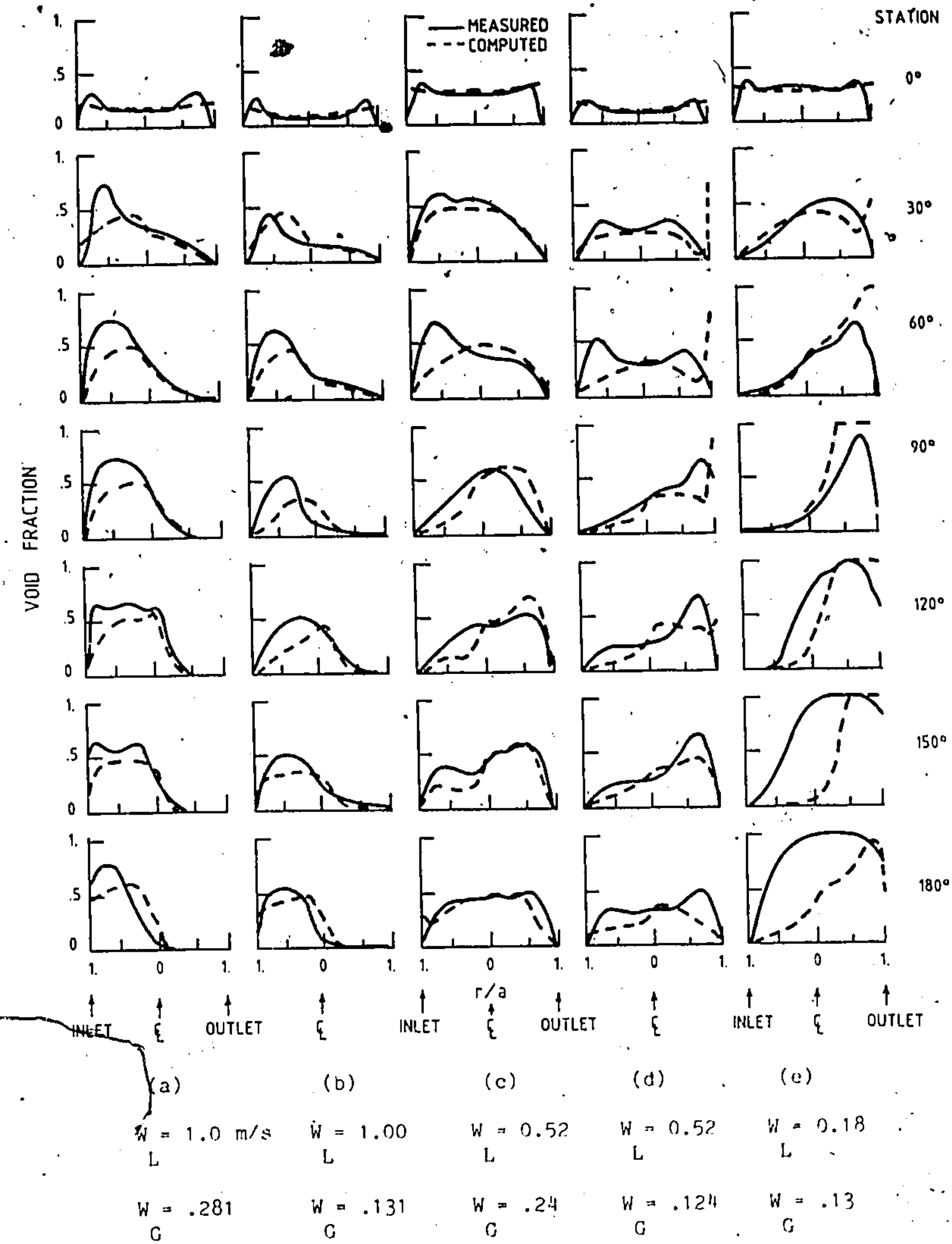

Fig. 7.8 Measured and Computed Volume Fraction Profiles
for Particular Cases of
the Experiments of Usui et al (1983)

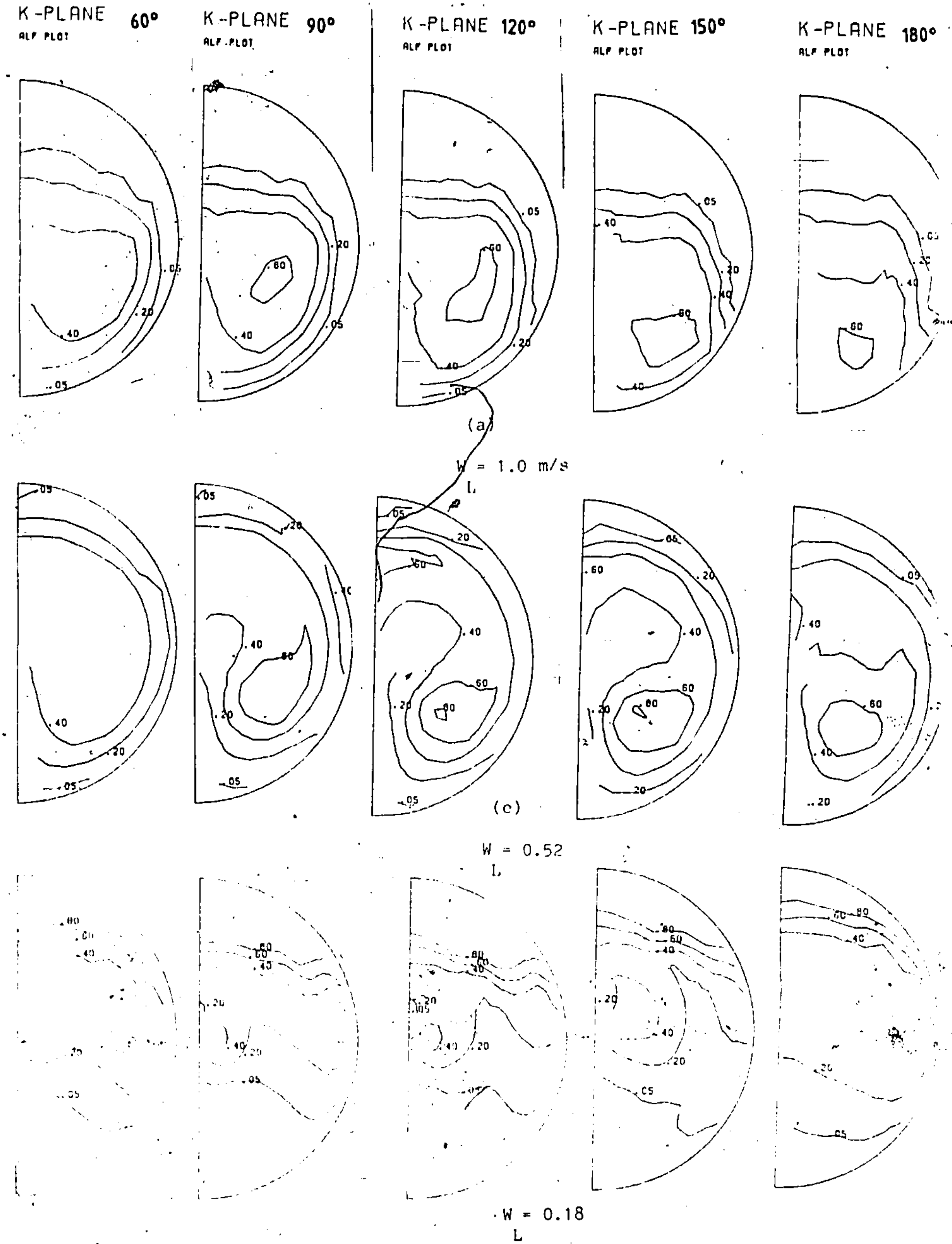

Fig. 7.9 Computed void contours for three cases of the Usui et. al.

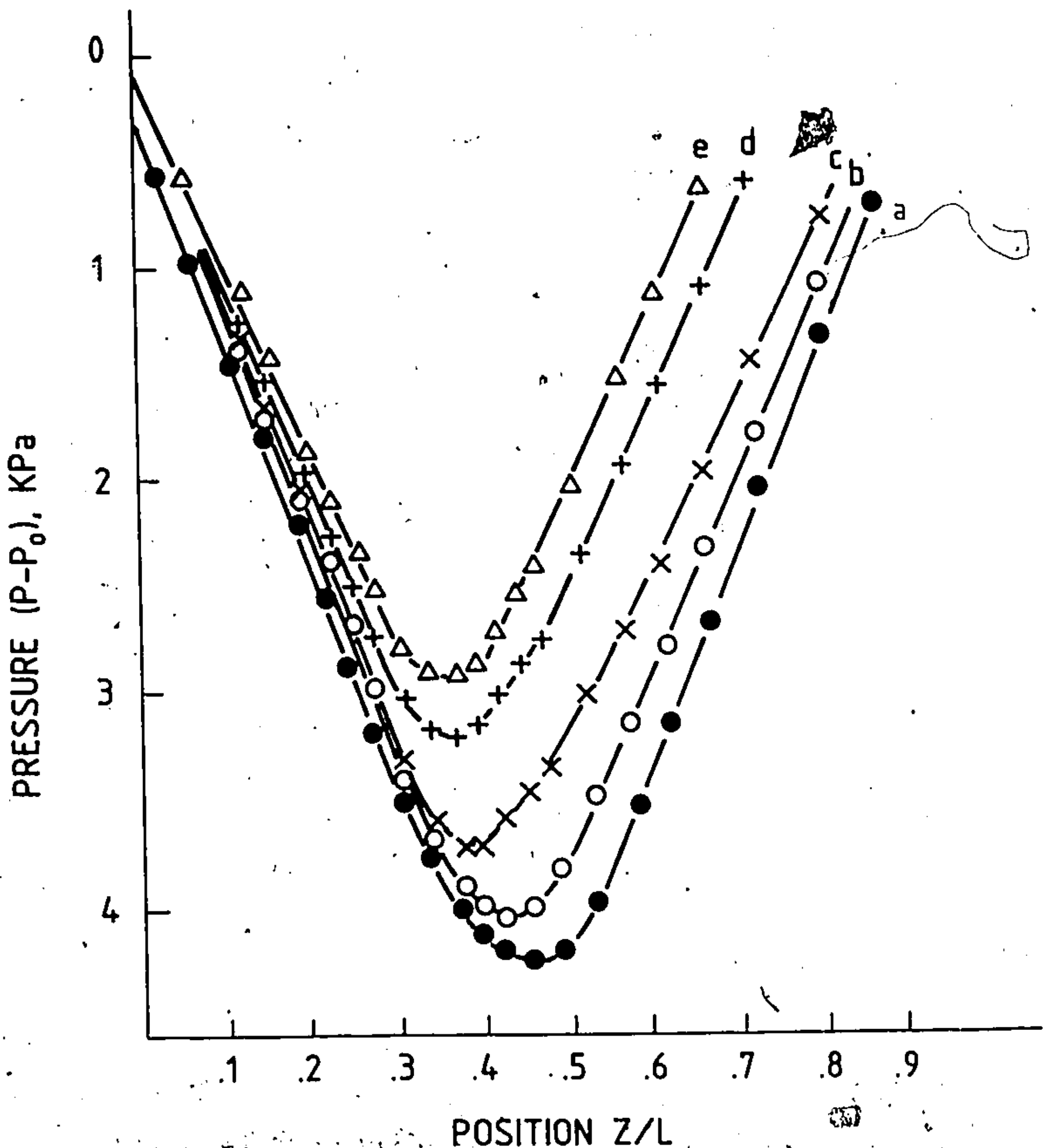

Fig. 7.10 Computed Pressure Profiles for the Usui et al. Experiments(1983).

7.4 Sensitivity Studies

As mentioned, the comparisons given in the previous sections were obtained using a fixed set of relations, as this is more informative than tuning parameters to fit particular cases. A number of sensitivity studies were also performed and are now discussed with reference to the Gardner and Neller case (a), as this shows a sufficiently strong variation in distribution to illustrate differences clearly.

The first case shown in figure 7.11b, illustrates the effect of increasing effective viscosity by a factor of 2 from the reference case, 7.11a. This is not a major effect, but the increased viscosity does slightly retard the separation in the horizontal section. This also suggests that the computation is not overwhelmed by numerical diffusion and may explain why the agreement with the experiments is quite good.

The second case, figure 7.12, shows the effect of increasing bubble diameter by 20%, and hence decreasing interphase surface area and drag. As expected, this slightly accelerates the separation in the horizontal pipe.

The third case, figure 7.13, shows the effect of decreasing the axial grid spacing by 25%. The contours shown are taken in planes which correspond to the same distance from the entrance to the bend, and show very little change.

The fourth case, figure 7.14, shows the effect of using the molecular viscosity, rather than the effective viscosity in the computation of interphase drag only. This has a marked effect as drag is reduced considerably and separation is accelerated significantly.

The penultimate case, figure 7.15, shows the effect of using the formula for drag coefficient proposed by Zuber and Ishii(1979). This is discussed in Appendix B. As noted by Lahey(1979), the difference is small, but there is a slightly slower migration of void to the top of the pipe.

Finally , figure 7.16 shows results obtained after 60 and 120 iterations. The void fraction distribution seems to be well established after 60 iterations, and figure 4.1 tends to support this.

These studies show that this computation is not particularly sensitive to reasonable changes in effective viscosity, or grid spacing, but, as expected is quite sensitive to interphase friction.

Also of interest are the velocity fields in the cross-section of the bend. The recirculation patterns typical of single phase flow, similar to those in figures 7.1 and 7.2, were computed only when centrifugal force was dominant. When gravity became dominant, a more complex flow pattern evolved. To illustrate this, computed velocity fields for water and air are shown for the reference case in figure 7.17 ,at station 9, 23^0 into the bend and at the exit plane station 18. This type of transition occured in all cases; the position at which it occured was case dependant.

7.5 Summary of Results for Bends

The numerical computation has successfully reproduced the changes in void distribution in flow around three types of bends. The following phenomena observed in the experiments were reproduced in detail.

(a) recirculation in the plane normal to the bend

(b) migration of the air to the inside of the bend due to centrifugal action

(c) migration of the air to the top of the pipe due to gravity

(d) the detailed interaction of (b) and (c)

(e) the effect of radius on (d)

(f) the effect of velocity on (d)

Some minor departures between calculated and measured void profiles did occur, but the major departure was the inability of the calculation to produce the expansion of the air in the downcomer for the very low flow U-bend case 7.8e. The expansion could not be simulated by increasing bubble diameter nor by invoking the transition to slug-type flow in the interphase drag model.

Considering the approximate nature of the models of interphase friction and effective viscosity, and the fact that the solution is prone to numerical diffusion, the computed results compare very well to the experiments.

This study has been published in a paper in Numerical Heat Transfer, Carver and Salcudean (1986).

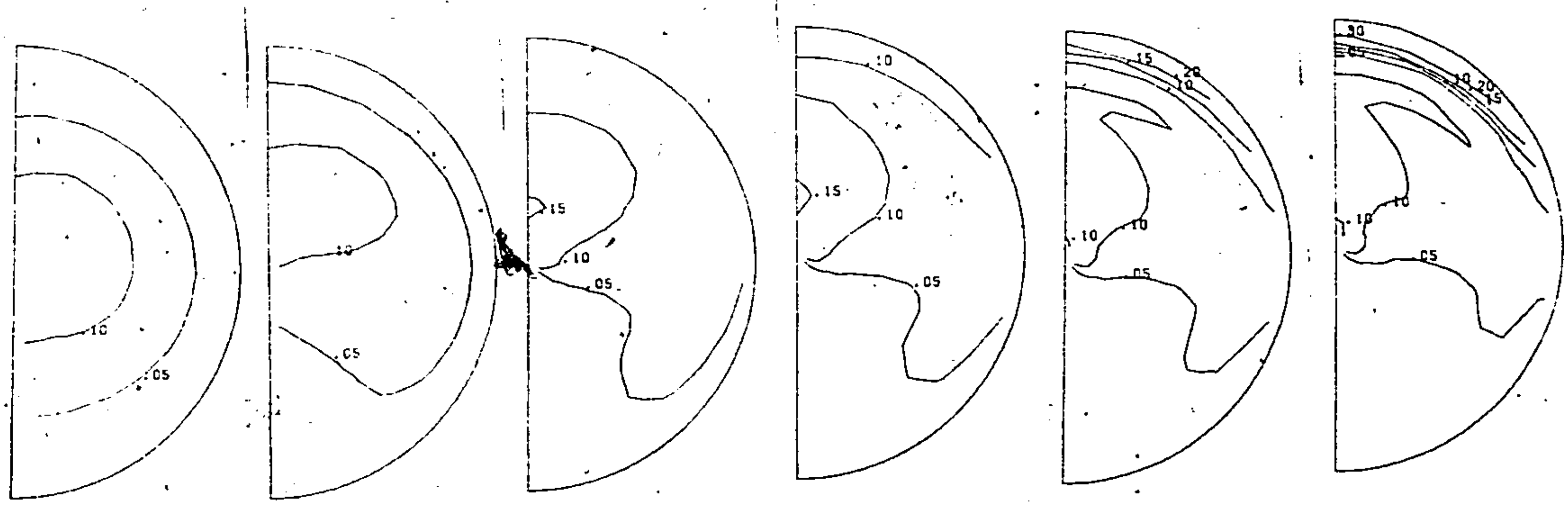

(a) Reference case

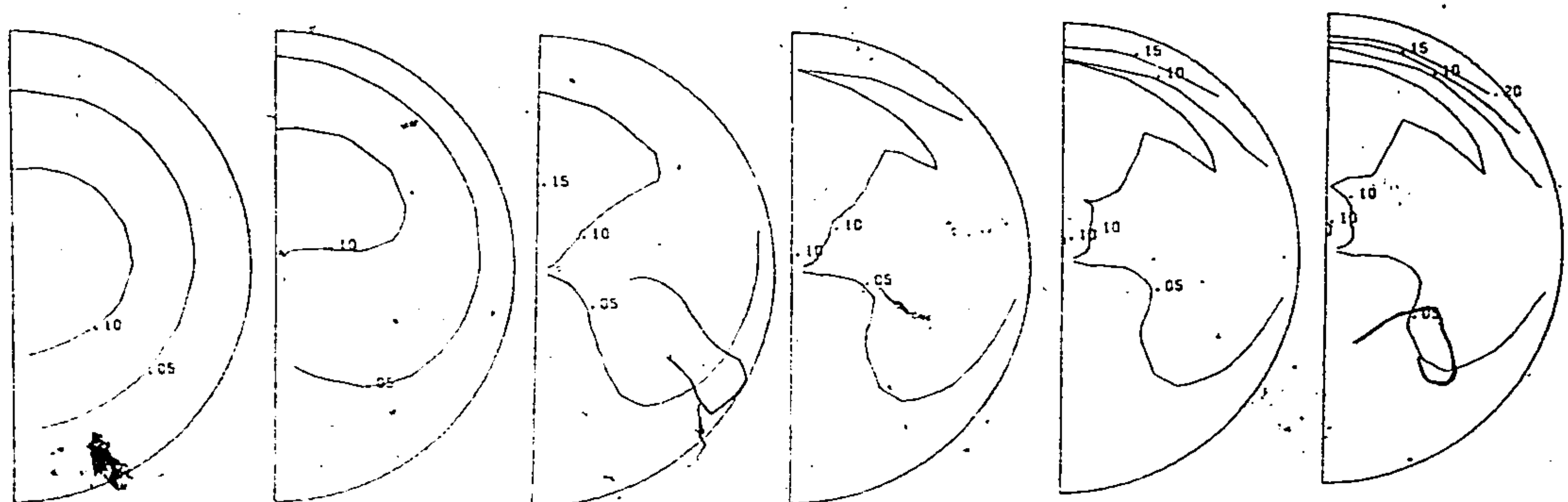

(b) Effect of 100% increase in viscosity

Fig. 7.11 Sensitivity studies (Case (a) of Gardner and Neller):

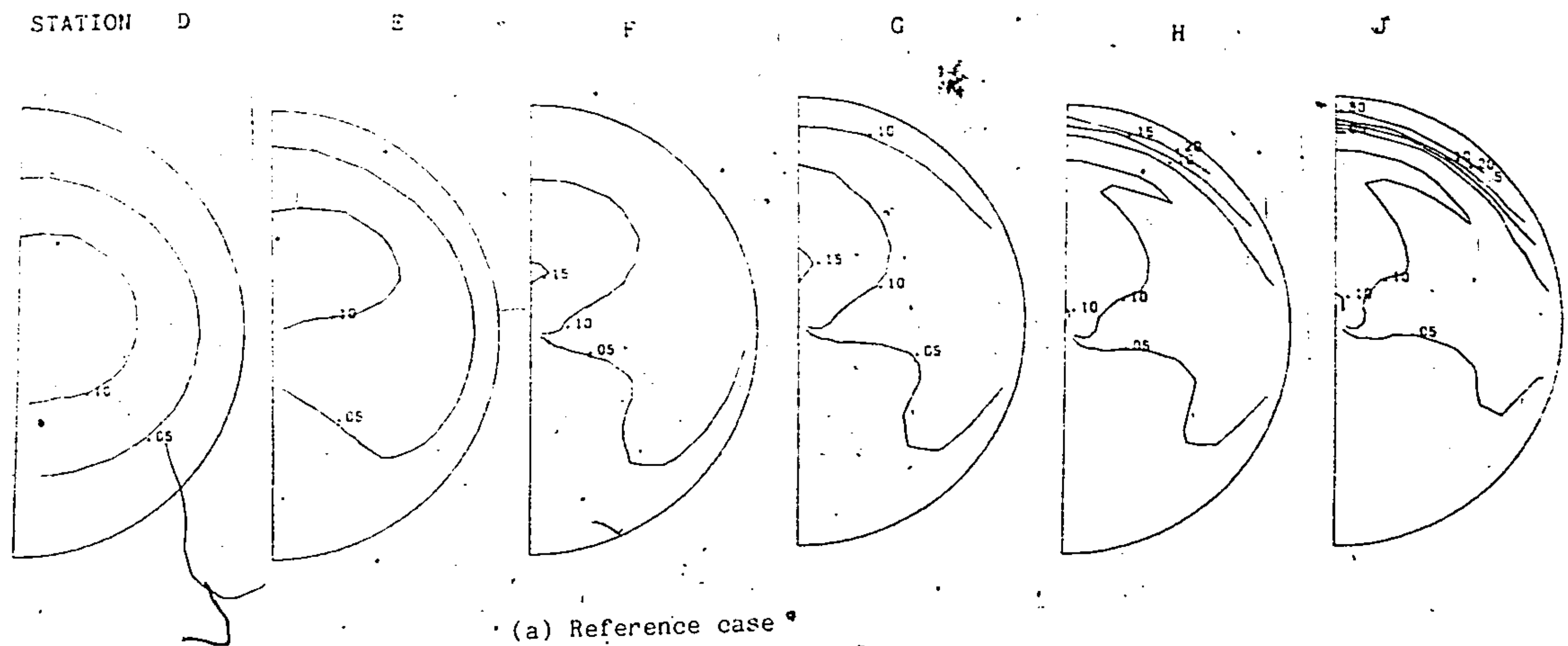

(a) Reference case

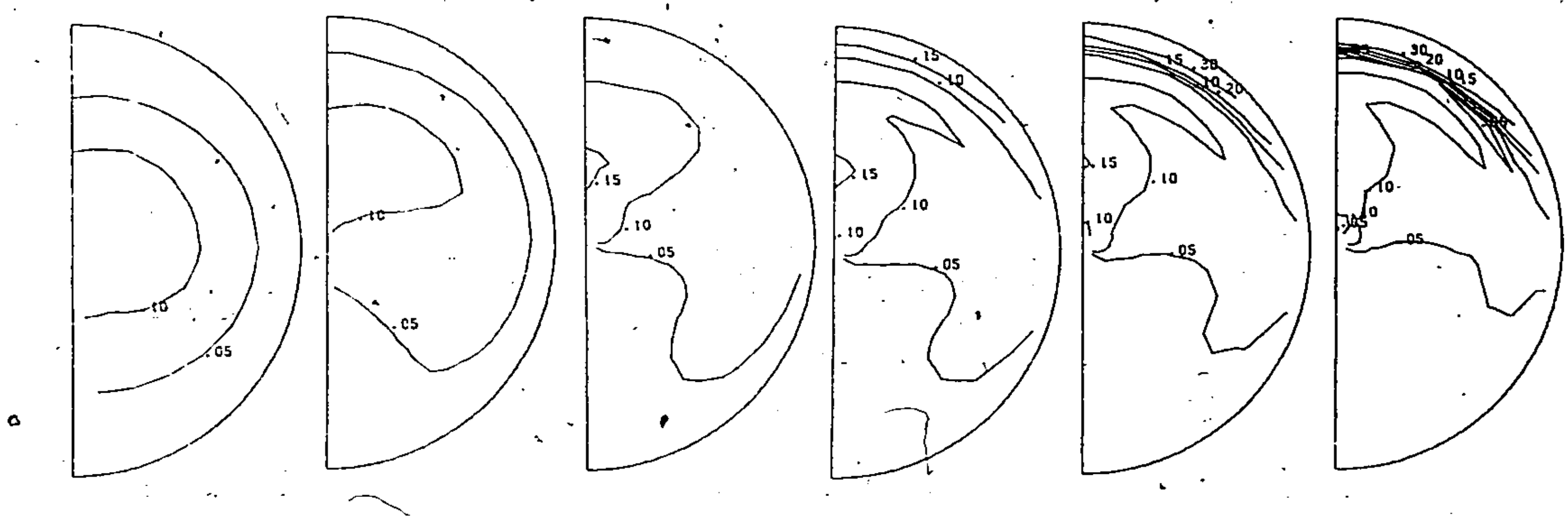

(b) Effect of 20% increase in Bubble size

Fig. 7.12 Sensitivity studies [Case (a) of Gardner and Neller]

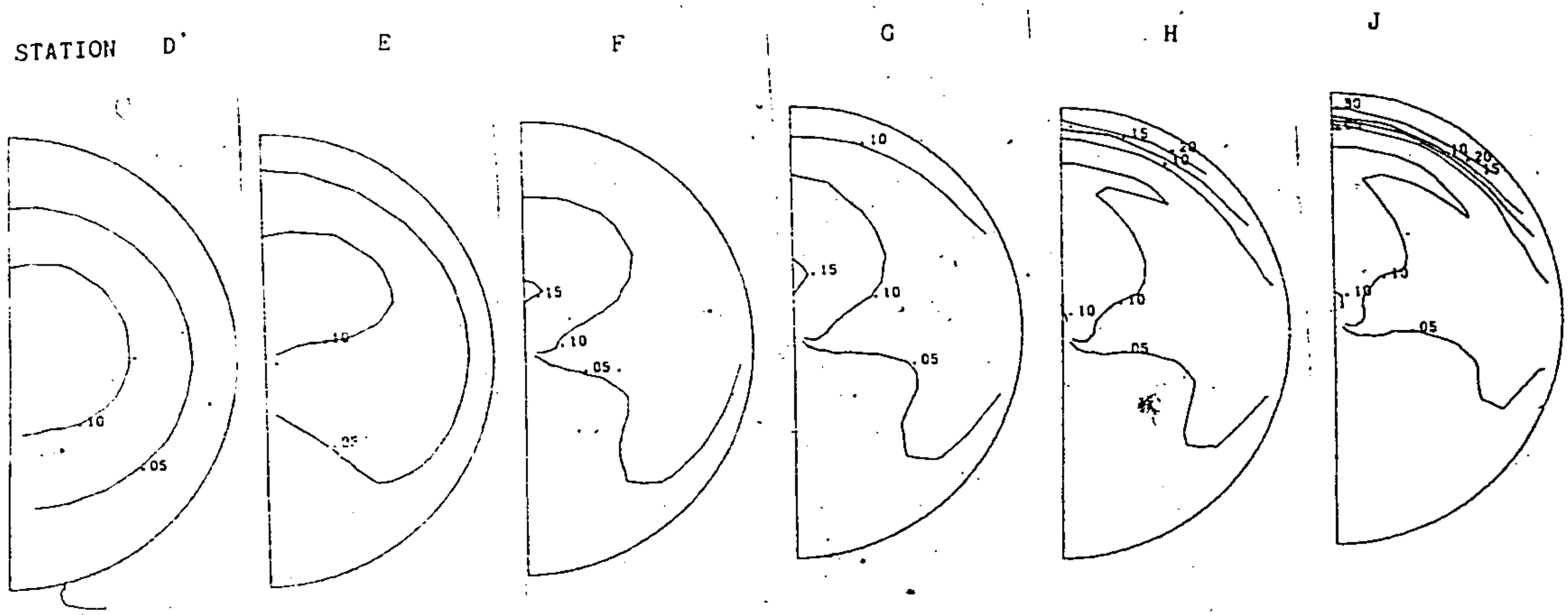

(a) Reference case

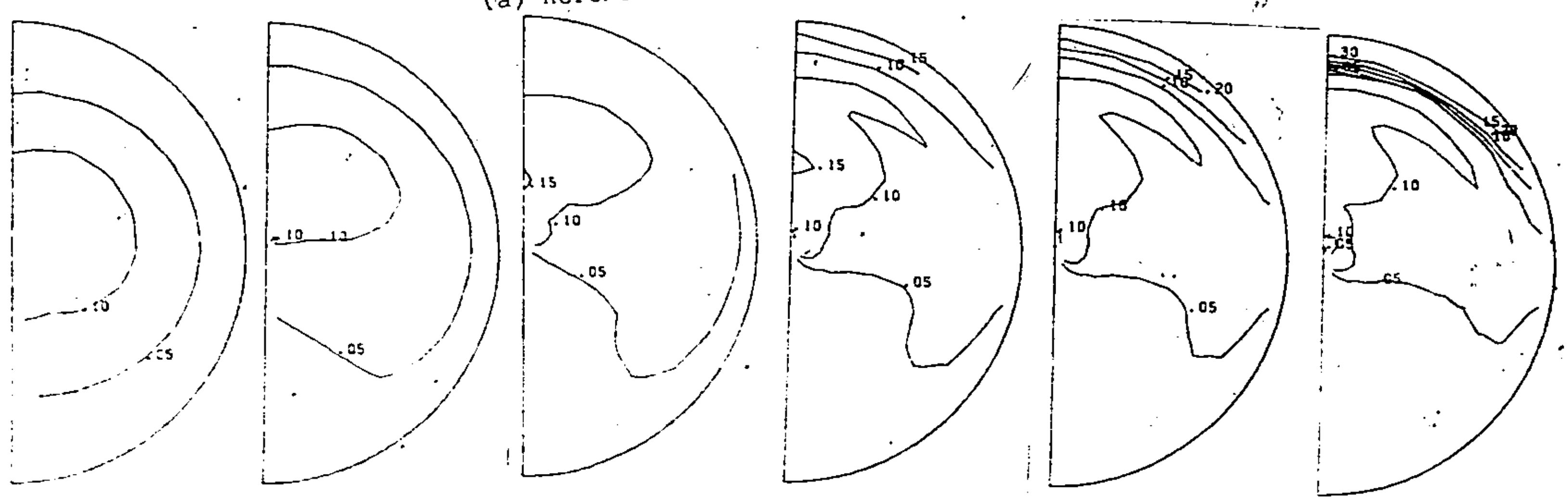

(b) Effect of 25% decrease in axial node size

Fig. 7.13 Sensitivity studies (Case (a) of Gardner and Neller):

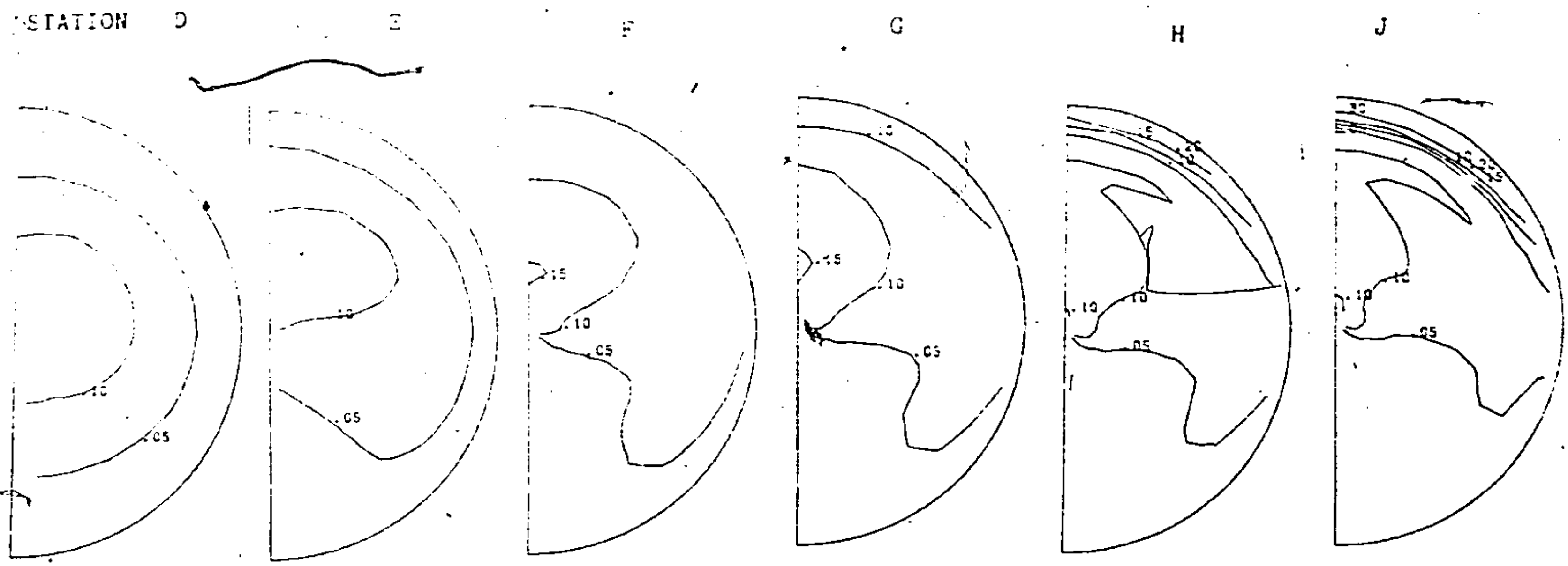

(a) Reference case

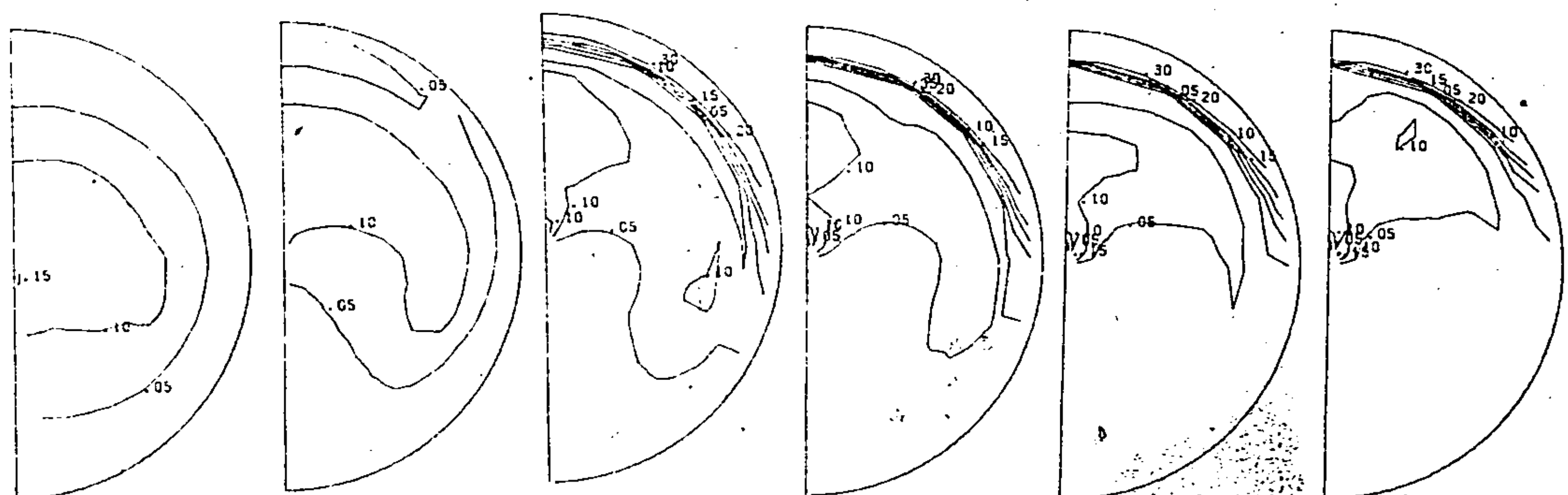

(b) Effect of using molecular viscosity in Drag Reynolds Number.

Fig. 7.14 Sensitivity studies (Case (a) of Gardner and Neller):

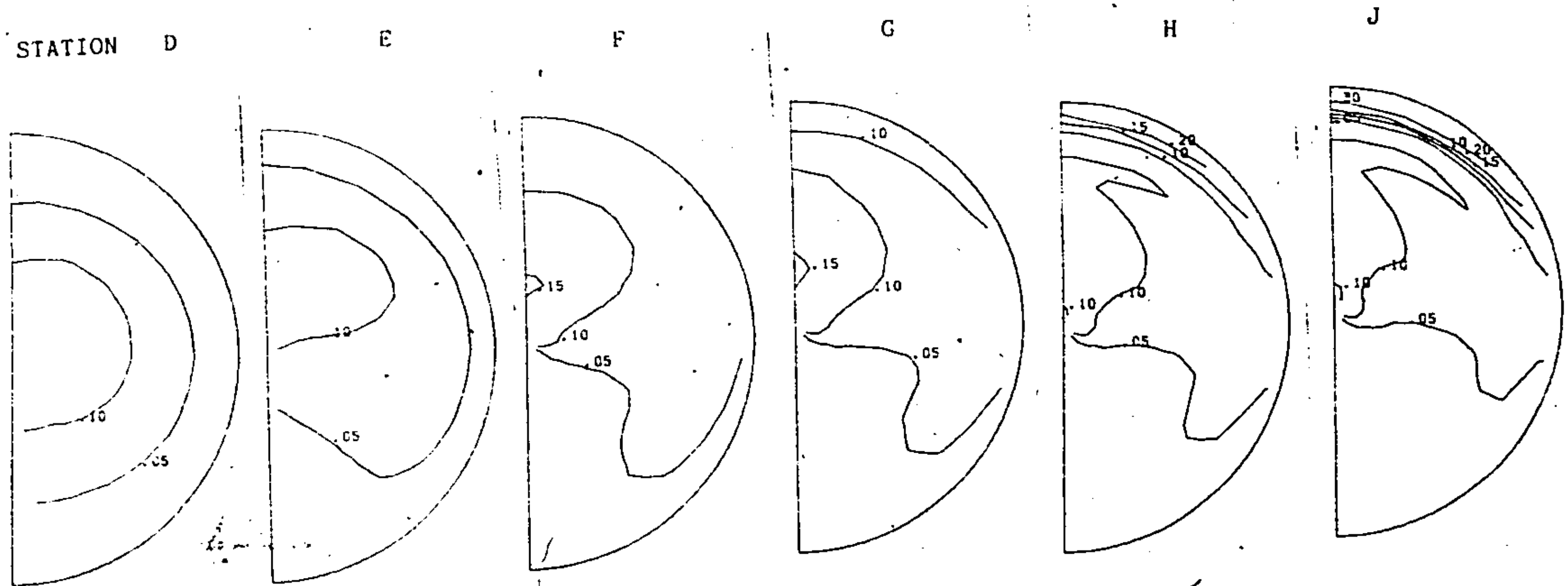

(a) Reference case

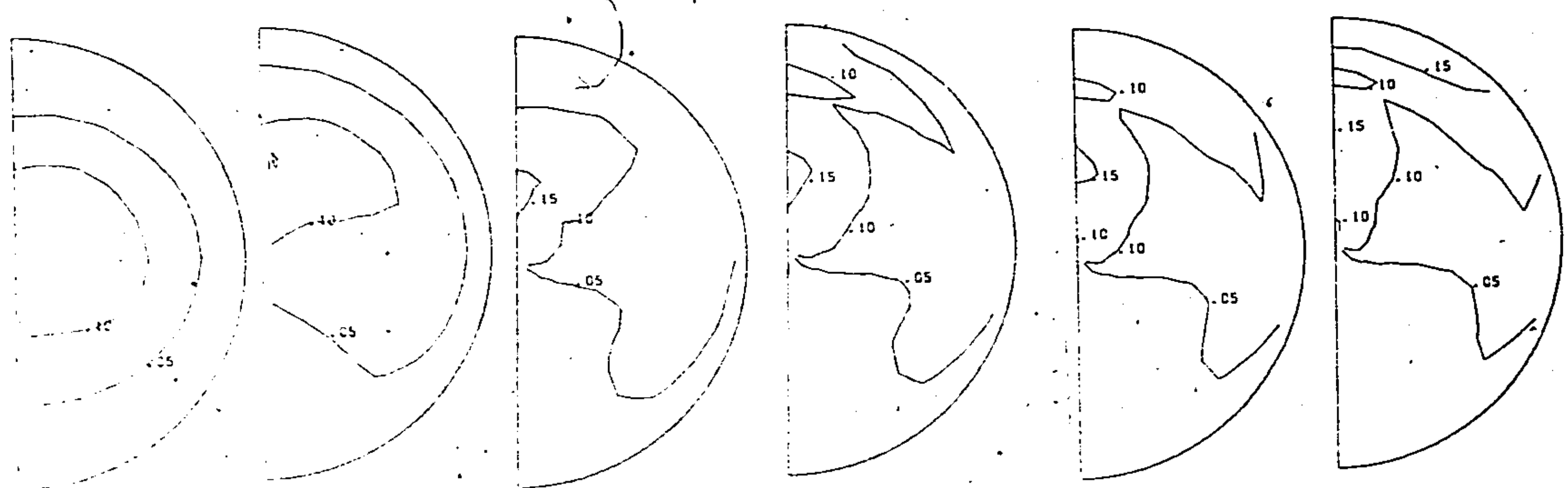

(b) Effect of using Zuber Drag Coefficient

Fig. 7.15 Sensitivity studies [Case (a) of Gardner and Neller]:

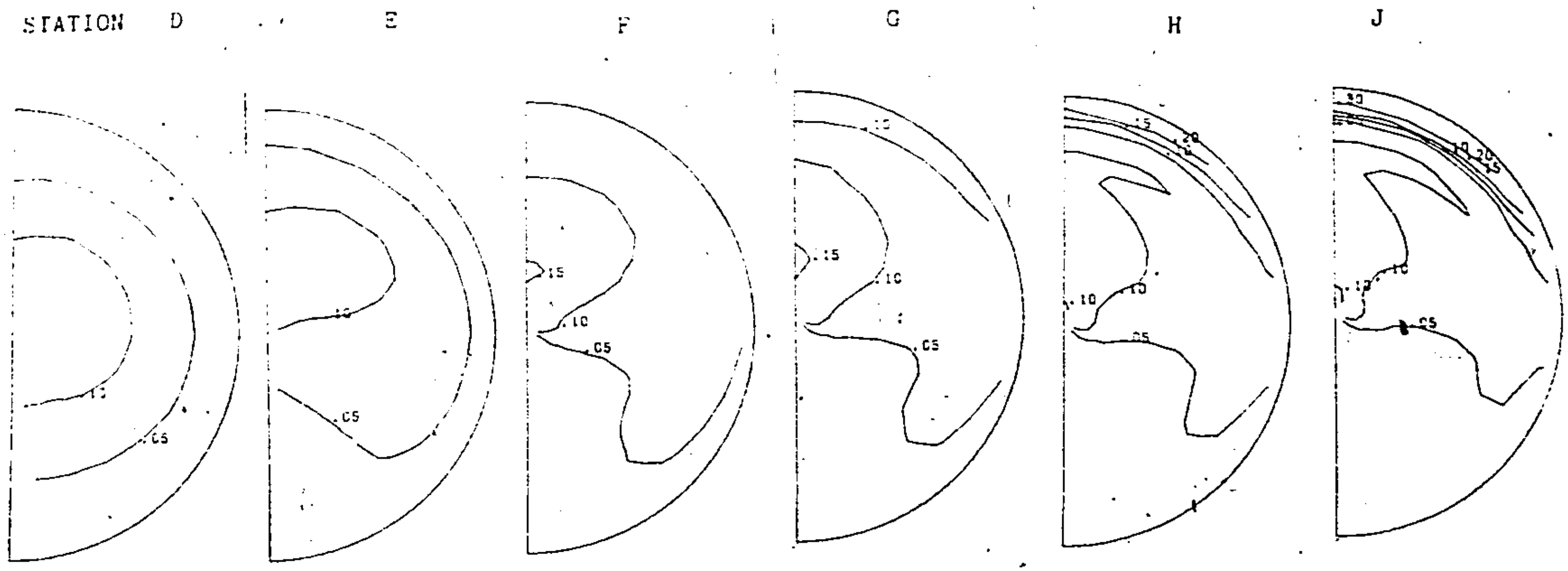

(a) Reference case 60 iterations

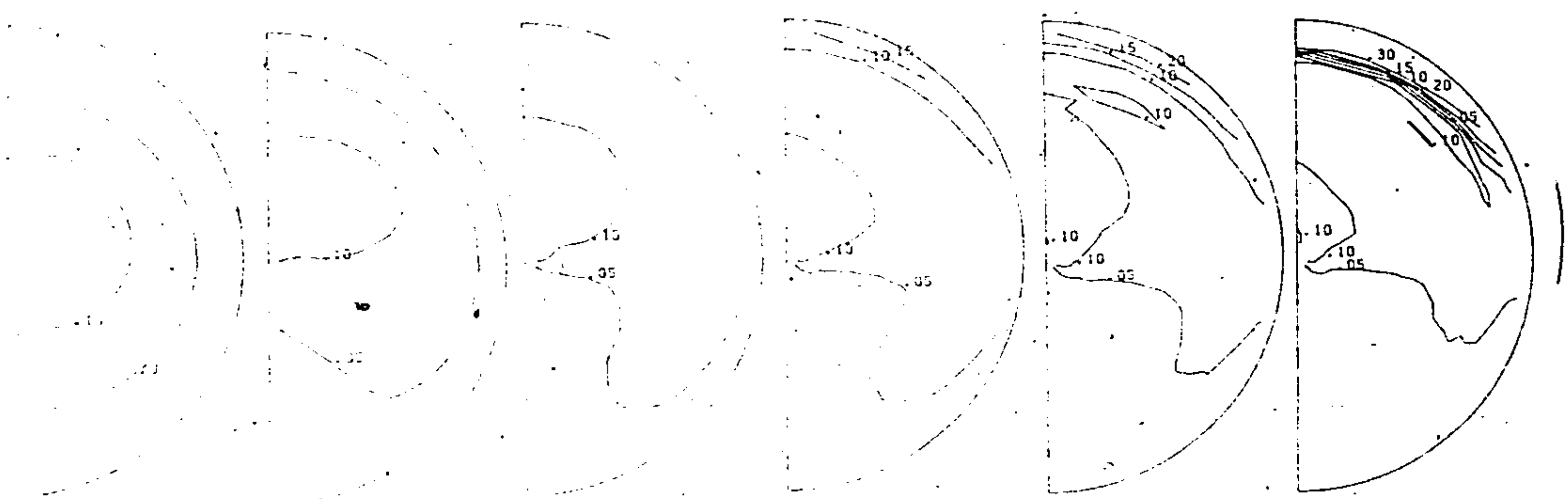

Fig

(b) Reference case 120 iterations

Fig. 7.16 Sensitivity studies (Case (a) of Gardner and Neller):

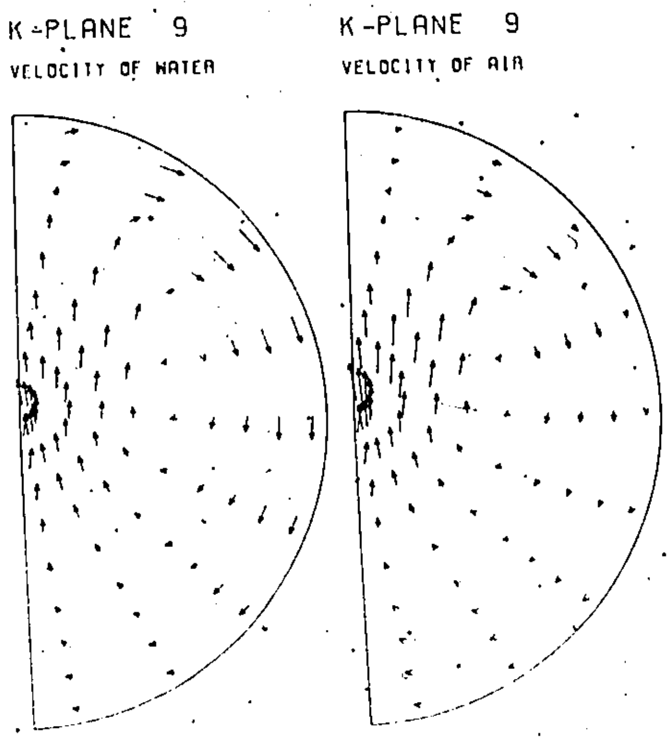

(a) Centrifugal Dominance

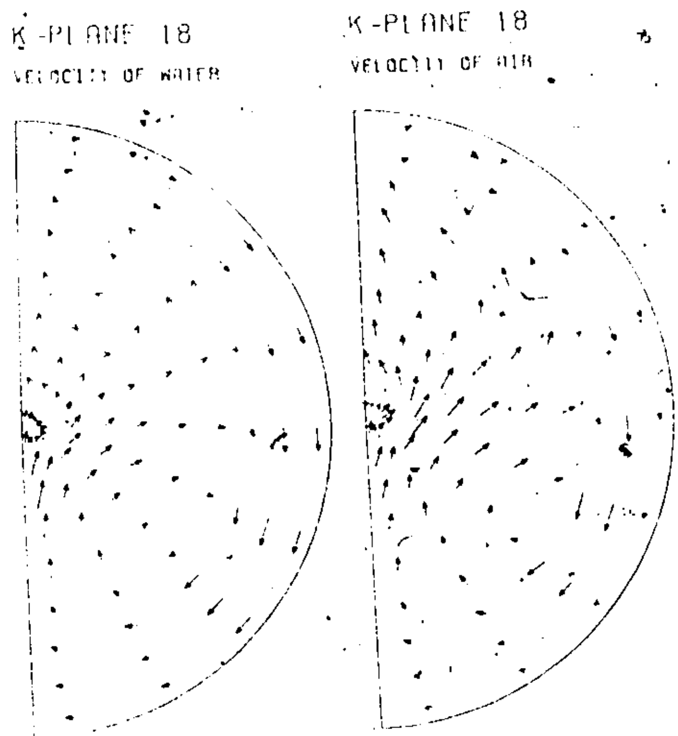

(b) Gravity dominance.

Fig. 7.17 Computed Velocity Fields for Typical Cases

CONCLUDING REMARKS

In this study, existing numerical methods for the three-dimensional computation of two-fluid flow has been reviewed and found inadequate, so a new algorithm was devised. This has been implemented by developing a two-fluid algorithm using an existing single phase computer program as a starting point. The resulting program was applied to predicting changes in phase distribution caused by the interaction of forces in vertical pipes, horizontal pipes with obstructions and in bends in various orientations, including Γ, C and U bends. It has been shown that the model appropriately predicts trends in phase distribution and relative velocity observed in experiments, and in cases where sufficient measurements were reported to make detailed comparisons, the completed distribution and migration of phases also gave good quantitative agreement.

As the two-fluid algorithms were implemented by extending a single phase program, the basic approach to solving the matrix equations in this program was maintained. The resulting computations usually converged smoothly, even for high density ratios, and for cases in which approached complete separation. However convergence is not rapid, and convergence of the two-fluid scheme could be accelerated by implementing a more rapid single phase scheme. Some enhancements were made to the basic matrix solution schemes, but a more efficient single phase scheme would clearly enhance overall convergence.

Although the interphase drag function used was a simple model based on bubbly flow, its main features follow widely accepted models quite closely, and as a range of parameters was used in sensitivity studies, it is unlikely that these more complex models would give significantly better results.

The interphase drag model directly controls the relative velocity between phases, so it is not surprising that results were sensitive to this model. However, results, were less sensitive to reasonable changes in grid position or grid density.

Further research is required to establish a definitive model of turbulence in two-phase flow, and more comprehensive models are still under investigation elsewhere. However in this study the approach was simplified by modelling effective viscosity based on the liquid field and this gave a useful approximation which appeared to give reasonably behaved results.

The greatest uncertainty associated with the simulation results is the effect of false diffusion. Because these calculations were limited by the inflexible memory limit of the CRNL CDC 175 computer, the grids used were inevitably quite coarse, and the numerical diffusion thus introduced is significant. This is judged to be less for the bend cases than for the obstruction cases. To date, all studies on mimimising false diffusion have been restricted to two dimensions. However, there is active research in the area and any new studies which extend such techniques to three dimensions could readily be incorporated in the current algorithm.

ACKNOWLEDGEMENTS

As supervisor of the research, Prof. M Salcudean has contributed many suggestions, and encouragement throughout the project. Professor S. Mirza, who took on the role of co-supervisor when Dr. Salcudean left Ottawa for U.B.C., was also very helpful. All the computing was funded by Atomic Energy of Canada, Chalk River Nuclear Laboratories; most of it was completed by means of a home personal computer link to the CRNL CDC 175 computer. J.D. Bugg and A.O. Banas have contributed extensively to the testing and the application of the single-fluid code, and G. Holloway confirmed the cylindrical formulation in connection with an application of the single fluid code. D.J. Latornell discussed many of the convergence enhancement techniques.

REFERENCES

Amsden, A.A., and Harlow, F.H. (1978) KACHINA: An Eulerian Computer Program for Multifield Flows, LA-NUREG-5680, 1978.

Amsden, A.A., and Harlow, F.H. (1977) KTIF: A Two-Fluid Computer Program for Downcomer Flow Dynamics, LA-NUREG-6994, 1977.

Apizatis, N. (1985), On the Two-Dimensional Laminar Flows of a Particulate Suspension on the Presence of a Gravity Field.

Austin, L.R. (1970) Development of Viscous Flow in Helical Coils, PhD Thesis Univ. Utah, University Microfilms.

Baliga, B.R., Pham, T.T, Patankar, S.V.(1983) Solution of Some Two-Dimensional Incompressible Fluid Flow and Heat Transfer Problems Using a Control Volume Finite Element Method, Numerical Heat Transfer, 6, p245-261.

Benodeckar, R.W., Goddard,R.I., Gosman, A.D., Issa,R.I.(1985) Numerical Prediction of Flow over Surface Mounted Ribs, AIAA J, 23, 359-366.

Beyerlein, S.W., Crossman, R.K. and Richter, H.J. (1985), Prediction of Bubble Concentration Profiles in Vertical Turbulent Two-Phase Flow. I. J. Multiphase Flow, 11, p108-121.

Biesheuvel, A., VanWijgaarden, J., (1980) Two Phase Flow Equations for a Dilute Dispersion of Gas Bubbles in a Liquid, J. Fluid Mech. 148, pp. 301-318.

Boussinesq, J.(1877) Theorie de l'ecoulement tourbillant, Mem Pres Acad. Sci., XXIII, 46.

Bradshaw, P., Cebeci, T., and Whitelaw, J.H., (1981), Engineering Calculation Methods for Turbulent Flow, Academic Press.

Bugg, J.D.(1985) Flow Distribution in Adjacent Subchannels of Unequal Size, Atomic Energy of Canada Limited, AECL-8962, 1985.

Carslaw, H.S. and Jaeger, J.C. Conduction of Heat in Solids, Oxford, 1959.

Carver, M.B.(1980) Pseudo Characteristic Method of Lines Solution of the Conservation Equations, J Comp Phys., 35, pp 57-76.

Carver, M.B.(1981) Conservation and the Pressure Continuity Relationship in Multidimensional Two-Fluid Computation, in R Vichnevetsky, Ed., Advances in Computer Methods for Partial Differential Equations, IV (IMACS Press, 1981) pp 168-172.

Carver, M.B.(1982) A Method of Limiting Values of Volume Fraction in Iterative Two Fluid Computations, J Mech Eng Sci V24, pp 221-224.

Carver, M.B.(1983) Numerical Computation in Two-Fluid Flow Using the Two-

Dimensional Computer Code TOFFEA, Atomic Energy of Canada Limited, AECL-8066.

Carver, M.B.(1984a), Numerical Computation of Phase Separation in Two-Fluid Flow, J Fluids Eng., 106, pp 147-153.

Carver, M.B.(1984b) Multidimensional Computational Analyses of Flow in Nuclear Reactor Components, SCS Transactions, 1, pp 97-116.

Carver, M.B., Carlucci L.N. and Inch,W.R.(1979) Thermalhydraulics in Re-Circulating Steam Generators, THIRST Code User's Manual, Atomic Energy of Canada Report, AECL 6346.

Carver, M.B. and Hinds, H.W.(1978) The Method of Lines and the Advective Equation, Simulation, 59-69.

Carver, M.B and Salcudean, M., (1984), Two-Dimensional Modelling of the Homogenizing Effects of Flow Obstructions in Two-Fluid Flow, Math and Comp. in Simulation,1984, XXVI, pp 475-484.

Carver, M.B and Salcudean, M., (1986), Three-Dimensional Numerical Modelling of Phase Distribution of Two-Fluid Flow in Elbows and Return Bends, Numerical Heat Transfer, 10, 229-251.

Carver, M.B. and M. Salcudean,(1987) Three Dimensional Modelling of the Effects of Flow Obstructions in Two-Fluid Flow, Math & Comp. in Simulation, in press.

Carver, M.B., Tahir, A., Rowe, D.S., Tapucu, A., Ahmad, S.Y.(1984) Computational Analysis of Two-Phase Flow in Horizontal Bundles, Nucl Eng Des.; 82, pp 215-226.

Chang, Y.F. and Skears, J.(1977) SOPHT - A Computer Model for CANDU-PHWR Heat Transport Networks and their Control, Nucl Tech., 35, pp 381-395.

Chen, B.C., Vanka, S.P., Sha, W.T.(1980) Recent Computations of Rod Bundle Thermalhydraulics Using Boundary Fitted Coordinates, Nucl Eng Des., 62, pp 123-136.

Chexal, B.(1986) The EPRI Full Range Drift-Flux Model, EPRI-NP-1487.

Chun, J.H.(1980) Flow Stratification of Two-Phase Flow in Horizontal Channels M.Sc. Thesis, U. Ottawa.

Chisholm, D. and Sutherland L.A. (1979) Prediction of Pressure Gradient in Pipeline Systems under Two-Phase Flow, Proc Inst. Mech Eng. 184, 24-31

Chorlton, F.(1967)Textbook of Fluid Dynamics, Van Nostrand.

Cook, T.L and Harlow, F.H., (1984), VORT, A Computer Code for Bubbly Two-Phase Flow, LA-10021-MS.

Courant, R., Isaacson, R. and Rees, M.(1952) On the Solution of Non-Linear Hyperbolic Differential Equations by Finite Differences, Comm., Proc. Appl Math., 5, pp 243-255.

Dean, W.R.(1927) Notes on the motion of Fluid in Curved Pipes,Phil. Mag.,4,243-255.

Delhaye, J.M. (1979) Basic Equations for Two-Phase Flow Modelling and Two-Phase Flow Patterns, Two-Phase Flow and Heat Transfer in the Power and Process Industries, Bergles et al.Editors, Hemisphere,New York.

DeVahl Davis, G. and Mallinson,G.D. (1976) An Evaluation of Upwind and Central Difference Approximations in Computational Fluid Dynamics, Computers and Fluids,4,29-43.

Drew, D.A. and Lahey, R.T.(1979) Application of Constitutive Principles to the Derivation of Multidimensional Two-Phase Flow Equations,I.J. Multiphase Flow,5,243-263.

Drew, D.A. and Lahey, R.T., (1981), Phase Distribution Mechanisms in Turbulent Two-Phase Flow in Channels of Arbitrary Cross Section, J. Fluids Engng 103, pp. 583-589.

Egely, G. and Saha, P.(1984) A Study of Momentum Transfer in Two-Fluid Formulations, in Multiphase Flow nad Heat Transfer III, Veziroglu and Bergles editors, Elsevier, Amsterdam.

Ellul, I.R., and Issa, R.I. (1986) Numerical Computation of Multidimensional Multiphase Flow, 4th Conference on numerical methods in Laminar and Turbulent Flow, Swansea.

Ellul, I.R. and Issa, R.I.. (1987) Prediction of Flow of Interspersed Gas and Liquid Flow through Pipe Bends. Submitted to Transactions of the Institute of Chemical Engineers.

Ferch, R.L. (1979) Method of Characteristics Solution for Non-Equilibrium Transient Flow Boiling, Int J Multiphase Flow, 5, p 265.

Galpin, P.F., Huget, R.G. and Raithby, G.D.(1986) Fluid Flow Simulation in Complex Geometries, proceedings 2nd. CNS/ANS Int. Conf. on Simulation Methods in Engineering, Montreal.

Gardner, G.C.and Neller, P.H. (1970) Phase distributions in Flow of an Air-Water Mixture Around Bends and Obstructions, Proc. Inst. Mech. Eng.,184,93-101.

Gosman, A.D. and Pun, W.M.(1974) Notes for Course on Calculation of Recirculation Flow, Imperial College Report HTS/74/2.

Gosman, A.D., Khalil, C.E. and Whitelaw, J.H.(1979) The Calculation of Turbulent Recirculating Flows, in Turbulent Shear Flows, Springer Verlag, Berlin, 1, pp 287-302.

Hackman, L.P., Raithby, G.D. and Strong, A.B.(1984) Numerical Prediction of Flow over a Backward Facing Step, Int. J. Num. Meth. in Fluids,4, p711-724.

Hanna,B. and McDonald,B.H. (1982) , Development of 1-D Two-Fluid Model for RAMA, CNS Symposium on Reactor Dynamics and Control,McMaster Univ.

Hancox, W.T. and Banerjee, S.(1977) Numerical Standards for Flow Boiling Analysis, Nucl Sci & Eng., 64, p 106.

Harlow, F.H. and Amsden, A.A.(1971) A Numerical Fluid Dynamics Method for All Speeds, J Comp Phys., 8, p 197.

Harlow, F.H. and Nakayama, P.I.(1967) Turbulent Transport Equation, Physics of Fluids, 10, pp 2323-2335.

Hassan, Y.A., Rice, J.G. and Kim, J.H.(1983a) A Stable Mass Flow Weighted Two-Dimensional Skew Upwind Scheme, Num. Heat Transfer, 6, p395-408.

Hassan, Y.A., Rice, J.G. and Kim, J.H.(1983b) Comparison of Measured and Predicted Thermal Mixing Tests using Improved Finite Difference Schemes Num. Eng. Des., 76, p153-160.

Hessami, M.A. and Pollard, A.(1984) Numerical Calculation of Convective Heat Transfer Between Horizontal Concentric Cylinders, ASME J. Heat Transfer, 106, 668-675.

Hewitt, G.F. and Roberts, D.N.(1969) Studies of Two Phase Flow Patterns by X-Ray and Flash Photography, AERE-M 2159.

Hogg, J.D. and Seader, G.W.(1969) Peripheral Velocity Components for Turbulent Flow in Curved Tubes, AICHE annual Meeting, Washington.

Huang, K. Davis, M.R., The Influence of Return Bends in Velocity Ratio in Gas Liquid Pipe Flow, Int. J. Multiphase Flow, V6, p.267-272, 1979.

Inoue, A., Aoki, S., Koga, T. and Yaegashi, H., (1976), Void Fraction, Bubble and Liquid Velocity Profiles of Two-Phase Bubble Flow in a Vertical Pipe. (In Japanese,referenced by Sato et al) Trans. JSME, 42-360, pp. 2521-2531.

Ishii, M., and Zuber, N.,(1979) Drag Coefficient and Relative Velocity in Bubbly, Particulate and Droplet Flows, AIChE Journal, 25, p. 843-850.

Ishii, M., (1975), Thermo-Fluid Dynamic Theory of Two-Phase Flow, Eyrolles Press.

Ishii, M. and Chawla, I.C., (1979), Two-Fluid Model Momentum Interaction Between Phases, 7th NRC Water Reactor Safety Research Information Meeting, Gaithersburg.

Judd, R.A., Tahir, T., Kiteley, J.C., Carver, M.B., Rowe, D.S., Stewart, D.G., and Thibeault, P.R.(1984) ASSERT-4(Version 1) User's Manual, Atomic Energy of Canada Limited, AECL-8573.

Kocamustafaogulari, G.(1971) Thermo-Fluid Dynamics of Separated Two-Phase Flow, PhD Thesis, Georgia Tech., University Microfilms.

Lahey, R.T., (1979), Phase Distribution and Separation Phenomena,USNRC Water Reactor Safety Research Information Meeting, Gaithersburg.

Launder, B.E. Spalding, D.B.,(1972) Mathematical Models of Turbulence,Academic Press, London.

Launder, B.E and Spalding, D.B., (1974), The Numerical Computation of Turbulent Flows Comp Math Appl Mech and Eng., 3, pp 269-289.

Latimer, B.R. and Pollard, A.(1985) A Comparison of Pressure-Velocity Coupling Solution Algorithms, Numerical Heat Transfer,8,635-653.

Leonard, B.P. (1979) A Stable and Accurate Convective Modelling Procedure Based on Quadratic Upstream Interpolation, Comp Meth Appl Mech. and Eng., 19, pp 59-78.

Liles, D.R.(1978) The Three Dimensional Two-Fluid Numerical Treatment of a Reactor Vessel in TRAC, Proceedings ANS Meeting on Computational Methods in Nuclear Engineering, Williamsburg, 1979, pp 1-33, also TRACP1: An Advanced Best Estimate Computer Program for PWR LOCA Analyses, LASL Report NUREG/CR-0063, LA-7279 MSV1.

Lillington, J.N.(1981) A Vector Upstream Differencing Scheme for Problems in Fluid Flow Involving Significant Source Terms, Int. J. Num. Meth. Fluids, 1, p3-16.

Lumley, J.L.(1983) Turbulence Modelling, J Applied Mech., 50, pp 1097-1103.

Lyczkowski, R.W. and Sha, W.T.(1981) Foundations of Rational Multiphase Flow and Heat Transfer Field Equations, Advances in Computer Methods for Partial Differential Equations, IV, R Vichevestksy, editor, IMACS press, pp 160-167.

Mahaffy, J.H. et al.,(1981) TRAC-PD2, An Advanced Best Estimate Code for Pressurized Water Loss of Coolant Accident, NUREG/CR-2054.

Malnes, D., (1966), Slip Ratio and Friction Factors in Bubble Flow Regime in Vertical Tubes, KR-110, Kjeller, Norway.

Moody, L.F.(1984) Friction Factors for Pipe Flow, Trans ASME, Nov 1944, p 676.

Moore, K.V. and Rettig, W.H.(1975), RELAP4, A Computer Program for Transient Thermalhydraulic Analysis, ANCR-1127.

Mori, W. Nakayama, Y.,(1967) Study of Forced Convective Heat Transfer in Curved Pipes, Int. J. Heat & Mass Transfer, 8, p.1170-1185.

Mundhane, J.M, Gregory, G.A. and Aziz,K.(1974) A Flow Pattern Map for Gas-Liquid Flow in Horizontal Pipes, I.J.Multiphase Flow,1,537-553.

Oshinowo, M.E. Charles, T.,(1974) Vertical Two Phase Flow Pattern Correlations, Can. J. Chem. Eng., 52, pp. 25-35, 1974.

Patankar, S.V., (1972), A Calculation Procedure for Heat Mass and Momentum Transfer in Three-Dimensional Parabolic Flow, I.J Heat and Mass Transfer, 15, pp 1787-1891.

Patankar, S.V.(1980) Numerical Heat Transfer and Fluid Flow, Hemisphere, New York.

Prandtl, U.(1925) Uber die ausgebidete Turbulenz, ZAMM5, pp 136-139.

Pratap, V.S., Patankar, S.V., Spalding, D.B.(1976) Prediction of Turbulent Flow in Curved Pipes, J Fluid Mech., pp 539-551.

Pratap, V.S.(1976) Flow and Heat Transfer in Curved Ducts, PhD Thesis, U London.

Raithby, G,D.(1976) Skew Upstream Differencing Schemes for Problems Involving Fluid Flow Comp Meth Appl Mech and Eng., 9, pp 153-164.

Raithby, G.D. and Schneider, C.E.(1979) Numerical Solution of Problems in Incompressible Fluid Flow: Treatment of the Velocity-Pressure Coupling, Num Heat Transfer, 2, p 417.

Ransom, V.H. and Hick, D.E.(1984) Hyperbolic Two-Pressure Models for Two-Phase Flow, J Comp Phys., 53, pp 124-151.

Ransom, V.H. et al.,(1982) RELAP5/Mod1 Code Description System Models and Numerical Methods NUREG/CR-1826.

Ransom, V.H. et al.,(1985) RELAP5/Mod2 Code Description System Models and Numerical Methods NUREG/CR-4312.

Restivo, A., Gosman, A.D and Issa,R.I.(1980)Flow Properties of Rooms with Small Ventilation Openings, J. Fluids Eng, 12, pp 316-320.

Rietema ,K. and Van den Akker,H. (1982) On .the Momentum Equations in Dispersed Two-Phase Systems, I.J.Multiphase Flow, 9, 21-36.

Rivard W.V. and M.D Torrey,(1978) KFIX: A Program for Transient Two Dimensional Two-Fluid Flow, LA-NUREG-6623.

Roache, P,J.(1976) Computational Fluid Dynamics, Hermosa, Abuquerque .

Rohatgi, P. Saha, U.S.,(1980) Constitutive Relationships in TRACP1A, NUREG/CR-1651.

Rouhani, Z., (1976), The Effect of Wall Friction and Vertex Generation on Radial Void Distribution, the Wall Vortex Effect, I.J Multiphase Flow, 3, pp 35-50.

Rowe, D.S.(1973) COBRA-III C, A Digital Program for Steady State and Transient Thermalhydraulics Analyses of Rod Bundle Nuclear Fuel Elements, BNWL-1695.

Salcudean, M. and Adbelrehim,Z.(1980) Heat Transfer in Turbulent Recirculating Flows Affected by Bouyancy in Rectangular Cavities, Chem Eng Commun., V4, pp 249-268.

Salcudean, M., Chun, J.H., Groeneveld, D.C. Leung, L.(1983) Effect of Flow Obstruction Geometry in Pressure Drop in Horizontal Air Water Flow, Int. J. Multiphase Flow 9 (1) 73-85.

Salcudean, M., Groeneveld, D.C., Leung, L.(1983) Effect of Flow Obstruction on Void Distribution in Horizontal Air-Water Flow. Int. J. Multiphase Flow, 9, pp. 91-96.

Salcudean, M., Lai, K., Guthrie, R.I.L.(1985) Mass and Multidimensional Heat, Flow Phenomena in Gas Stirred Reactors, Can. J. Chem. Eng., 63, pp. 57-61.

Salcudean, M., Leung, L.K.H.,(1985) Effect of Flow Obstruction on Two-Phase Pressure Drops in Horizontal and Vertical Flows, 2nd Int. Conf. Multiphase Flow, London, Sponsored by BHRA.

Sato, Y. Sadatomi, M. and Sekoguchi, K., (1981), Momentum and Heat Transfer in Two-Phase Bubble Flow, I.J Multiphase Flow I-Theory, pp 167-177, II A Comparison Between Experiment and Theoretical Calculations, pp 179-190.

Sato, Y. and Sekoguchi, K., (1975), Liquid Velocity Distribution in Two-Phase Bubble Flow, Int J Multiphase Flow, 2, pp 79-95.

Schlichting, H., (1979), Boundary Layer Theory, McGraw-Hill, New York.

Serizawa, R., Katasha, I and Michiyuki, I., (1975), Turbulent Structure of Air-Water Bubbly Multiphase Flow, 2, pp 221-259.

Sha, V.L. et al.,(1979) Numerical Procedures for Calculating Steady/Unsteady Single/Two Phase Three Dimensional Fluid Flow with Heat Transfer, NUREG-CR-0789.

Soh, W.Y. and Berger, S.A.(1984) Numerical Prediction of Laminar Flow in Helical Coils, J.Fluid. Mech.,184,109-135.

Soo, S.L.(1967) Fluid Dynamics of Multiphase Systems, Blaisdell, Waltham, Ma.

Spalding, D,B.(1972) A Novel Finite Difference Formulation for Differential Expressions Involving First and Second Derivatives, Int J Num Meth. Eng,551-559.

Spalding, D.B. et al.,(1978) The Ursula Steam Generator Code, EPRI-NP-1315.

Spalding, D.B. et al.,(1979) Calculation of Two Dimensional Two-Phase Flows, Two-Phase Momentum, Heat Transfer in Chemical Process, and Energy Engineering Systems, F Durst, et al., editors, Hemisphere Press, Washington.

Spalding, D,B.(1980) Mathematical Methods in Nuclear Reactor Thermalhydraulics, Proceedings ANS Meeting on Nuclear Reactor Thermalhydraulics, Saratoga, N.Y., R.T Lahey, ed., pp 1979-2023.

Sun, T.Y. and Faeth, G.M.(1986) Structure of Turbulent Bubbly Jets, I.J. Multiphase Flow,12,99-126.

Tapacu, A. and Gencay, P.(1980) Measurement of Air and Water Flow in Interconnected Subchannels. Ecole Polytechnique report EP/NP 1768.

Usui, K., Aoki, S. and Inoue, A., (1983), Flow Behaviour and Pressure Drop of Two-Phase Flow Around Inverted U-Bend, J Nucl Science and Tech., 20, 11, pp 915-928.

Van der Welle, R.(1981) Turbulent Viscosity in Vertical Adiabatic Liquid Flow I.J. Multiphase Flow,6,461-475.

VanDoormaal, J.P. and Raithby, G.D. (1984) Enhancements of the SIMPLE Method for Predicting Incompressible Flows, Num. Heat. Transfer,7,147-164.

Von Rosenburg, D.U.(1969) Methods for the Numerical Solution of Partial Differential Equations, Elsevier, New York.

Wallis, G.B.,(1976) EPRI-NP-275, The Separated Flow Model of Two Phase Flow.

Wallis, G.B.,(1979) One-Dimensional Two-Phase Flow, McGraw-Hill.

Wong, H.H. and Raithby, G.D.(1979) Improved Finite Difference Methods Based on Critical Evaluation of the Approximation Errors, Num. Heat Transfer, 2, p139-163.

Zuber, N. and Findlay, J.A., (1965), Average Volumetric Concentration in Two-Phase Flow Systems, J. Heat Transfer, pp. 453-468.

Zuber, N., (1960), On the Variable Density Single-Fluid Model for Two-Phase Flow, Trans. ASME, J. Heat Transfer, 82, pp. 255-258.

Zuber, N., Steady State and Transient Void Fraction in Two Phase, et al. Flow Systems, GEAP5417, 1967.

Zun, I., Richter, H.J. and Wallis, G.B., (1975), The Transverse Migration of Bubbles in Vertical Two-Phase Flow, Dartmouth College, Thayer School of Engineering, Hanover, N.H.

APPENDICES

A : GRID LAYOUT AND COMPUTATIONAL FUNDAMENTALS

This appendix contains the fundamental details of the computational algorithms. Refinements are discussed in Appendix B.

A.1 Grid Layout and Control Volumes

The staggered grid used in the FAITH code differs from conventional grids only in that the velocity components are stored ahead of the pressure node with the same index instead of upstream of the node as in most other codes, for example Patankar(1980), Carver et al(1981).

The arrangement of velocities and grid points is summarized in Table A1 and Figures A1 to A4, as are the geometrical variables associated with the grid. Note that only internal velocities are stored; this results in significant storage saving. Velocity components perpendicular to a wall or a line of symmetry are zero. The y=0 boundary is a line of symmetry, x=0,XTOT can be solid walls usually for a cartesian option or lines of symmetry for the cylindrical option. The U velocity grid is not shown but is analogous to the V velocity grid in all respects but those concerning symmetry and radius.

Note that all scalars are stored at the main points and that for a scalar control volume the velocity vectors are centred at the scalar control volume faces. Vector control volumes are staggered only in the direction of the particular vector, such that they are centered on that vector. The various geometrical quantities required to define these control volumes are shown in Figures A2 and A3. Figure A4 shows a representation of the layout of a typical toroidal control volume.

Figure A4 Layout of a Typical Toroidal Scalar Control Volume

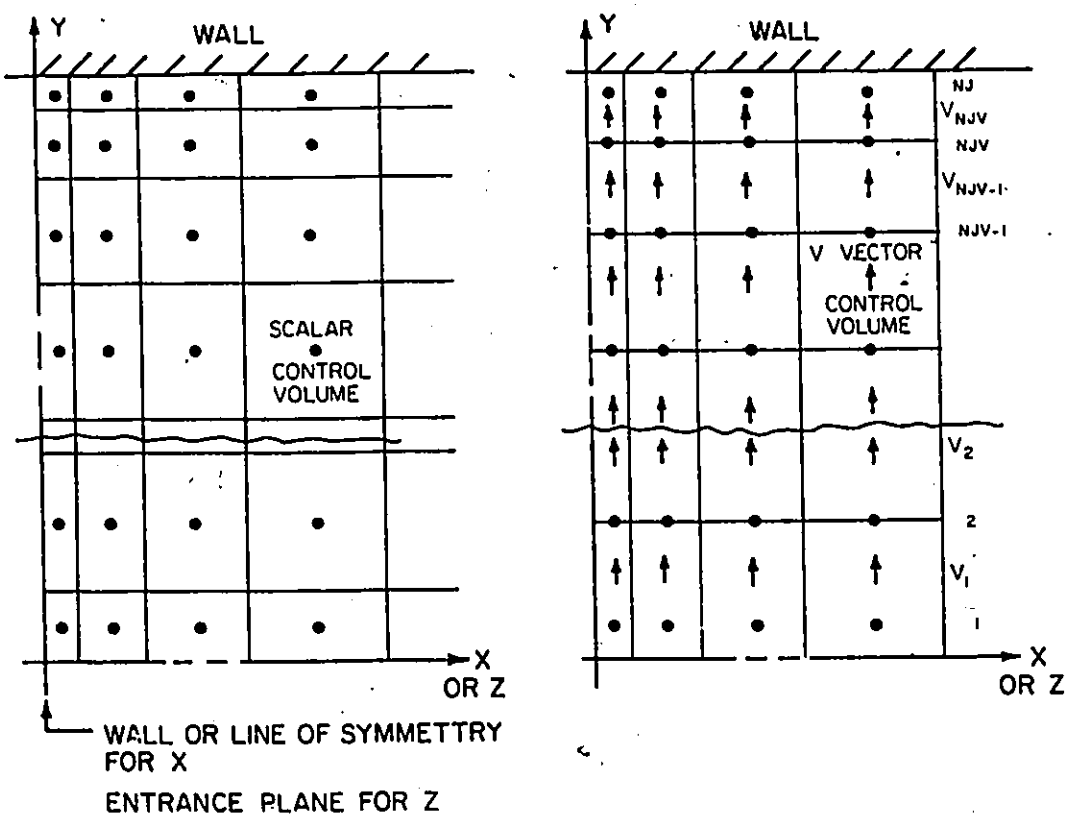

Figure A1: Scalar and Vector Control Volume Positions

FIGURE A2

AXIAL GRID LAYOUT

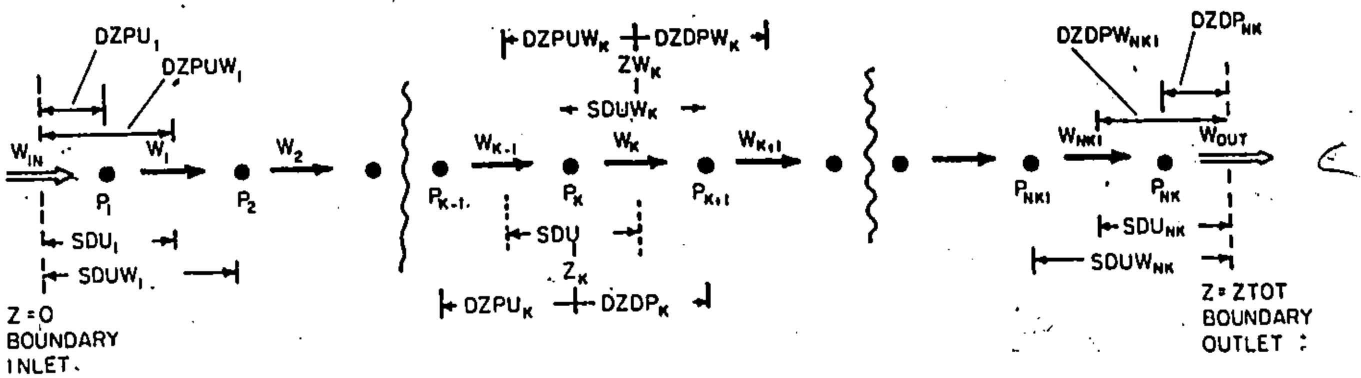

FIGURE A3

RADIAL GRID LAYOUT

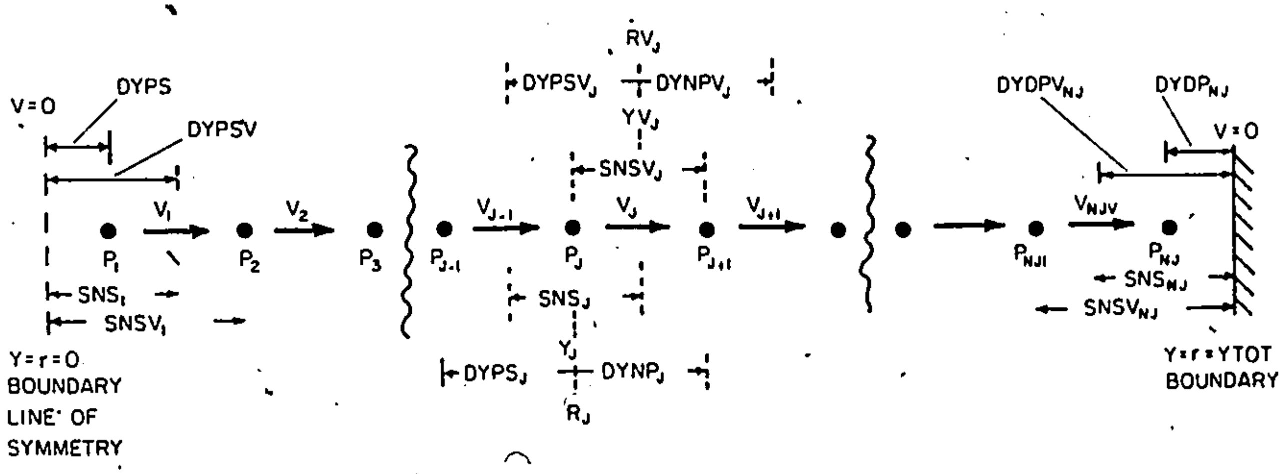

NOTE $RCV_J = 0.5\ (R_J + R_{J-1})$

X GRID IS SIMILAR, EXCEPT BOTH BOUNDARIES CAN BE LINES OF SYMMETRY

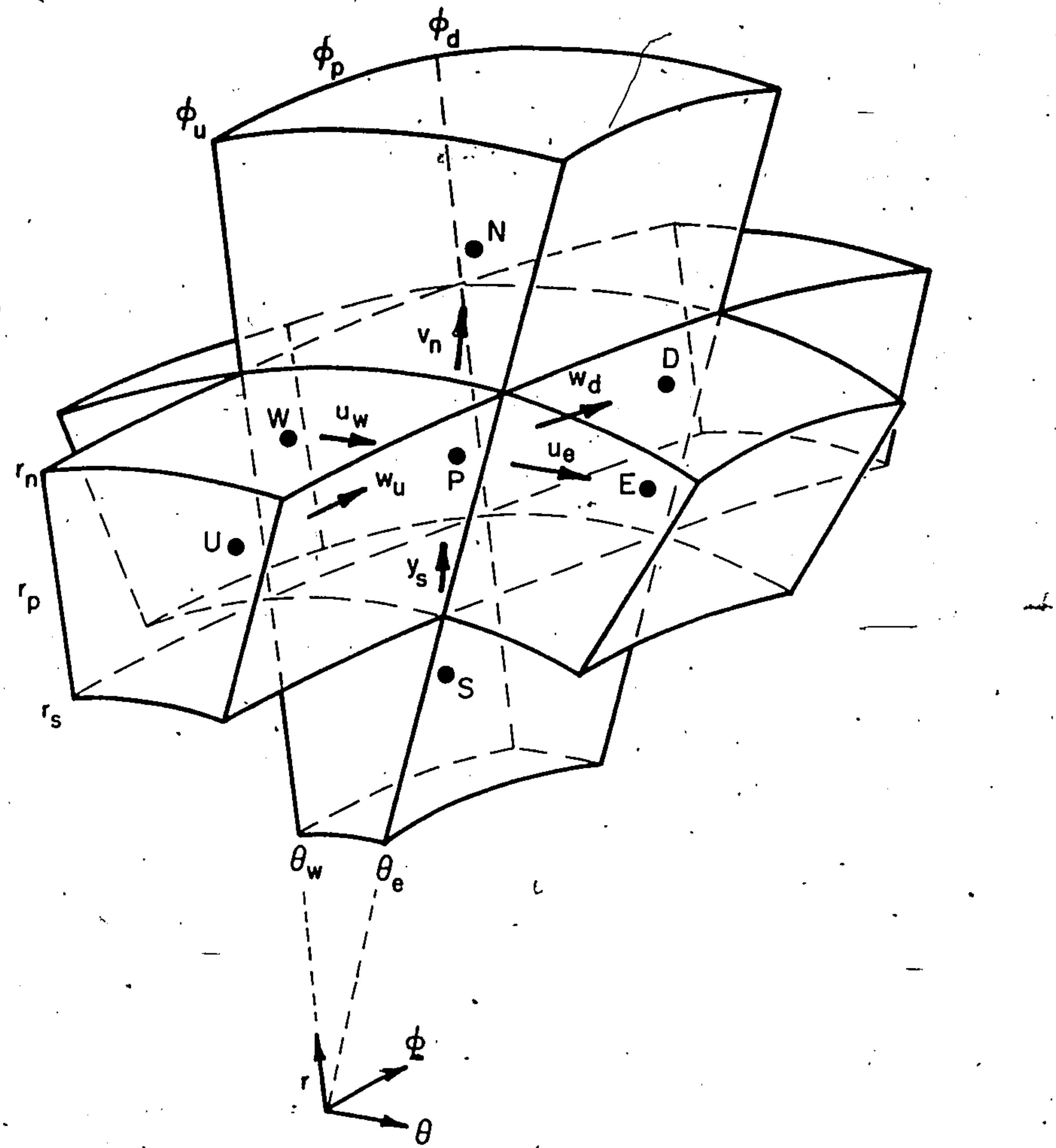

Figure A4 Layout of a Typical Toroidal Scalar Control Volume

TABLE A1

Assignment of Variables

Variable	Symbol	Fluid 1	Fluid 2	Dimensions	Location
Pressure	p	P		NX,NX,NZ	X,Y,Z
θ velocity	u	u	uu	NX1,NY,NZ	XU,Y,Z
∂U/∂P	$\partial u/\partial P$	DU	DUU	"	"
r velocity	v	V	VV	NX,NY1,NZ	X,YV,Z
∂V/∂P	$\partial v/\partial P$	DV	DVV	"	"
ψ velocity	w	W	WW	NX,NY,NZ1	X,Y,ZW
∂W/∂P	$\partial w/\partial P$	DW	DWW	"	"
Pressure Correction	dp	PP		NX,NY,NZ	X,Y,Z
Density	ρ	DENS	DEN2	"	"
Viscosity	μ	VIS	VIS2	"	"
Volume Frac.	β,α	BET	ALF	"	"
Turbulent En.	k	TE		"	"
Turbulent Dissip.	ε	ED		"	"
Turbulent Gen.	G	GENER		"	"
Inlet Flow	W_{in}	WIN	WIN2	NX,NY	X,Y
Outlet Flow	W_{out}	WOU	WOU2	"	"
Inlet Vol. Frac.	β_{in},α_{in}	BETIN	ALFIN	"	"

A.2 Integration of the Equations

As discussed in chapter 2, the equations are integrated by applying Greens theorem, equation (2.13), where necessary to the standard form, equation (2.12), to produce (2.14). For the cartesian form, the portion of the viscous terms which must be attributed to the source terms is apparent from equation (2.27), and as noted, for the laminar case, is zero

$$\frac{\partial}{\partial x_j} \mu \frac{\partial U_j}{\partial x_i} = \tau_L \tag{A1}$$

The integrated forms of the viscous terms are given in Tables A2 to A7, and are labelled type 1, 2, 3, 4. The required areas and volumes are given in table A8.

Type 1 fits the standard form, equation (2.14)

Types 2–4 are terms which must be included in the source

Type 2 fits equation A1

Type 4 arise from the toroidal formulation

Type 3 are the remaining terms

TABLE A2

Integrated Form of the Non-Viscous Components

of the θ Momentum Equation (Equation 2.4)

Term	Integrated Form	Type
$\frac{1}{R'r}\{ \frac{\partial}{\partial\theta}(R'\alpha\rho uu) \}$	$\Delta_{EW}[(\alpha\rho uA)u]$	1
$\frac{1}{R'r}\{ \frac{\partial}{\partial r}(R'r\alpha\rho uv) \}$	$\Delta_{NS}[(\alpha\rho vA)u]$	1
$\frac{1}{R'r}\{ \frac{\partial}{\partial\phi}(R'r\alpha\rho wu) \}$	$\Delta_{UD}[(\alpha\rho wA)u]$	1
$Z_1 = \alpha\rho w^2 \sin\theta/R'$	Z_1VOL	4
$Z_2 = \alpha\rho uv/r$	Z_2Vol	4
$\frac{\alpha}{r}\frac{\partial p}{\partial\theta}$	$\alpha\bar{\Delta}_{EW}(pA)$	3
$Z_3 = \alpha\rho g\sin\phi\sin\theta$	Z_3VOL	3
$Z_4 = \Psi(u_l - u_l)$	Z_4VOL	3

TABLE A3

Integrated Form of the Non-Viscous Components

of the r Momentum Equation (Equation 2.5)

Term	Integrated Form	Type
$\frac{1}{R'r}\{ \frac{\partial}{\partial\theta}(R'\alpha\rho uv) \}$	$\Delta_{EW}[(\alpha\rho uA)v]$	1
$\frac{1}{R'r}\{ \frac{\partial}{\partial r}(R'r\alpha\rho vv) \}$	$\Delta_{NS}[(\alpha\rho vA)v]$	1
$\frac{1}{R'r}\{ \frac{\partial}{\partial\phi}(R'r\alpha\rho wv) \}$	$\Delta_{UD}[(\alpha\rho wA)v]$	1
$Z_1= \alpha\rho w^2\cos\theta/R'$	Z_1VOL	4
$Z_2= \alpha\rho u^2/r$	Z_2Vol	4
$\alpha\frac{\partial p}{\partial r}$	$\bar{\alpha}\Delta_{NS}(pA)$	3
$Z_3= \alpha\rho g\sin\phi\cos\theta$	Z_3VOL	3
$Z_4= \Psi(v_{\iota}- v_{\iota})$	Z_4VOL	3

TABLE A4

Integrated Form of the Non-Viscous Components

of the ϕ Momentum Equation (Equation 2.6)

Term	Integrated Form	Type
$\frac{1}{R'r}\{ \frac{\partial}{\partial\theta}(R'\alpha\rho uw) \}$	$\Delta_{EW}[(\alpha\rho uA)w]$	1
$\frac{1}{R'r}\{ \frac{\partial}{\partial r}(R'r\alpha\rho vw) \}$	$\Delta_{NS}[(\alpha\rho vA)w]$	1
$\frac{1}{R'r}\{ \frac{\partial}{\partial\phi}(R'r\alpha\rho ww) \}$	$\Delta_{UD}[(\alpha\rho wA)w]$	1
$Z_2 = \alpha\rho w(u\cos\theta - v\sin\theta)/R'$	$Z_2 Vol$	4
$\frac{\alpha}{R'}\frac{\partial p}{\partial\psi}$	$\bar{\alpha}\Delta_{UD}(pA)$	3
$Z_3 = \alpha\rho g\cos\psi$	$Z_3 VOL$	3
$Z_4 = \Psi(w_l - w_l)$	$Z_4 VOL$	3

TABLE A5

Integrated Form of the Viscous Components (Equation 2.7) of the θ Momentum Equation (Equation 2.4)

	Term	Integrated Form	Type
1.	$\frac{1}{Rr}\frac{\partial}{\partial r}\left[Rr\,\alpha\mu\left(r\frac{\partial}{\partial r}\frac{u}{r}\right.\right.$	$\Delta_{NS}\left[\alpha\mu\frac{\partial u}{\partial r}A\right]$	1
	$\left.\left.+\frac{1}{r}\frac{\partial V}{\partial\theta}\right)\right]$	$-\Delta_{NS}\left[\frac{\alpha\mu u}{r}A\right]$	2
		$+\Delta_{NS}\left[\frac{\alpha\mu}{r}\frac{\partial v}{\partial\theta}A\right]$	3
2.	$\frac{1}{Rr}\frac{\partial}{\partial\theta}\;2R\alpha\mu\left[\left(\frac{1}{r}\frac{\partial u}{\partial\theta}+\frac{v}{r}\right)\right]$	$2\Delta_{EW}\left[\frac{\alpha\mu}{r}\frac{\partial u}{\partial\theta}A\right]$	1+2
		$+\Delta_{EW}\left[\frac{2\mu V\alpha}{r}A\right]$	3
3.	$\frac{1}{Rr}\frac{\partial}{\partial\phi}\left[r\alpha\,\mu\left(\frac{R}{r}\frac{\partial}{\partial\theta}\frac{W}{R}+\frac{1}{R}\frac{\partial u}{\partial\phi}\right)\right]$	$\Delta_{UD}\left[\frac{\alpha\mu}{r}\frac{\partial W}{\partial\theta}A\right]$	2
		$\Delta_{UD}\left[\alpha\mu\frac{W}{R}\sin\theta\,A\right]$	4
		$+\Delta_{UD}\left[\frac{\alpha\mu}{R}\frac{\partial U}{\partial\phi}A\right]$	1
4.	$\left[\frac{\alpha\mu}{r}\left(r\frac{\partial}{\partial r}\frac{U}{r}+\frac{1}{r}\frac{\partial v}{\partial\theta}\right)\right]$	$\left[\frac{\alpha\mu}{r}\frac{\partial U}{\partial r}-\frac{U}{r}\right]\mathrm{VOL}$	3
		$+\left[\frac{\alpha\mu}{r^2}\frac{\partial V}{\partial\theta}\right]$	3
5.	$\frac{2\alpha\mu}{R^2}\left[\frac{\partial W}{\partial\phi}+v\cos\theta-u\sin\theta\right]\sin\theta=Z$	Z.VOL	3

TABLE A6

Integrated Form of the Viscous Components (Equation 2.8)

of the r Momentum Equation (Equation 2.5)

Term	Integrated Form	Type
1. $\frac{1}{Rr}\left[\left(\frac{\partial}{\partial r} 2\ Rr\alpha\ \mu \frac{\partial V}{\partial r}\right)\right]$	$\Delta_{NS}\left[2\alpha\mu \frac{\partial V}{\partial r}\ A\right]$	1+2
2. $\frac{1}{Rr}\ \frac{\partial}{\partial \theta}\ R\alpha\mu\left[\left(r \frac{\partial}{\partial r} \frac{U}{r} + \frac{1}{r}\frac{\partial V}{\partial \theta}\right)\right]$	$\Delta_{EW}\left[\frac{\alpha\mu}{r}\ \frac{\partial V}{\partial \theta}\ A\right]$	1
	$+\ \Delta_{EW}\left[\alpha\mu \frac{\partial U}{\partial r}\ A\right]$	2
	$-\ \Delta_{EW}\left[\frac{\alpha\mu U}{r}\ A\right]$	3
3. $\frac{1}{Rr}\ \frac{\partial}{\partial \phi}\left[r\alpha\mu\ \left(\frac{1}{R}\frac{\partial V}{\partial \phi} + R\ \frac{\partial}{\partial r}\frac{W}{R}\right)\right]$	$\Delta_{UD}\left[\frac{\alpha\mu}{R}\ \frac{\partial V}{\partial \phi}\ A\right]$	1
	$+\ \Delta_{UD}\left[\alpha\mu\ \frac{\partial W}{\partial r}\ A\right]$	2
	$+\ \Delta_{UD}\left[\alpha\mu\ \frac{W}{R}\ \cos\ \theta\ A\right]$	4
4. $-\ \frac{2\alpha\mu}{r}\left[\left(\frac{1}{r}\ \frac{\partial V}{\partial \theta} - \frac{v}{r}\right)\right] = Z_4$	$Z_4 VOL$	3
5. $+\ \frac{2\alpha\mu}{R}\ \left(\frac{\partial W}{\partial \phi} + v\cos\ \theta - u\sin\ \theta\right)\ \frac{\cos\ \theta}{R} = Z_5$	$Z_5 VOL$	3

TABLE A7

Integrated Form of the Viscous Components (Equation 2.9)

of the ϕ Momentum Equation (Equation 2.6)

Term	Integrated Form	Type
1. $\frac{1}{Rr}\left[\frac{\partial}{\partial r}\left[\bar{R}r\alpha\mu\left(\frac{1}{R}\frac{\partial V}{\partial \phi}\right.\right.\right.$	$\Delta_{NS}\left[\frac{\alpha\mu}{R}\frac{\partial V}{\partial \phi}A\right]$	2
$\left.\left.\left.+ R\frac{\partial}{\partial r}\frac{W}{R}\right)\right]\right]$	$+ \Delta_{NS}\left[\alpha\mu\frac{\partial W}{\partial r}A\right]$	1
2. $\frac{1}{Rr}\left[\frac{\partial}{\partial \theta}\left[R\alpha\mu\left(\frac{R}{r}\frac{\partial}{\partial \theta}\frac{W}{R}\right.\right.\right.$	$\Delta_{EW}\left[\frac{\alpha\mu}{r}\frac{\partial W}{\partial \theta}A\right]$	1
$\left.\left.\left.+\frac{1}{R}\frac{\partial U}{\partial \phi}\right)\right]\right]$	$+ \Delta_{EW}\left[\frac{\alpha\mu}{R}\frac{\partial U}{\partial \phi}A\right]$	2
	$- \Delta_{EW}\left[\frac{\alpha\mu W}{R}\sin\theta\, A\right]$	4
3. $\frac{1}{Rr}\left[\frac{\partial}{\partial \psi}2\alpha\mu r\left(\frac{1}{R}\frac{\partial W}{\partial \phi}\right.\right.$	$\Delta_{UD}\left[\frac{2\alpha\mu}{R}\frac{\partial W}{\partial \phi}A\right]$	1+2
$\left.\left.+ (v\cos\theta - u\sin\theta)/R\right)\right]$	$+ \Delta_{UD}\left[\frac{2\alpha\mu}{R}(v\cos\theta - u\sin\theta)\, A\right]$	3
4. $\frac{\alpha\mu}{R}\left[\left(\frac{1}{R}\frac{\partial V}{\partial \phi} + R\frac{\partial}{\partial r}\frac{W}{R}\right)\right]\cos\theta = Z_4$	Z_4VOL	4
5. $\frac{\alpha\mu}{R}\left[-\left(\frac{R}{r}\frac{\partial}{\partial \theta}\frac{W}{r} + \frac{1}{R}\frac{\partial V}{\partial \phi}\right)\right]\sin\theta = Z_5$	Z_5VOL	4

TABLE A8

AREAS AND VOLUMES

Term	Integrated Form	Variable
$R'd\phi r dr d\theta$	$R\ \Delta\phi\bar{r}\Delta r\Delta\theta(1+\varepsilon)$ $\varepsilon<\bar{r}\Delta\sin\theta/R\Delta\theta$	VOL
$rdrd\theta$	$\bar{r}\Delta\theta\Delta r$	AU=AD
$R'd\phi dr$	$R\ \Delta\phi r\Delta\theta(1+\varepsilon)$ $\varepsilon<\bar{r}\cos\theta/R$	AE=AW
$R'd\phi r d\theta$	$R\ \Delta\phi r\Delta\theta(1+\varepsilon)$ $\varepsilon<r\Delta\sin\theta/R\Delta\theta$	AN=AS

Note that as $\varepsilon<r/R$, the correction has been neglected by Austin(1971) , Pratap(1976) and Soh and Berger(1984). It was also neglected in this study. This is clearly justifiable for the bends of Gardner and Neller(1969), but is marginal for the bends of USUI et. al.(1983), however, in comparison with other approximations in the modelling, this is not unreasonable.

With reference to Figure A4, the following then apply to the scalar control volume p :

$$A_N = r_n(\theta_e-\theta_w)R'(\phi_d-\phi_u)$$
$$A_S = A_N r_s/r_n$$
$$A_E = A_W = .5R(\phi_d-\phi_u)(r_n+r_s)(r_n-r_s)$$
$$A_U = A_D = .5(r_n+r_s)(r_n-r_s)(\phi_e-\phi_w)$$

A.3 Convective Derivative Formulae

In chapter 4, it was pointed out that the integration of the standard equation (2.12) resulting in the detailed expression (2.15) could be reduced to the concise form (2.16) using appropriate expressions for interpolating values at the control volume faces. The interpolation expressions result from various Taylor series expansions of the convective derivative terms. The relation between Taylor derivative expression and Lagrangian interpolation polynominals is discussed by Carver and Hinds (1978), so it will be introduced very simply here. Two examples suffice

First Order Directional Difference

$$\left(\frac{\partial\phi}{\partial x}\right)_P = \frac{\phi_P - \phi_W}{x_P - x_W} = \frac{\phi_P - \phi_W}{\Delta x} \qquad \text{(A2)}$$

Second Order Central Difference

$$\left(\frac{\partial\phi}{\partial x}\right)_P = \frac{\phi_E - \phi_W}{X_E - X_W} = \frac{\phi_E - \phi_W}{2\Delta x} \qquad \text{(A3)}$$

Using the control volume integral method:

$$\int \left(\frac{\partial\phi}{\partial x}\right)_P dx = \phi_e - \phi_w \qquad \text{(A4)}$$

The interpolants $\phi_e = \frac{1}{2}(\phi_E + \phi_P)$ (A5)

$$\phi_w = \frac{1}{2}(\phi_P + \phi_W)$$

yield $\phi_e - \phi_w = \frac{1}{2}(\phi_E - \phi_W)$ (A6)

The interpolants $\phi_e = \phi_P$, $\phi_w = \phi_W$

yield $\phi_e - \phi_w = \phi_P - \phi_W$ (A7)

Clearly (A6) is equivalent to (A3) and (A8) to (A2).

Neglecting the higher order terms in the Taylor and Lagrange expansions produces a numerical diffusion. This is illustrated simply here by comparing the first order expression (A2) to the second order (A3):

$$\left(\frac{\partial\phi}{\partial x}\right)_P = (\phi_P - \phi_W)/dx = (\phi_E - \phi_W)/2dx + \{dx(\phi_E - 2\phi_P + \phi_W)/dx^2\} \qquad \text{(A8)}$$

Note that the {term} is a second derivative, thus the use of the first order expression has introduced an additional numerical diffusion. This is clearly detrimental to the accuracy, however, the fact that the central difference formula omits the point of interest is detrimental to diagonal dominance and hence to numerical stability.

The effect of these and higher order formulae on the accuracy and stability of numerical computation of 1D equations are widely discussed, for example see Carver and Hinds(1978), and their implications on the multidimensional convection diffusion equations are discussed at length in Patankar(1980), and will be discussed further in Appendix B. The appropriate direction for the directional difference is generally called upwind, and is dictated by the eigenvector of the characteristics equations Courant et al(1955), Carver(1980).

Considering only the convective and diffusive terms the general equation

$$\frac{d}{dx}(\rho u \phi) = \frac{d}{dx}\left(\xi \frac{d\phi}{dx}\right) \tag{A9}$$

becomes

$$(\rho u \phi)_e - (\rho u \phi)_w = (\xi/\Delta x)_e\,(\phi_E - \phi_P) - (\xi/\Delta x)_w\,(\phi_P - \phi_W) \tag{A10}$$

$$C_e \phi_P - C_w \phi_W = D_e\,(\phi_E - \phi_P) - D_w\,(\phi_P - \phi_W) \tag{A11}$$

Casting this into general form gives

$$A_p\,\phi_P = \sum_n A_n\,\phi_n\ ,\ n = E,W \tag{A12}$$

It is convenient to characterize the ratio of convection to diffusion by means of the dimensionless Peclet number.

$$P_t = C/D = \frac{\rho U \Delta x}{\xi}$$

It is well established that central difference formulae remain stable only for diffusion dominated flows (P_t small), and upwind formulae are stable for convective dominated flows (P_t large) . The hybrid differencing scheme introduced by Spalding (1972) uses these facts to introduce a sliding or hybrid difference scheme which uses upwind differencing for $|P_t| > 2$ and central for $|P_t| < 2$.

The resulting coefficients for each scheme are given in Table A9.

TABLE A9

Coefficients of the General Equation

Term	Central	Upwind	Hybrid
A_e	$D_e - C_e/2$	$D_e + \{-C_e\}$	$\{-C_e, D_e - C_e/2\}$
A_W	$D_w + C_w/2$	$D_w + \{C_w\}$	$\{C_w, D_w + C_w/2\}$
A_p	$D_e + D_w + (C_e - C_w)/2$	$D_e + D_w + \{C_e\} + \{-C_w\}$	
or	$A_e + A_w + C_e - C_w$	$A_e + A_w + C_e - C_w$	$A_e + A_w + C_e - C_w$

Note {A,B} denotes maximum of A,B,0

The coefficients for the three dimensional equations are assembled in analagous manner, hence :

$$A_p = \Sigma A_n + \Sigma C_{out} - \Sigma C_{in}$$

Further implications of the derivative formulation on accuracy are discussed in Appendix B.

A.4 Source Terms and Relaxation

Under-relaxation factors are applied to all the equations in prerelaxed form as discussed in chapter 2. Thus, the general equation

$$A_p \phi_p = \sum_n A_n\phi_n + S \tag{A13}$$

becomes

$$A_p' \phi_p = \sum_n A_n\phi_n + S' \tag{A14}$$

where $A_p' = A_p/\beta$, $S' = S + A_p' (1-\beta)\phi_p^0$

As noted, the iteration process is stable when all coefficients are positive, and stability is increased when diagonal domination (A_p) is increased. Thus, underrelaxation clearly stabilizes the iteration.

It is also not unusual for the source term to contain some functions of ϕ_p as all terms containing ϕ_p may not fit the standard form.

Thus, (A13) may be written to identify such terms

$$A_p\phi_p = \sum_n A_n\phi_n + S_c + S_p\phi_p \tag{A15}$$

To aid convergence, as many terms as possible must be implicit, so (A15) is written

$$(A_p - S_p)\phi_p = \sum_n A_n\phi_n + S_c \tag{A16}$$

Clearly, S_p must be retained negative to maintain diagonal dominance, hence many of the source terms are arranged to ensure this as follows. S_p is split into positive and negative portions

$$S_p = S_{pp} + S_{pm}$$

$$(A_p - S_{pm})\phi_p = \sum_n A_n\phi_n + S_c + S_{pp}\phi_p^0 \tag{A17}$$

A further scheme for enhancing diagonal dominance is used. From Table A8,

$$A_p = A_e + A_w + C_e - C_w \tag{A18}$$

or for the three dimensional case

$$A_p = \sum_n A_n + (\sum_O - \sum_I)\, C \tag{A19}$$

Note that the latter term is the divergence of the mass fluxes and is being driven to zero by the pressure correction process. Thus, to enhance diagonal dominance this term is included in A_p only when it is positive.

A.5 Initial and Boundary Conditions - General

The function of the calculation routines is given in table 4.1. To maintain the generality of the routines CALCU through CALCE, the equations are set up for all the internal grid as if there were no boundaries. Each routine calls instead the boundary condition routine PROMOD which has an entry point for each flow variable.

The program has not been set up with "user-friendly input", as the variety of cases to be addressed dictates that problems be set up within the program. As the definition of the geometrical framework comes entirely through the definition of coordinate system, initial and boundary conditions, a problem may be specified completely by modifying only EXEC, INIT and PROMOD. The specification of coordinate system, grid points and initial conditions are self-evident in EXEC and INIT respectively simply by assignment. It is neccessary only to define the main grid points and all other grid variables are then automatically computed; the conversion to the selected coordinate system is also automatic. The program has been set up using FORTRAN PARAMETER statements, and so storage automatically expands to fit the specified number of grid points, although the absolute size on the CRNL CDC 175 computer is limited because it does not have a virtual memory system.

As the above involves standard programming practice, no further details are required. However it is of interest to mention the boundary condition routine PROMOD. As shown in Figure A1, the grid is arranged so that boundaries are located in the position that would be occupied by an additional normal velocity vector. Hence, this velocity is zero. The velocity components near to and parallel to the wall are stored at a small distance from the wall, are non zero, and hence calculated. Normal components are taken as zero.

The only exception to this are the inlet and outlet planes where velocities are non-zero. In the original code Restivo et. al.(1980), inlet values had to be constant, however, inlet velocity, and volume fraction may now be specified as matrices in the x,y plane by assigning values to two-dimensional arrays WIN, WIN2 and ALFIN. In order to promote convergence, all internal values are also set to inlet values initially. At the outlet plane, WOUT, WOU2 are outlet mass flux matrices. In the routine FLEXIT, these are assembled from the final internal velocity vectors, summed and then adjusted to conserve axial flow continuity of each fluid, in the manner discussed in Chapter 4.

A.6 Boundary Conditions for Turbulent Flow

For the zero penetration boundary condition, no extra terms are required. However, the zero-slip condition must be imposed in terms of shear stress at the wall. First, a check is made to see whether the near-wall point is in the laminar sublayer or turbulent boundary layer by evaluating

$$y^+ = C_\mu^{0.25}\, k^{0.5}\, \rho dy/\mu \tag{A20}$$

where dy is the distance from the wall of the near-wall parallel velocity resultant Q_p.

For laminar sublayer $y^+ < 11.63$ Launder and Spalding(1974), and the shear stress is the same as for the laminar case.

$$\tau_w = \mu\,\frac{Q_p - Q_w}{dy} = \mu \frac{Q_p}{dy} \tag{A21}$$

For $y^+ \geqslant 11.63$, the shear stress at the wall is estimated by the generalized log law, Launder and Spalding(1974).

$$\tau_w = \kappa\, Q_p\, y^+ \mu/(dy \cdot \ln(E^+ y^+)) \tag{A22}$$

where E^+ is a surface roughness parameter, and κ is Von Karmans constant. These are assigned recommended values of 9.79 and 0.42 respectively; however, some variation of these values has been discussed, Bradshaw et. al.(1981).

Finally, the generation term G of equation (2.44) must be completed to incorporate the velocity gradient to the wall. Similarly, the value of turbulent kinetic energy k at the near wall points is modified using the assumption of zero diffusion to the wall. The dissipation rate ε is computed on the assumption that the length scale turbulence varies with distance from the wall in linear fashion. Hence,

$$\varepsilon_p = C_\mu^{0.75} \, k^{1.5} / \kappa \, dy \tag{A23}$$

Further details are given by Launder and Spalding(1974). In this study, the method used by Restivo et. al.(1984) in their single phase code was followed, invoking the common simplification that the shear stress components appearing in each momentum equation can be computed from the velocity components.

A.7 Structure of the CALC Routines

Each of the CALC routines has the same basic structure.

In the first section, the coefficients are assembled from the standard form, equation (2.15), for each k plane. Advantage is taken of the obvious cycle relationships, AW(I+1) = AE(I), etc. Following assembly of the standard coefficients, the nonstandard coefficients are inserted appropriately in the source terms.

In the second section, PROMOD is called to apply boundary conditions as discussed in A.6.

In the third section, the AP coefficient is assembled as described in section A.3, under-relaxation is applied as described in A.4, and finally the standard equation (A16) is solved after adjusting according to (A19) by calling the tridiagonal routine LISOLV, 2D option. This is repeated for each k plane.

There are two minor exceptions to this. The pressure equation (2.51) is solved in elliptic form, so all k planes are solved together using the tridiagonal LISOLV 3D option. Also in the CALC routine a block adjustment is made to ensure continuity is satisfied plane to plane in the Z direction. This adjustment is applicable only if the flow is predominantly in the Z direction. This is discussed in Chapter 4.

B. FURTHER NUMERICAL CONSIDERATIONS

B.1 Simplified Schemes

In a recent paper, Issa and Ellul (1986) have suggested that the momentum equation for the light phase can be reduced by considering only the dominant terms. The equations then become

$$0 = \psi \, (u_g - u_l) - \alpha \frac{\partial P}{\partial x_i} + (\alpha\rho)_g g_i \tag{B1}$$

This can then be solved in point Jacobi form for u_g, thus avoiding the solution of the complete equation involving the convective terms.

As this method clearly breaks down when the void fraction α becomes large, and, as if α is small, the full equation as programmed reduces to this equation anyway there is very little practical advantage to this simplification. A more general way of economizing used in this study is to use a smaller number of iteration sweeps in the light phase momentum equations, one sweep being sufficient unless considerable stratification takes place.

In the same publication Issa and Ellul (1986) obtain the pressure equation from the liquid phase continuity only. However in a more recent paper (1987), they reported that this led to some instability for large α, and now use the pressure equation based on the sum of the normalized or volumetric continuity equation of each fluid as originally outlined by Carver (1984).

B.2 Implicit Pressure Correction Formulation

One of the schemes suggested by Spalding (1983) attempts to make the momentum equations less interdependent, by eliminating the terms containing the velocity of the second fluid. The argument can be obscured by the algebra, so the equations are here first stated in simplified form.

$$a_p u_p = \sum_n a_n u_n + b\Delta P + d(u'_p - u_p) \tag{B2}$$

$$a'_p u'_p = \sum_n a'_n u'_n + b'\Delta P + d'(u_p - u_p) \tag{B3}$$

If we now combine these equations to eliminate u'_p from B2:

$$(a_p + d \ (1 - \frac{d'}{a'_p}))u_p = \Sigma a_n u_n + b\Delta P + \frac{d}{a'_p}(\Sigma a'_n u'_n + b'\Delta p) \tag{B4}$$

It would seem that no advantage is gained, until the derivative $\partial u/\partial \Delta P$ is evaluated.

$$\partial u/\partial \Delta P = \frac{b + d(b'/a'_p)}{a_p + d - d(b'/a'_p)} \tag{B5}$$

Clearly the effect of pressure on u is now influenced by the second fluid parameters. By contrast differentiating (B2) gives:

$$\partial u/\partial \Delta P = b/(a_p + d) \tag{B6}$$

It is quite straight forward to use (B5) for DU instead of the usual formula (B6), and Spalding suggests this gives improved convergence. In our case it had no detectable effect. Spalding was doing his tests with a constant drag function d. It seems that when a realistic drag function is used and $\gamma = f(v_r)|v_r|$, nonlinear effects must remove any advantage.

B.3 Convergence Enhancing Modifications to SIMPLE

Some of the minor modifications introduced by Raithby and VanDoormaal (1983) and reviewed by Latimer and Pollard (1985) were implemented in the FAITH code.

SIMPLECTS The first is the consistent time step formulation of Raithby (1978). Simply stated, this uses the fact that when the equations are stated in transient form, the time step is equivalent to a relaxation factor

$$(e_p + a_p)\, u_p = \sum_n a_n u_n + b\Delta P + d(u_p' - u_p) + e_p\, u_p^0 \tag{B7}$$

The coefficient e_p varies as $1/\Delta t$, hence a small time step is heavily under relaxed. Clearly, in a transient, the time step used in all equations must be the same.

Comparing equation (A11) to the implicitly prerelaxed equation

$$\left(\frac{a_p}{\beta}\right) u_p = \Sigma a_n u_n = \text{etc} + \left(\frac{1-\beta}{\beta}\right) a_p u^0 \tag{B8}$$

it is clear that

$$e_p^* = [(1 - \beta)/\beta]a_p \tag{B9}$$

Similarly, the pressure equation is derived from the continuity equation, thus the relaxation on the momentum equations must be the same, and that in the pressure equation must be equivalent to the same time step. This reduces to

$$\beta_p = 1 - \beta \tag{B10}$$

SIMPLEC

This modification notes that the pressure derivative normally used, B6, may be innacurate, as the effect of pressure on the neighbouring fluxes is ignored. In order to take these in to account, A6 is modified:

$$(a_p - \Sigma a_n)u_p = \{\Sigma a_n u_n - \Sigma a_n u_p\} + b\Delta P + \text{etc} \tag{B11}$$

The contention is that the {term} is now very small so that the new pressure derivative is more representative.

$$\partial u_p/\partial \Delta P = b/(a_p - \Sigma a_n) \tag{B12}$$

As SIMPLEC corrects the inaccuracy in the pressure equation to some extent, β_p=1.0 is recommended.

The Combination

Both SIMPLECTS and SIMPLEC may be used individually or together in the FAITH code. Invoking either gives improvement in convergence over the standard SIMPLE technique, but the improvement was usually small even for single phase flows. Latimer and Pollard reported a significant improvement in two dimensional studies, however they also showed the benefit of using an axial mass flux correction (Chapter 4.) to be much greater.

SIMPLER

The SIMPLER procedure due to Patankar (1980) has also been implemented in the program. In this method, the pressure is solved for directly as follows. First the momentum equations are solved in point Jacobi form for the so called pseudo velocities. The general momentum equation was written as

$$a_p u_{pi} = \Sigma a_n u_n + b_i \Delta P_i + S_i \qquad \text{(B13)}$$

The pseudo velocities are obtained from a point Jacobi-step, omitting the pressure term.

$$\tilde{u}_{pi} = (\Sigma a_n u_n + S_i)/a_{pi} \qquad \text{(B14)}$$

Equation B14 can now be written

$$u_{pi} = \tilde{u}_{pi} + b_i(P_+ - P_-)_i \qquad \text{(B15)}$$

A pressure equation can now be developed in a similar manner to the SIMPLE method of deriving a pressure correction equation

$$\vec{B}\,\vec{P} + \vec{D} = 0 \qquad \text{(B16)}$$

where now

$$D = \sum_{\iota} \sum_{n} (\alpha\tilde{u}A_+ - \alpha\tilde{u}A_-) \qquad \text{(B17)}$$

The only differences are that the pressure equation (B16) is based on the imbalance of the pseudo volumetric fluxes, where as the pressure correction equation is based on the imbalance of the volumetrix fluxes. This means that the pressure equation no longer lags behind the velocity field as in the pressure correction method. However the velocities must still be corrected to maintain continuity through a pressure correction equation in the same manner as SIMPLE.

$$\vec{B}'\ \delta\vec{P} + \vec{D}' = 0 \qquad \text{(B18)}$$

where

$$D = \sum_{\iota} \sum_{n} (\alpha uA_+ - \alpha uA_-) \qquad \text{(B19)}$$

and

$$\delta u_i = b_i(\delta P_+ = \delta P_-)_i/a_{pi} \qquad \text{(B20)}$$

Unlike SIMPLE, this pressure correction is applied only to correct the velocities and not the pressure.

The SIMPLER procedure requires about 1.4 times the work per iteration and also requires auxiliary storage for the pseudo velocities. The advantage cited is that the pressure field is established more quickly (although the pressure equation should also be iterated more than the correction equation). In this study the SIMPLE method and its 'C' and 'CTS' extensions were found to operate as efficiently as SIMPLER providing the block correction was imposed axially, because the latter also establishes the pressure field very quickly.

B.4 ARTIFICIAL OR NUMERICAL DIFFUSION AND RELATED ERRORS

As mentioned in Appendix A, higher order formulae have been proposed to minimize false diffusion, a phenomenon causing wave fronts to be unrealistically diffused. This diffusion is minimum when the predominant velocity is parallel to the grid lines. Raithby(1976) took advantage of this in his skewed differencing, in which derivatives are taken in the direction of the predominant velocity. These methods have not been incorporated in the code, so the user should be aware of the possibility of false diffusion. Some analytical methods of estimating the magnitude of false diffusion are discussed by Patankar(1980), who notes also that some idea can also be gained by completing successive calçulations with increasing viscosity. False diffusion may be so large that increasing viscosity will not significantly change the solution until the imposed viscosity approaches a significant fraction of the effective viscosity due to false diffusion.

Artificial diffusion and other related errors can be generated in any numerical solution because in the discretisation process, the equations are transformed into finite difference analogs which only approximate the mathematical equations. Errors can arise from a number of sources.

Diffusion due to Low Order Approximation in One Dimensional Equations

As discussed in Appendix A, equivalent formulae for derivatives may be obtained from Taylor series or by differentiating interpolants. By either route, higher order terms are usually neglected. Also, the appropriate direction of differentiating for hyperbolic equations is dictated by the characteristic loci. This leads to the so called donor-cell, upwind, or pseudo-characteristic differencing methods of which some higher order versions are reviewed in Carver (1980). The most common, donor cell method or first order upwind method, while guaranteeing stability, also causes undue smoothing of the solution due to the implicit addition of false diffusion terms mentioned in Appendix A. This can also lead to errors in pressure, Raithby (1976). This can be rectified by using higher order upwind methods, see for example Leonard (1980).

False Diffusion in Multi-Dimensional Grids

Derivatives in multidimensional methods are usually evaluated by applying locally one dimensional formulae in the various component directions. False diffusion can be minimized by using higher order formulae as above, but only when the streamlines coincide with a particular coordinate direction. Once the streamlines cross a control volume at an angle to the coordinates, the locally one dimensional formulae no longer retain the appropriate characteristic influence.

For example in a normal uniform two dimensional grid, upwind derivatives would normally be expressed as (Figure A1)

$$\frac{\partial\phi}{\partial x} = (\phi_P - \phi_W)/\Delta X \ (u>0)$$

$$\frac{\partial\phi}{\partial Y} = (\phi_P - \phi_S)/\Delta Y \ (v>0) \tag{B22}$$

These show the appropriate influence precisely only for either U=0 or V=0. For the case U=V however it is clear that the true upwind derivative is

$$\frac{\partial\phi}{\partial S} = (\phi_P - \phi_{SW})/\Delta S \ (u,v>0) \tag{B23}$$

and that the appropriate components should be obtained from (B23) not (B22). The results of applying B22 to the latter case will be to smear any changes across the streamline in a similar manner that lower order methods smear changes along a streamline. Clearly a method that smears neither along or across the streamline is required.

A method of resolving this problem by differentiating along streamlines by rotating a local reference coordinate system, thus in effect using a version of B23 was developed by Raithby (1975) and a number of variations on this 'skew upwind' system have been proposed, for example by Wong and Raithby (1979), Leonard (1979), Lillington (1981). The payoff of skew upwinding is of course that more accurate solutions can be obtained more economically by using substantially coarser grids.

These methods suffer from two disadvantages. Most do not guarantee positive coefficients and this can detract from diagonal dominance, leading to numerical stability problems. They have all been developed for two dimensions and involve considerable computational effort, so much in fact that they have not been generalized to three dimensions.

Because of this, more straight forward methods are sought, and according to Galpin, Huget and Raithby(1986), the most promising at the moment appear to be 'mass weighted schemes' see for example, Hassan et al (1983a).

Hackman et. al.(1984) have shown that to accurately simulate the recirculation zone generated by single phase flow over a simple step required a 150*150 grid with an upwind scheme, whereas skewed differences could give grid independant results for about 42*42. Benodeckar et. al.(1985) have completed a similar study for single phase flow over surface ribs, a case more akin to the peripheral obstruction, and reach similar conclusions. By contrast, Hassan et. al.(1983b) show that the velocity field for flow around a bend can be computed quite well using upwind differences, but that the skewed formulae were required in the energy equation. The above suggests that the current studies of flow around bends may be prone to less severe numerical diffusion than the obstruction case.

All the studies reported on numerical diffusion were single phase two-dimensional cases. The general form of the skewed differencing scheme must address 8 neighbouring points. For equal generality, an equivalent 3D scheme must address the task of incorporating at least 26 neighbouring points. This may be one reason why none have been reported.

As no 3D schemes are yet established, an approximate way of evaluating false diffusion was used in this study, based as follows on the work of DeVahl Davis and Mallinson(1976).

The false diffusion terms introduced by first order upwinding in one dimension have been introduced in Appendix A, and may now be combined to comprise three dimensions :

$$\Gamma_{false} = 0.5(\ u\Delta\phi_{xx} + v\Delta\phi_{yy} + w\Delta\phi_{zz}) = \Gamma_x\phi_{xx} + \Gamma_y\phi_{yy} + \Gamma_z\phi_{zz} \qquad \text{(B24)}$$

This is analogous to diffusion in an anisotropic medium, when the axes coincide with the principal axes of diffusion. Carslaw and Jaeger(1954) show that if the flux has direction cosines l,m,n, the conductivity in this direction is :

$$1/\bar{\Gamma} = l^2/\Gamma_x + m^2/\Gamma_y + n^2/\Gamma_z \qquad \text{(B25)}$$

In two dimensions this can be resolved following DeVahl Davies and Mallinson(1976), who assume that the flux is normal to the local velocity, thus, as n=0 :

$$\bar{U} = u\,\bar{i} + v\,\bar{j} = U(\cos\gamma\,\bar{i} + v\sin\gamma\,\bar{j})\ ,\ l=-\sin\gamma\ ,\ m=\cos\gamma$$

$$\Gamma = \Gamma_x\Gamma_y/(\ \Gamma_x m^2 + \Gamma_y l^2\ ) = \frac{0.5U\Delta x\Delta y\sin\gamma\cos\gamma}{(\Delta x\cos^3\gamma + \Delta y\sin^3\gamma)} \qquad \text{(B26)}$$

This formula appears to contain the appropriate trends, for example ,if $\Delta x=\Delta y$, it has a maximum at $\gamma=\pi/2$. Raithby(1976) and Patankar(1980) recommend using this formula to assess the magnitude of false diffusion, and hold that numerical results will be acceptable if $\Gamma_{false} < \Gamma_{effective}$. In fact Hessami and Pollard obtained good comparison with experimental data for laminar flows even when Γ_{max} approached the molecular viscosity.

It would be useful to have such a guide for 3D computations, however it is not possible to derive one along the same lines, as diffusion normal to the resultant velocity can be anywhere in the normal plane. Faced with this dilemma, it is necessary to use an even rougher estimate of 3D false diffusion.

Equation B26 was evaluated in each of the coordinate planes. It was clear that the estimates were strongly affected by the coördinate grid spacing and aspect ratio, and that the computed results must be regarded as having a larger effective viscosity than that computed. For the bend cases, taken at the point of maximum cross flow, which is at the start of the bend in the pipe centre, $v/w\approx0.03$, and Γ is estimated to be about 0.005 in the uv and uw planes, which is of the same order as the effective viscosity. However in the vw plane, $\Gamma\approx0.1$, which is considerably larger, hence the overall false diffusion must be regarded as being near the latter. Nevertheless quite reasonable results were obtained for phase and velocity distribution in bends. For the obstruction, the radial velocities are much larger, and the maximum ratio $v/w\approx0.4$ upstream of the obstruction. In this case the values of Γ are computed to be .01,.02,0.5 in the uv,uw,vw planes.

Developing a 3D skew scheme is a major undertaking and was considered beyond the scope of the present work. Instead the study has concentrated on developing a viable framework for the solution of the 3D two-fluid equations and introducing sufficient modelling to demonstrate that experimentally observed phenomena can be reproduced with reasonable felicity.

Grid Curvature Related Errors

In addition to the false diffusion errors, Galpin, Huget and Raithby (1986) have shown that the pressure field can become distorted in uniform flows across a curved grid simply due to the fact that the coordinate direction changes while the flow direction does not. This error is maximum when the flow is uniform across the curved grid, and can then be as much as half a (transverse) velocity head. In the current study however, flows across the grid are not uniform but circulatory and are dominated by centrifugal momentum terms, so this error may not be major.

B.6 Drag Coefficient Formulae

The remaining problem of definition is the bubble diameter. Codes such as TRAC use a bubble diameter based on critical Weber number. The formulation is as follows

$$d_b = \frac{W_b \sigma}{\rho_1 v_r^2} \tag{B27}$$

where a value of 25 for W_b is deemed appropriate. This formulation is also used by D.S. Rowe (1981) in 1D studies and by Spalding (1981) in the URSULA code.

The flaw here is that any dynamic evaluation of d_b then depends on evolution of relative velocity. For obvious reasons, when V_r is small the formula generates enormous bubbles. In the URSULA code, Spalding (1978) imposes a limit on bubble size as an arbitrary fraction of the available hydraulic diameter, but this is an artifice. Early calculations using the TOFFEA code showed that the use of equation (B27) to determine bubble size led to numerical instability due to the vast range of sizes produced.

One way to circumvent this is to base the bubble size on a more stable relative velocity, for example, that obtained from drift flux considerations

$$w_\infty = C_1 \frac{\{(\rho_1 - \rho_v).\sigma\}^{0.25}}{\rho_1^{0.5}} \tag{B28}$$

There is a philosophical aversion to this, however, as the two fluid model is no longer independent of the drift flux simplification. A more satisfying approach is to merely use the bubble size formulation due to Wallis (1979)

$$d = 2 \left\{\frac{\sigma}{g(\rho_f - \rho_g)}\right\}^{1/2} \tag{B29}$$

This, of course, does give constant bubble size unless ρ_g is a strong function of P, but this is a simplification as opposed to the obvious distortion given by equation B27. This belief is also confirmed by Hanna et al (1982).

The specification for C_d is also open to some doubt. However, a survey by Lahey(1979) showed that several proposed formulae gave approximately the same results. However, this was over a limited range of Reynolds number. The formula for drag on a sphere in the Stokes region is $C_D = 24/Re$, and most formulae are extensions of this. The Reynolds number for the bubble case is again that based on relative velocity

$$Re = \frac{V_r d_b}{(\mu/\rho)_l}. \tag{B30}$$

Thus in any 2D or 3D computation, a large range of velocities can be produced throughout the field.

Some proposed formulae for C_D are :

Wallis (1979)	$6.3Re^{(-0.385)}$	(B31)
Zuber and Ishii (1979)	$\frac{24}{Re}(1 + 0.1R^{0.75})$	(B32)
TRAC, Liles(1978)	$\min(240, 24/Re, 18.7Re^{(-0.68)})$	(B33)

Results from these formulae are given in Table B1 for a range of relative velocities and Reynolds numbers. Also included are bubble sizes predicted by equation B27 based on this Reynolds number, and bubble size predicted by B29 and B27 for comparison. It is clear that B31 and B32 give about the same value of C_d for the expected range, but B33 is quite different. Following a recommendation by Lahey(1979), B31 was used in these studies, but B32 was used in the sensitivity studies discussed in Chapter 7.

Table B1

Comparison of Drag Coefficient and Bubble Size Formulae

Re_b	v_r m/s	C_d(B31)	C_d(B32)	C_d(B33)	d_b(B27) m	d_b(B29) m
.01	$2*10^{-6}$	37.	2400.	240.	10^8	.005
.1	.00002	15.	244.	90.	10^6	"
1.	.002	6.3	26.4	18.7	10^4	"
10.	.02	2.7	3.7	2.4	10^2	"
100.	.2	1.1	1.0	0.24	4.	"
10^3	2.	.44	.45	.024	.04	"
10^4	20.	.18	.25	.0024	.004	"